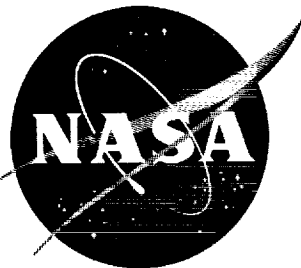94

N63-13180

Code 1

NASA

TECHNICAL NOTE

D-1432

LARGE-SCALE WIND-TUNNEL TESTS OF A CIRCULAR PLAN-FORM

AIRCRAFT WITH A PERIPHERAL JET FOR LIFT,

THRUST, AND CONTROL

By Richard K. Greif and William H. Tolhurst, Jr.

Ames Research Center
Moffett Field, Calif.

M-FI IC

B 27 1962

Code 1

NATIONAL AERONAUTICS AND SPACE ADMINISTRATION

TECHNICAL NOTE D-1432

LARGE-SCALE WIND-TUNNEL TESTS OF A CIRCULAR PLAN-FORM

AIRCRAFT WITH A PERIPHERAL JET FOR LIFT,

THRUST, AND CONTROL

By Richard K. Greif and William H. Tolhurst, Jr.

SUMMARY

/ 3 / 8 0

Full-scale tests have been conducted in the Ames 40- by 80-Foot Wind Tunnel to determine the performance, stability, and control characteristics of a research aircraft having a circular plan form and employing a peripheral jet for lift, thrust, and control. The aircraft was 18 feet in diameter and 18 percent thick. Propulsion was provided by a 5-foot-diameter rotor which took in air through the wing upper surface and drove it through internal ducting to a peripheral nozzle designed to provide thrust vector control.

Six-component aerodynamic data and propulsion system flow data were obtained at various angles of attack over a range of jet-momentum coefficients from 0 to 3.4. Flight characteristics in the cruise configuration were determined at altitudes ranging from 12 feet 7 inches to 2 feet 8 inches. Transition-flight characteristics were studied only at the lowest ground height. Some effects of forward speed on rotor performance were also investigated.

INTRODUCTION

The ability of an annular nozzle to augment thrust both statically and at forward speeds near the ground has led to the consideration of this device for use in vehicles ranging from simple ground-effect machines to high-speed VTOL aircraft. The principles on which these nozzles work have been explained in reference 1, and results from small-scale static and wind-tunnel tests of a circular wing with an annular nozzle are presented in reference 2. Additional information on the subject can be found in references 3 through 6.

Use of an annular nozzle as the hovering device in practical VTOL or GETOL (Ground Effect Take-Off and Landing) applications requires some scheme for the eventual conversion of its jet into conventional horizontal thrust for wing-supported flight. For the circular-winged aircraft of this investigation, the conversion was accomplished in the following

manner. In the hovering condition, its peripheral jet was highly focused (directed radially inward), providing augmentation near the ground while avoiding the thrust reduction associated with unfocused annular jets away from the ground (ref. 2). For transition and cruise conditions, an alternate passage was provided in the annular nozzle duct to permit the rear and lateral portions of the jet to exhaust radially outward in a manner characteristic of a jet wing.

The purpose of this test was to obtain aerodynamic force and moment data and propulsion system flow data which would enable determination of the aircraft's performance, stability, and control characteristics in transition and cruise flight. The flow data were also used to study aerodynamic effects on the propulsion system during in-flight operating conditions. The transition studies were influenced by the fact that the aircraft (which was intended for flight) had a thrust deficiency which prohibited hovering out of ground effect. As a result, the aircraft was tested as a GETOL vehicle, although it was originally designed for VTOL operation.

The purpose of this report is to present the principal results of the investigation. Additional data can be found in reference 7 along with some performance calculations for the aircraft based on a 4,500 pound gross weight.

NOTATION

C_D drag coefficient, $\dfrac{\text{drag}}{qS}$

C_Y side-force coefficient, $\dfrac{\text{side force}}{qS}$

C_L lift coefficient, $\dfrac{\text{lift}}{qS}$

C_l rolling-moment coefficient, $\dfrac{\text{rolling moment}}{qSD}$

C_m pitching-moment coefficient, $\dfrac{\text{pitching moment}}{qSD}$

C_n yawing-moment coefficient, $\dfrac{\text{yawing moment}}{qSD}$

C_J jet momentum coefficient, $\dfrac{\text{jet momentum}}{qS}$

C_{p_t} turborotor total pressure coefficient,
$$\frac{\text{(fan outlet total pressure)} - \text{(ambient static pressure)}}{q}$$

D wing diameter, ft

h height of undersurface center from ground, ft

i_T horizontal-tail incidence (positive when trailing edge is down), deg

J_A lateral control position (right gives a right rolling moment), fraction of total travel from neutral[1]

J_E longitudinal control position (negative gives pitch-down moment), fraction of total travel from neutral[1]

J_T transition control position[1]

M_J total jet momentum, lb

q free-stream dynamic pressure, lb/ft^2

r radius from center of turborotor axis, ft

r_F total turborotor radius, 5.0 ft

S wing area, ft^2

V velocity, knots

W gross weight, lb

δ_v deflection of roll and pitch control vanes from neutral (Neutral was 30°, trailing edge down, from horizontal. See fig. 2(b).)

ρ air density, slugs/ft^3

θ azimuth angle measured from airplane's fore and aft center line, deg (see fig. 2(a))

---

[1]See "Model and Apparatus" section for more details.

MODEL AND APPARATUS

Test Aircraft

Wind-tunnel installation.- Several views of the aircraft installed
in the 40- by 80-foot wind tunnel are shown in the photographs of figure
1. A support system using variable-height struts allowed the aircraft to
be raised and lowered for a simulation of ground proximity. Figures 1(a)
and 1(b) show the aircraft at the maximum test height, which was
12 feet 7 inches from the tunnel ground plane to the center of the air-
craft undersurface. Figure 1(c) shows the aircraft at the minimum test
height of 2 feet 8 inches. (This photograph was taken after the wing
was modified to extend the upper surface trailing edge of the wing.)

Geometric details of the aircraft, including those of its propulsion
system, control system, and test modifications, are presented in figure 2.
The general arrangement of these items and the major dimensions of aero-
dynamic importance are shown in figure 2(a). It should be noted that the
moment center was located at the geometric center of the wing rather than
near its aerodynamic center, because of symmetry requirements in the
hovering condition. While this would ordinarily cause a large instability
problem at forward speeds, it was anticipated that certain features of the
design (discussed below) would help to minimize it.

Propulsion system.- The essential element of the propulsion system
was a 5-foot-diameter turborotor (rotor with tip turbines) driven by the
exhaust of three J-69 jet engines. Turborotor and engine intakes were
located in the upper surface of the wing. Both turborotor outlet flow
and tip-turbine discharge gases were ducted radially outward to the
peripheral nozzle. The arrangement of these items is shown in figure 2(a).

Control system.- The principal features of the control system are
shown in the section views of figure 2(b). To aid in the description of
this rather complex system, an artist's sketch of the peripheral jet flow
regimes produced by it are presented in figure 3.

The focusing ring was continuous, encircling the annular portion of
the nozzle. Its double function was to focus the annular jet and, through
longitudinal and lateral movement, control its direction to provide thrust
and moment control for hovering and flight at low forward speeds (figs.
3(a) and 3(b)). The symbols J_E and J_A denote the displacement of the
focusing ring in fractions of its total longitudinal and lateral travel,
respectively. Positive J_E indicates a nose-up control input; right J_A
indicates a right roll control input. Calibrations of these items are
given in figure 4.

For use during flight at higher speeds, an alternate nozzle was installed in conjunction with the annular nozzle around the rear 240° of the wing periphery. The design of the alternate nozzle (shown in fig. 2(b)) allowed the jet to exhaust radially from the wing "trailing edge" in a manner equivalent to the flow from a jet flap. The lateral portions of the jet were turned partially aft by means of cascades located in the nozzle exit. Examples of the flow produced by the system are illustrated in figures 3(c) and 3(d). The purpose of the alternate nozzle arrangement was to provide solutions to drag, lift, and pitching-moment problems anticipated during operation at higher speeds. To overcome drag, its function was to provide greater horizontal thrust than could be achieved by controlling the thrust vector with the focusing ring system. In regard to lift and pitching moment, benefits were expected in the forms of increased trailing-edge lift induced by the jet flap and increased effective aspect ratio due to the radial fanning of the jet. These would have the combined effects of increasing lift, reducing nose-up pitching moment, and reducing instability. (Since the center of gravity was located at the center of the wing, it was desirable from a pitching-moment standpoint to keep the center of pressure as far aft of the wing aerodynamic center as possible. Twelve transition doors located around the aft 240° of the duct controlled the distribution of flow between the annular nozzle and the alternate nozzle. Instead of operating independently, the doors were separated into two coupled units. The six doors located in the two lateral 60° sectors of the duct formed one independently operated unit while the six doors located in the rear 120° sector formed the other. The symbol J_T was used to describe a "transition control position" in terms of "rear door position"/"side door position." (This is not to be confused as a ratio.) Door position in each case was expressed as a fraction of the total angular travel of the doors from their position required for hovering. (For example, a $J_T = 0.25/1$ indicates the rear doors to be 25 percent open and the side doors to be 100 percent open.)

Movable vanes located in the exit of the rear 120° portion of the thrust nozzle provided control moments for pitch and roll. These vanes were actuated by a linkage connected to the focusing ring so that all phases of flight would have one common input control. The calibrations of vane deflection versus J_E and J_A are shown in figure 4. Note that positive δ_v is given as the angular deflection of the vane trailing edge up from the vane's neutral position. Neutral position was 30°, trailing edge down, from horizontal.

Limited tests were made with the aircraft equipped with a horizontal tail as shown in figure 2(a). The tail was studied primarily as a stabilization and trim device.

Modifications.- In addition to the tail studies mentioned above, the aircraft was tested for the effects of three modifications.

The most important modification consisted of a faired extension to the upper surface trailing edge of the rear 120° portion of the thrust nozzle. This modification (shown in fig. 2(b)) was made early in the tests in an effort to increase nose-down control effectiveness. It was left on the aircraft for the remainder of the tests.

In another attempt to increase the nose-down control effectiveness, a 25-percent chord flap was extended at a 30° angle from the trailing edge of each pitch and roll control vane. The effect of these flaps was studied only briefly.

A portion of the test was conducted with the turborotor intake fitted with a set of guide vanes as shown in figure 2(c). The purpose was to determine the effectiveness of these vanes in relieving the asymmetric loading in the turborotor when operating at forward speeds.

Instrumentation

Measurement of aerodynamic forces and moments.- Measurements of lift, drag, and pitching moment were obtained by means of strain-gage load cells located at the attachment points of the aircraft to the three variable-height struts. Use of the system made it unnecessary to account for the large tare forces on the unfaired struts. Only the exposed area of the load cells themselves could introduce tare forces and these were negligible.

Measurements of side force, rolling moment, and yawing moment were obtained from the conventional floating frame balance of the 40- by 80-foot wind tunnel. Strut tares in these lateral measurements were assumed to be cancelling.

Measurement of jet momentum.- The jet momentum was the product of the total mass flow through the system and the exit jet velocity at the peripheral nozzle. Total mass flow consisted of the mass flow measured through the turborotor and the mass flow of the jet engines. Turborotor mass flow was determined from six radial pitot-static pressure rakes spaced at 60° intervals around the rotor azimuth. A check using two other systems (believed to be somewhat less reliable) gave mass flows which agreed within the order of ±10 percent. To calculate the exit velocity of the jet, total pressure was measured at the nozzle periphery and the jet was assumed to expand isentropically to free-stream conditions. This method of calculating jet velocity was subject to some question because of the presence of a swirl effect in the duct flow. However, it generally checked to within 10 percent of an alternate method whereby jet velocity was determined from continuity considerations using the total mass flow (described above) and the exit geometry of the nozzle. In view of the foregoing, it can be stated with reasonable certainty that the probable error in nozzle jet momentum is no greater than 10 percent.

Since it was difficult to hold constant values of jet momentum and tunnel free-stream dynamic pressure during the test, it was necessary to state C_J as a nominal value in all figures herein except figure 6. The deviation of actual values of C_J from the nominal was generally within ±5 percent, or less than the probable error in C_J itself.

PROCEDURE

Range of Variables

The investigation covered a range of free-stream dynamic pressures from 3 to 25 pounds per square foot, corresponding to an approximate Reynolds number range from 5 to 15 million, based on the wing's 18-foot diameter. The majority of power-on runs were made with a constant jet momentum of about 3,000 pounds. Combined with the range of tunnel speeds, this gave a C_J variation from 0 (power off) to 3.4. Total mass flow through the turborotor and engines was approximately 390 pounds per second for the 3,000-pound thrust condition.

The aircraft was tested at ground heights of 2 feet 8 inches $(h/D = 0.15)$, 3 feet 10 inches $(h/D = 0.21)$, 5 feet 0 inches $(h/D = 0.28)$, and 12 feet 7 inches $(h/D = 0.70)$. At the lower height, angle of attack was restricted for mechanical reasons to a range from -9.5° to $+2.5^\circ$. At the maximum height, angle of attack was varied from -10° to $+24^\circ$.

The characteristics of the longitudinal, lateral, and transition controls were studied over their full ranges of available travel. For those tests with the horizontal tail, stabilizer incidence was varied from -20° to -32°.

Method of Testing

The C_J parameter.- The majority of the tests were conducted at a constant value of jet momentum, with tunnel speed as the variable to obtain a range of jet momentum coefficients. To confirm the validity of this technique, a brief investigation was made at zero angle of attack for the forward flight configuration $(J_T = 1/1)$ to determine whether jet momentum or tunnel speed had any effects on the correlation of aerodynamic coefficients with C_J.

GETOL transition studies.- Since the transition doors operated in two independent units, a wide variety of transition control techniques was available for testing. However, it was not practical to perform the extensive tests necessary to determine the optimum of these techniques, especially in view of the other variables involved (ground height, etc.). Three door opening sequences representative of a transition from hover to cruise flight were therefore selected for exploratory study. These were: (1) a sequence in which the side doors remained closed until the rear doors were fully opened; (2) a sequence in which all doors

opened together; and (3) a sequence in which the rear doors remained closed until the side doors were opened. The method that produced the best combination of high lift and large nose-down moment for a balanced thrust-drag condition was then selected for a complete transition study, which was carried out as follows: At each of nine transition control settings (9 J_T) selected to give the desired door-opening sequence, data were obtained at the ground height of 2 feet 8 inches to determine the effects of angle of attack along with longitudinal and lateral control position. Each J_T was tested over a range of momentum coefficients selected to correspond with its particular area of operation during a transition.

Cruise flight tests.- Tests to determine the aircraft's characteristics in the cruise flight condition were conducted at a ground height of 12 feet 7 inches. For each of several C_J, the effect of longitudinal control position was studied through a range of angles of attack. Measurements of lateral control effects were less extensive.

The foregoing was repeated for the tail-on configuration after a very brief test to determine a tail incidence that would be somewhat near optimum (from considerations of maximum trimming capability without an excessive drag penalty).

Power-off base runs.- A circular cover was placed in the turborotor intake and conventional angle-of-attack variations were made with power off at both the maximum and minimum test heights. Both tail-on and tail-off data were obtained.

CORRECTIONS

Standard wind-tunnel wall corrections were not incorporated in the data reduction for this report. Corrections were applied, however, to account for a slight inclination of the wind axis caused by the presence of the variable-height strut system. Uncorrected values of angle of attack and drag coefficient based on the tunnel goemetric axis were corrected as follows:

$$\alpha_{corr} = \alpha_{uncorr} + \Delta\alpha$$

$$C_{D_{corr}} = C_{D_{uncorr}} + C_L \sin \Delta\alpha$$

(corrections to C_L were negligible); where, for the ground heights used in this investigation:

h/D	$\Delta\alpha$
0.70	2.9
.28	2.5
.21	2.5
.15	2.5

(These measurements were obtained during tests of the variable-height strut system in the absence of a model.)

RESULTS

Table I is an index to the figures discussed in the following section.

Longitudinal Characteristics

Power-off base runs.- The power-off longitudinal characteristics of the aircraft at two ground heights are presented in figure 5 for both the tail-on and tail-off configurations. The data were taken with a cover plate in the turborotor intake. Nominal q was 26 psf for each curve.

Correlation with momentum coefficient C_J.- The results in figure 6 indicate that the correlation of C_L, C_D, and C_m with C_J is independent of the value of free-stream dynamic pressure for the forward flight configuration ($J_T = 1/1$) at a ground height of 12 feet 7 inches ($h/D = 0.70$). Based on these results, results of reference 2, and unpublished data, the results for other configurations and ground heights tested in this investigation should show the same degree of correlation. Their application, therefore, should not be restricted to any particular value of wing loading as long as geometric similarity is maintained.

Transition characteristics.- The longitudinal characteristics of the aircraft at various stages of transition are shown in figures 7 through 9. Effects of angle of attack, longitudinal control position, and momentum coefficient are shown over a range of transition configurations varying from the hover configuration to the cruise configuration. A few results have been included throughout to show the effect of the horizontal tail. All results pertain to the modified trailing-edge configuration.

Figure 7 presents results corresponding to the initial stage of transition in which the aircraft is in the hover configuration (transition doors closed). The results are presented for several ground heights to show the general effect of ground proximity and to illustrate the necessity for a more efficient jet arrangement in free air flight. A better illustration of ground effect can be seen in figure 8, where the results of figure 7 at zero angle of attack and neutral longitudinal control have been cross plotted against h/D for several values of momentum coefficient.

Figure 9 presents characteristics corresponding to the intermediate stages of transition during which the transition doors move from their hover position toward their cruise flight position. Results are shown only for the sequence in which the side doors were opened before the rear doors, because this was the only technique found not to result in excessive nose-up pitching moments. The tests from which these results were

obtained were conducted at the lowest possible ground height $(h/D = 0.15)$, since it appeared that full advantage of the ground effect would have to be taken to enable transition.

In figures 8 through 9(d), the rear transition doors were in the hover position and the side doors were at increasing stages of opening. Under these conditions, increasing angle of attack produced wing leading-edge stall when the controls were set in nose-up positions $(J_E > 0)$. The corresponding results are presented as dashed curves in the figures. Figures 9(e) through 9(g) represent the high-speed phase of transition, during which the rear transition doors were at increasing stages of opening while the side doors were completely open. No stall characteristics were observed under these conditions.

Cruise flight characteristics.- The longitudinal characteristics of the aircraft in the cruise flight configuration are shown in figures 10 through 13. Results for various longitudinal control positions are presented for several momentum coefficients.

The characteristics of the aircraft with the trailing-edge modification are shown in figures 10 through 12. Figure 10 presents the results for low and intermediate ground heights. Characteristics out of ground effect (maximum test height) for both the tail-off and tail-on configurations are shown in figure 11. Figure 12 presents the results for the tail-off configuration with the addition of flaps on the pitch and roll-control vanes.

The characteristics of the aircraft prior to the trailing-edge modification (original configuration) are given in figure 13. The latter figure shows the effect of adding a horizontal tail and varying its incidence. It is interesting to note in figure 13(b) that the tail contributes very little to the stability of the aircraft. This result indicates that the tail was operating in a region of high downwash caused by the aircraft's propulsion system.

Lateral and Longitudinal Characteristics With and
Without Turborotor Intake Guide Vanes

Lateral characteristics.- The lateral characteristics of various transition configurations in the presence of ground effect are shown in figure 14.

The lateral characteristics of the cruise flight configuration in the absence of ground effect $(h/D = 0.70)$ are presented in figure 15. The variations of C_Y, C_l, and C_n with momentum coefficient are shown in figure 15(a) for several angles of attack and in figure 15(b) for various lateral control settings. Effects of the installation of guide vanes in the turborotor intake can be seen by comparing figure 15(b) to 15(c).

Longitudinal characteristics.- The longitudinal characteristics of the aircraft with intake guide vanes are shown in figures 16(a) and 16(b) for transition flight (h/D = 0.15) and cruise flight (h/D = 0.70), respectively.

Turborotor Outlet Pressure Distribution

Circumferential pressure profiles at the turborotor outlet are presented in figure 17 for various momentum coefficients, angles of attack, and longitudinal control settings. Variations of total pressure coefficient with azimuth angle are plotted for several radial stations. All results were obtained at h/D = 0.70 for the forward flight configuration without rotor intake guide vanes.

Performance Summary

An analysis of the results was performed to determine the available speed range through which the aircraft was capable of maintaining trimmed, level, unaccelerated flight (1 g flight). The results of this study are summarized in figure 18.

Momentum thrust to weight ratio, angle of attack, and longitudinal control position required for 1 g flight are plotted against a dimensionless speed parameter in figure 18(a) for several transition configurations operating in the ground effect. The same form of presentation is used in figure 18(b) to show the results for the cruise configuration out of the ground effect. Each curve was obtained by cross plotting the basic test results for the modified trailing-edge configuration without the horizontal tail. Momentum thrust to weight ratios were obtained from ratios of C_J to C_L, while the speed parameter is equivalent to $\sqrt{1/C_L}$.

It can be seen in figure 18(a) that a trim point at any given speed can be produced by more than one combination of airplane variables. A selection of trim points through the transition speed range can therefore be based on the desired variation of any one airplane variable (e.g., at constant angle of attack, or at minimum thrust (power) required). To illustrate this, cross plots of trim points for two cases of power variation (constant power and minimum power) are shown in figure 18(c).

It is interesting to note that the momentum thrust-to-weight ratios (see Instrumentation section regarding accuracy) required during transition appear rather large in comparison to what might be expected of a vehicle which utilizes an annular jet for thrust augmentation during hover. For this aircraft, however, there is little reason to expect any thrust augmentation effect to carry over into transition since its jet configuration, as dictated by the requirements of horizontal thrust and longitudinal

trim, does not remain annular at forward speeds. (This was illustrated in fig. 3.) Compounding the problem is the fact that the angles of attack required for trim did not permit full utilization of the aerodynamic lift available from the wing. A reduction in the thrust required for transition might be accomplished by: (1) performing the transition at lower ground heights; (2) developing schemes to provide horizontal thrust and longitudinal trim which would still allow the main jet configuration to be optimized for maximum lift; and/or (3) overcoming the pitch-up problems associated with wing operation at high angles of attack.

While the curves of figure 18 represent the trim conditions of zero drag and pitching moment, it should be noted that the aircraft does not in any instance have static aerodynamic stability. To make it a flyable vehicle, an automatic stabilization system of some type would have to be employed.

Ames Research Center
    National Aeronautics and Space Administration
        Moffett Field, Calif., July 19, 1962

REFERENCES

1. Chaplin, Harvey R.: Theory of the Annular Nozzle in Proximity to the Ground. DTMB Aero Lab; Aero Rep. 923, 1957.

2. Greif, Richard K., Kelly, Mark W., and Tolhurst, William H., Jr.: Wind-Tunnel Tests of a Circular Wing with an Annular Nozzle in Proximity to the Ground. NASA TN D-317, 1960.

3. Von Glahn, Uwe H.: Exploratory Study of Ground Proximity Effects on Thrust of Annular and Circular Nozzles. NACA TN 3982, 1957.

4. Chaplin, Harvey, and Stephenson, Bertrand: Preliminary Study of the Hovering Performance of Annular Jet Vehicles in Proximity to the Ground. DTMB Aero. Lab., Aero. Rep. 947, 1958.

5. Rethorst, Scott, and Royce, W. W.: Lifting Systems for VTOL Vehicles. IAS Paper No. 59-123, 1959.

6. Boehler, Gabriel D., and Spindler, Robert J.: Aerodynamic Theory of the Annular Jet. Part I. Aerophysics Co. Rep. AR 581-R, 1958.

7. Garland, D. B.: Report on Phase 2 Tests of an Avrocar in the 40- by 80-foot Wind Tunnel at NASA Ames Research Center. Avro Aircraft Ltd. Rep. 500/Aero Test/408, vols. 1, 2, and 3, 1961.

TABLE I.- LIST OF FIGURES

14

A-27748

(a) Three-quarter front view at maximum test height.

Figure 1.- Installation of the aircraft on the variable-height strut system of the Ames 40- by 80-Foot Wind Tunnel.

16
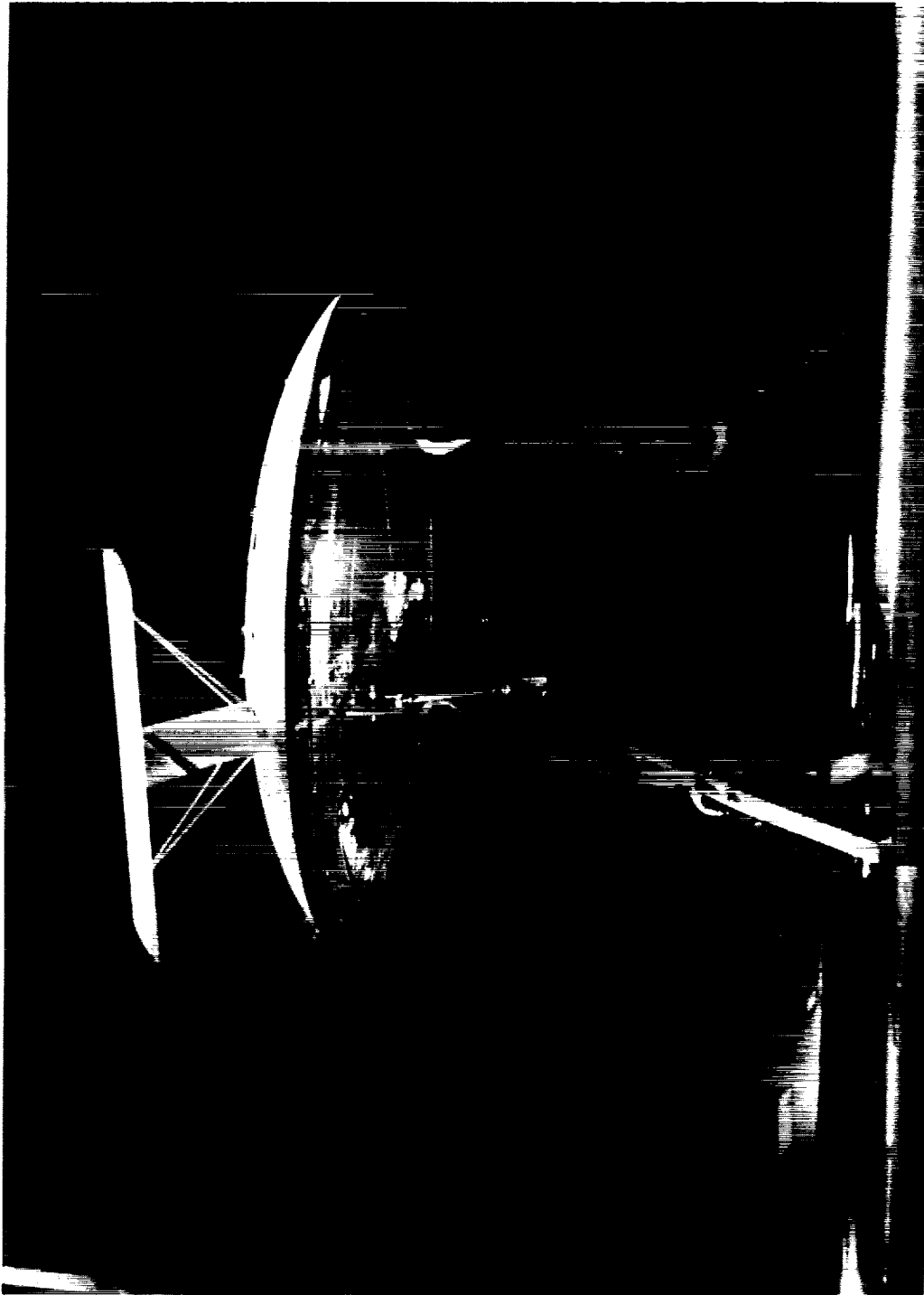
A-27749

(b) Three-quarter rear view at maximum test height (with horizontal tail).

Figure 1.- Continued.
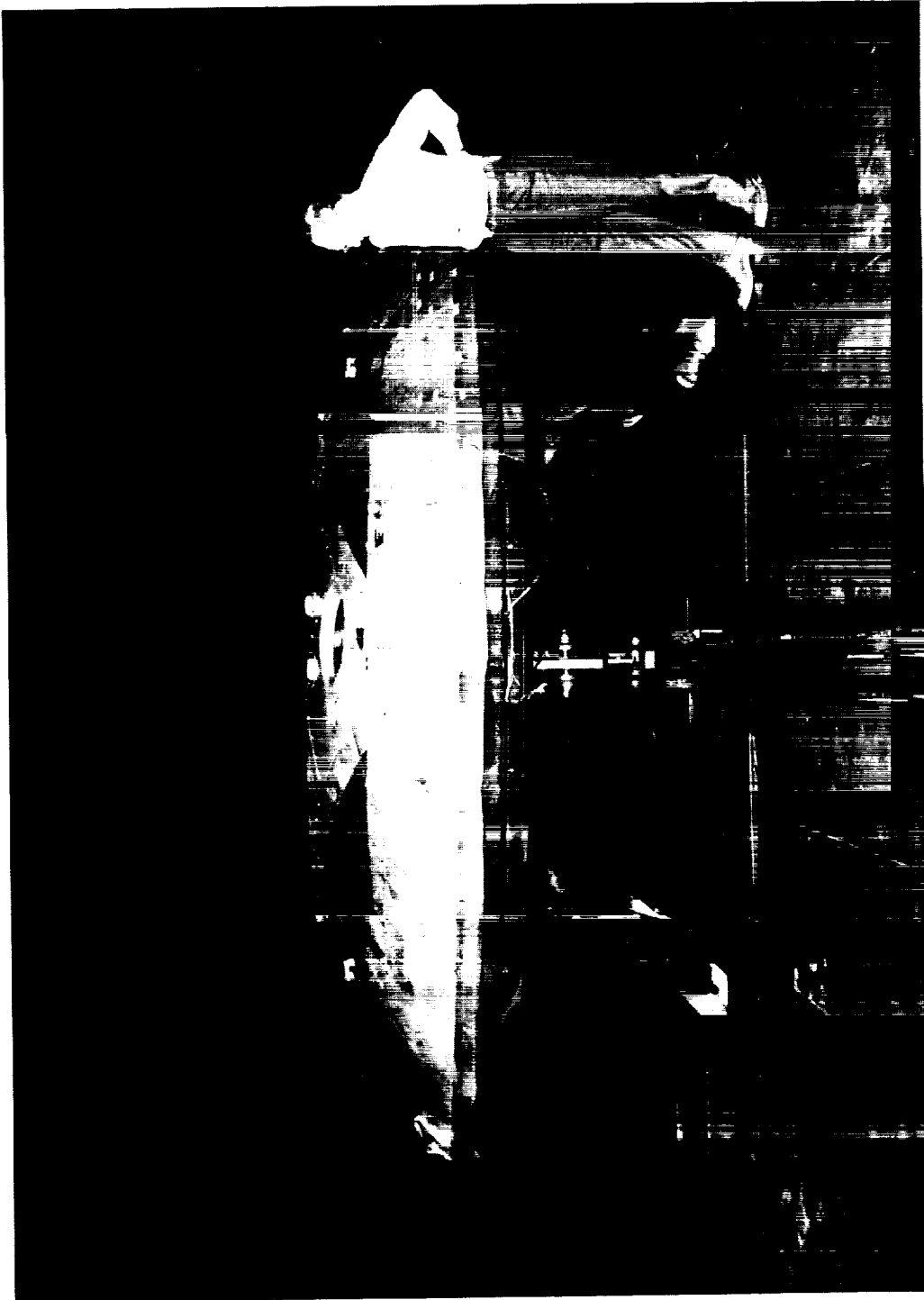
A-27772

(c) Rear view at minimum test height.

Figure 1.- Concluded.

18

Wing area = 254 ft²
Wing diameter = 18 ft
t/D = 0.18
Aspect ratio = 2/π
Tail area = 30 ft²
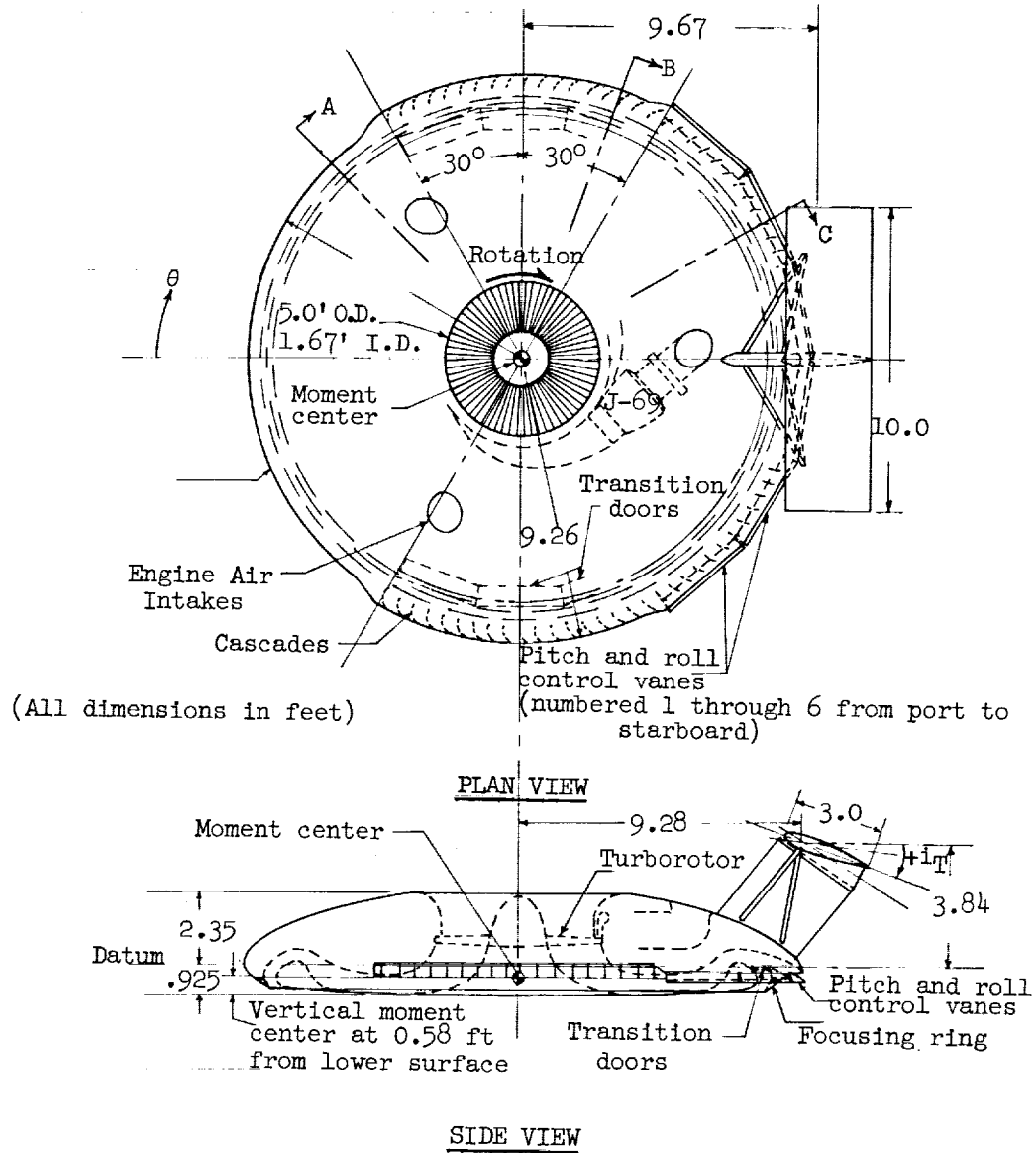
(a) General details.

Figure 2.- Geometrical details of the aircraft.

19

SECTION A

Datum

Annular nozzle

Focusing ring

SECTION B

Transition door in hover position

Transition door in cruise flight position

Datum

Alternate nozzle

Cascade

Focusing ring

Annular nozzle

SECTION C

Transition door

Datum

Annular nozzle

Focusing ring

Alternate nozzle

Trailing-edge modification (rear 120° only)

Pitch and roll control vane 6 in. chord 1.5 in. vane flap extension

δv down 30°

30°

Neutral control position, 300° torus

(b) Arrangement of control devices.

Figure 2.- Continued.

Wind
direction →

2.0

2.5

A   A

All dimensions in feet

2.18   1.37   .83   1.87   2.35

Aircraft Datum

SECTION A-A
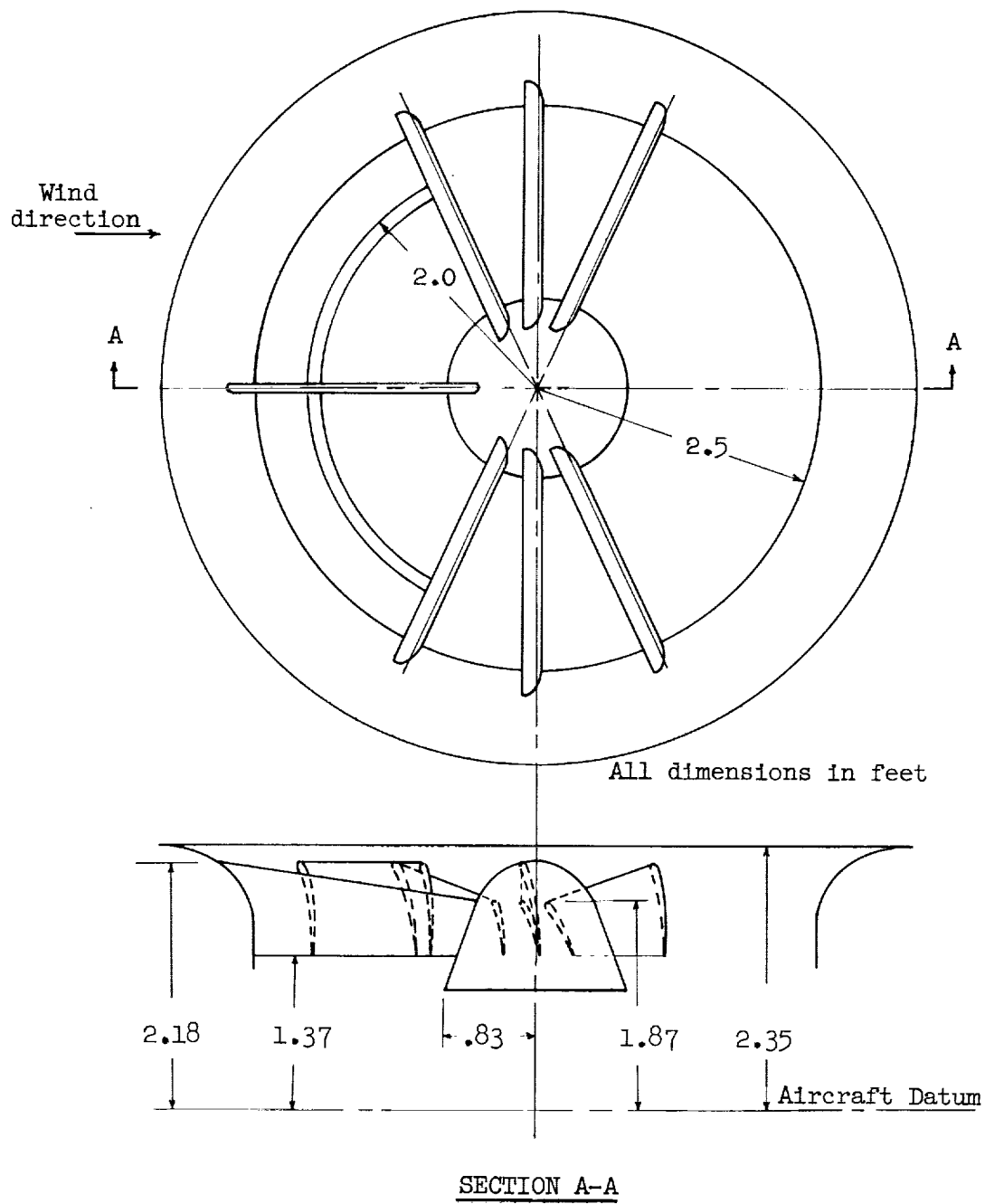
(c) Sketch of the turborotor intake guide vanes.

Figure 2.- Concluded.
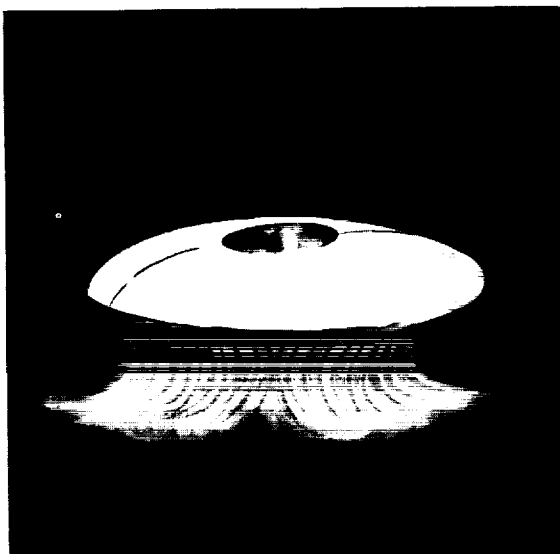
(a) Hover configuration
Transition doors closed.
Focusing ring neutral.
Pitch and roll controlled by
movement of focusing ring.

(b) Initial transition stage
Transition doors closed.
Focusing ring moved aft, but
with reserve travel for pitch
and roll control.

A-29196

(c) Mid-transition stage
Rear transition doors closed.
Side transition doors open.
Pitch and roll controlled by
movement of focusing ring.
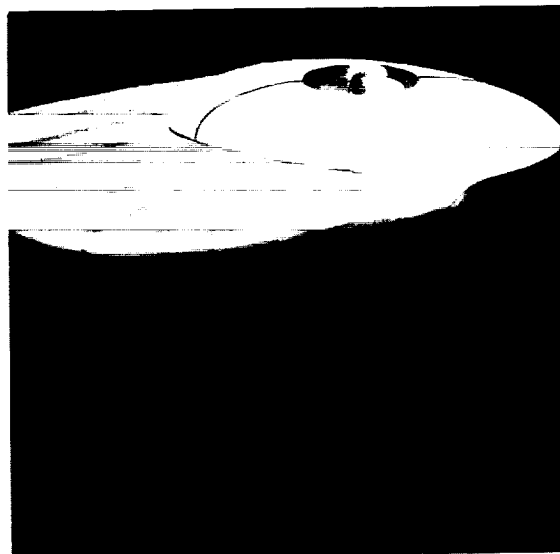
(d) Cruise flight out of ground
effect
All transition doors open.
Pitch and roll controlled by
movable vanes located in rear
120° of thrust nozzle.

Figure 3.- Sketch of the jet flow regimes produced by the control
system during various flight phases.
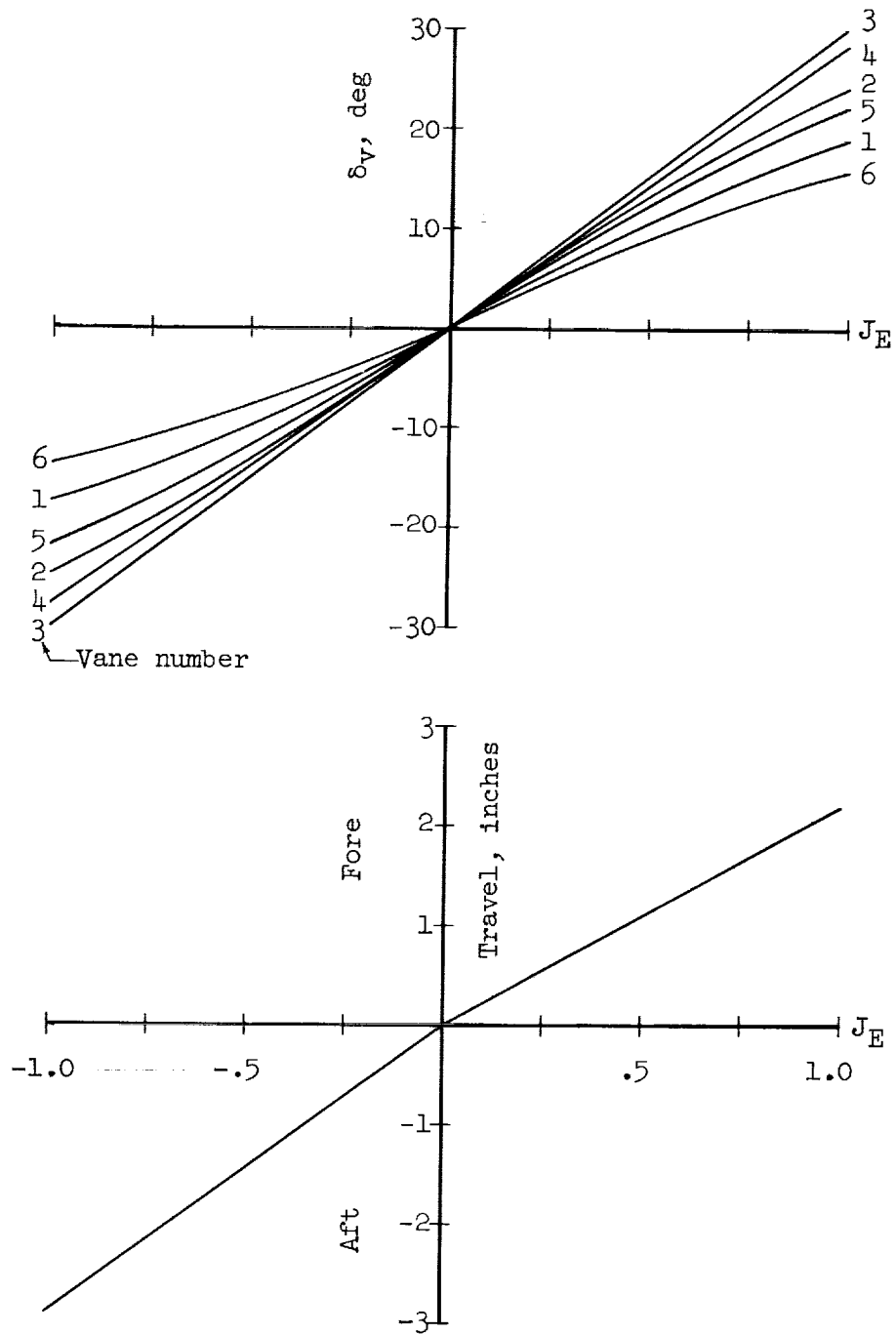
(a) Longitudinal control position with neutral lateral control.

Figure 4.- Calibration of focusing ring position and pitch and roll control vane deflection versus control position.
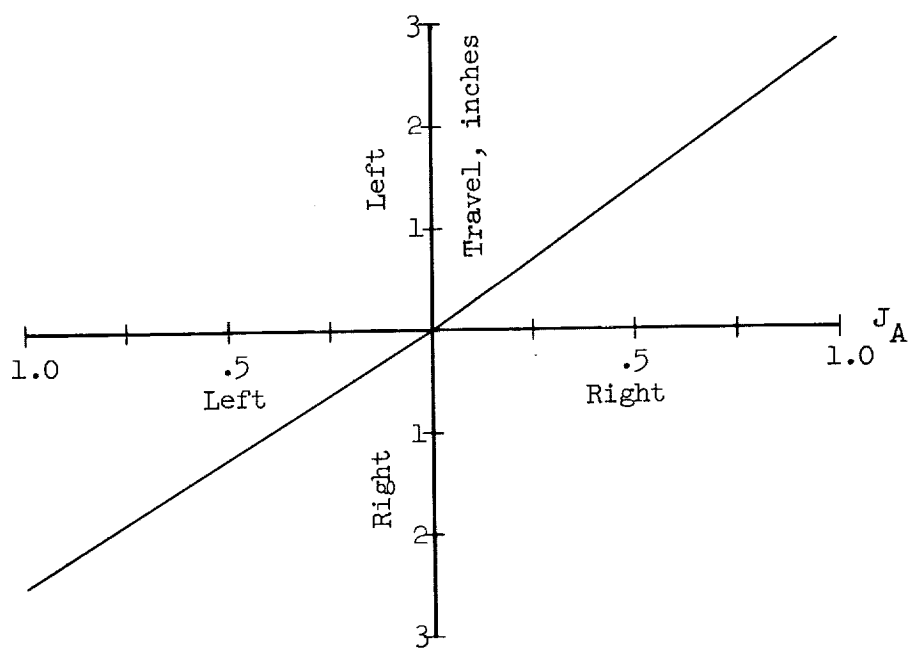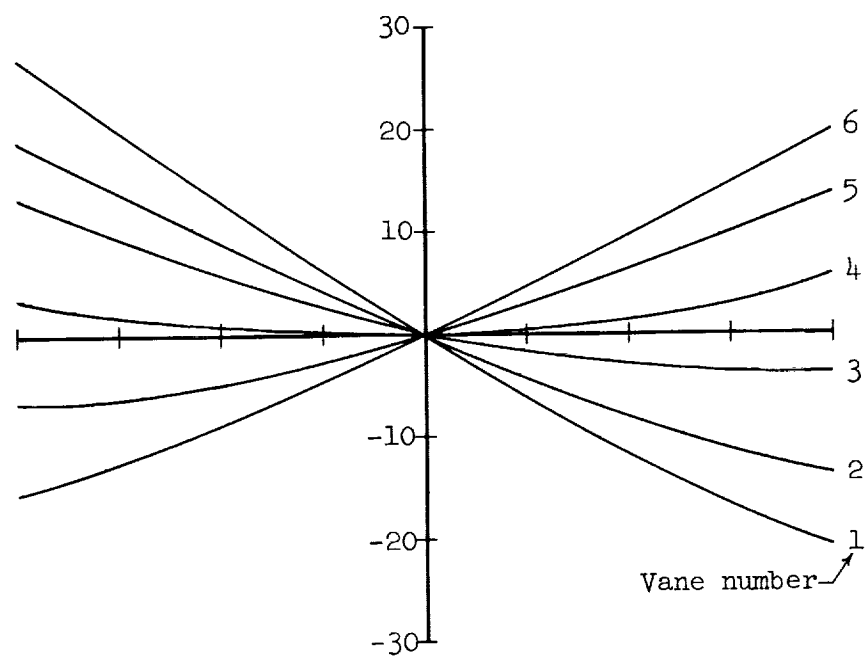
(b) Lateral control position with neutral longitudinal control.

Figure 4.- Concluded.
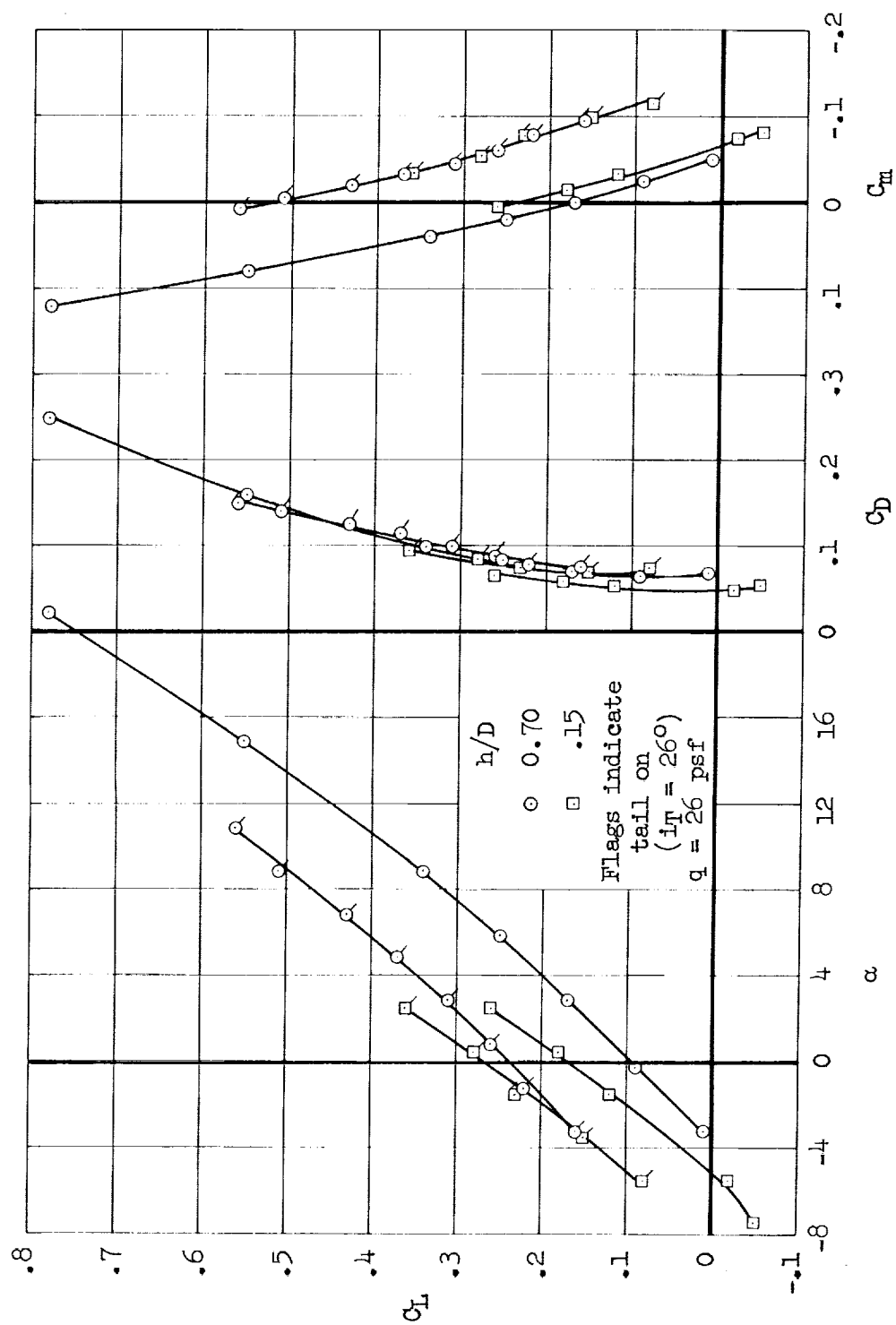
Figure 5.- Power-off longitudinal characteristics at the maximum and minimum test heights.
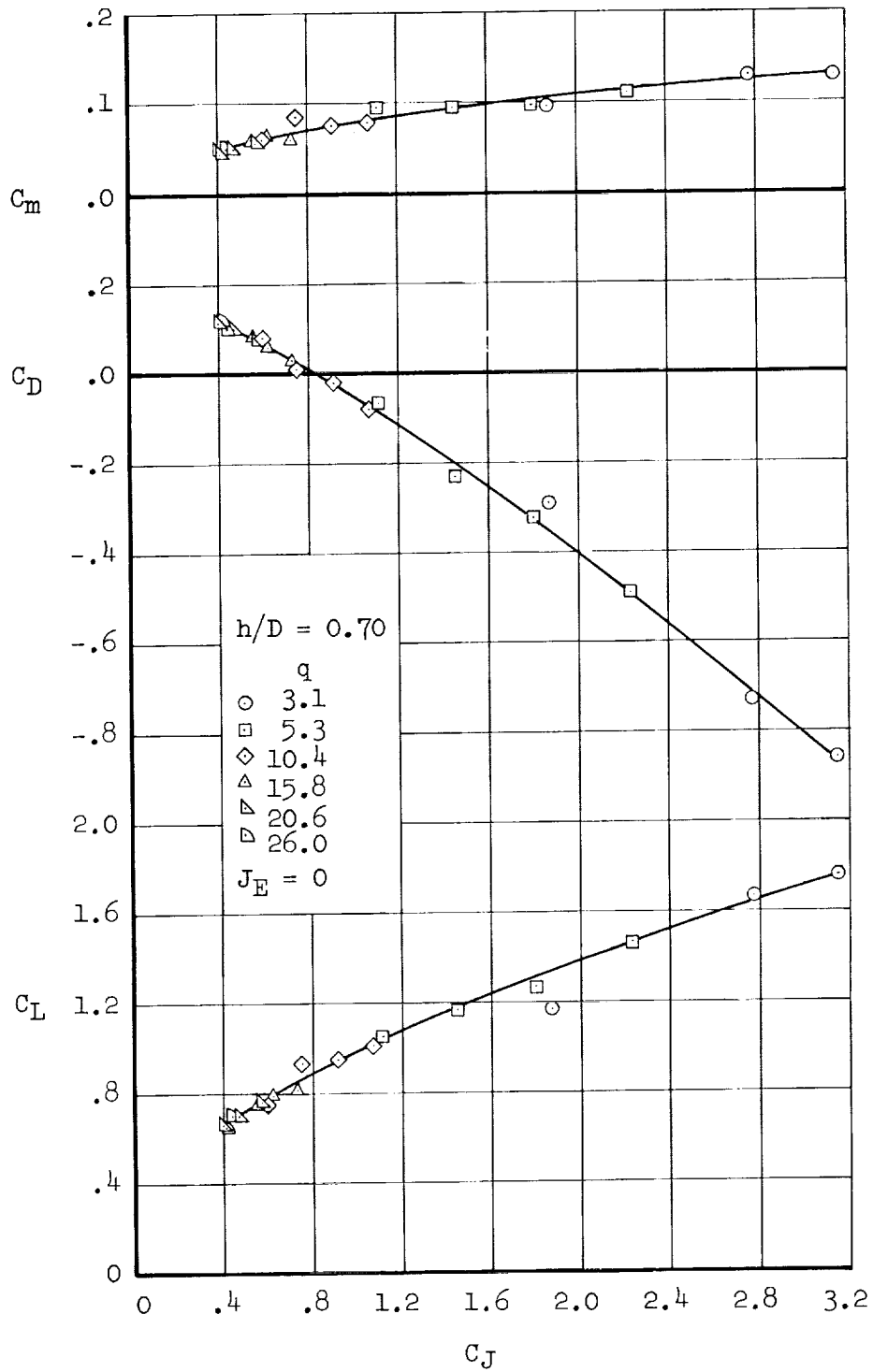
Figure 6.- Effect of free-stream dynamic pressure on the correlation of
longitudinal aerodynamic coefficients with the jet momentum
coefficient.
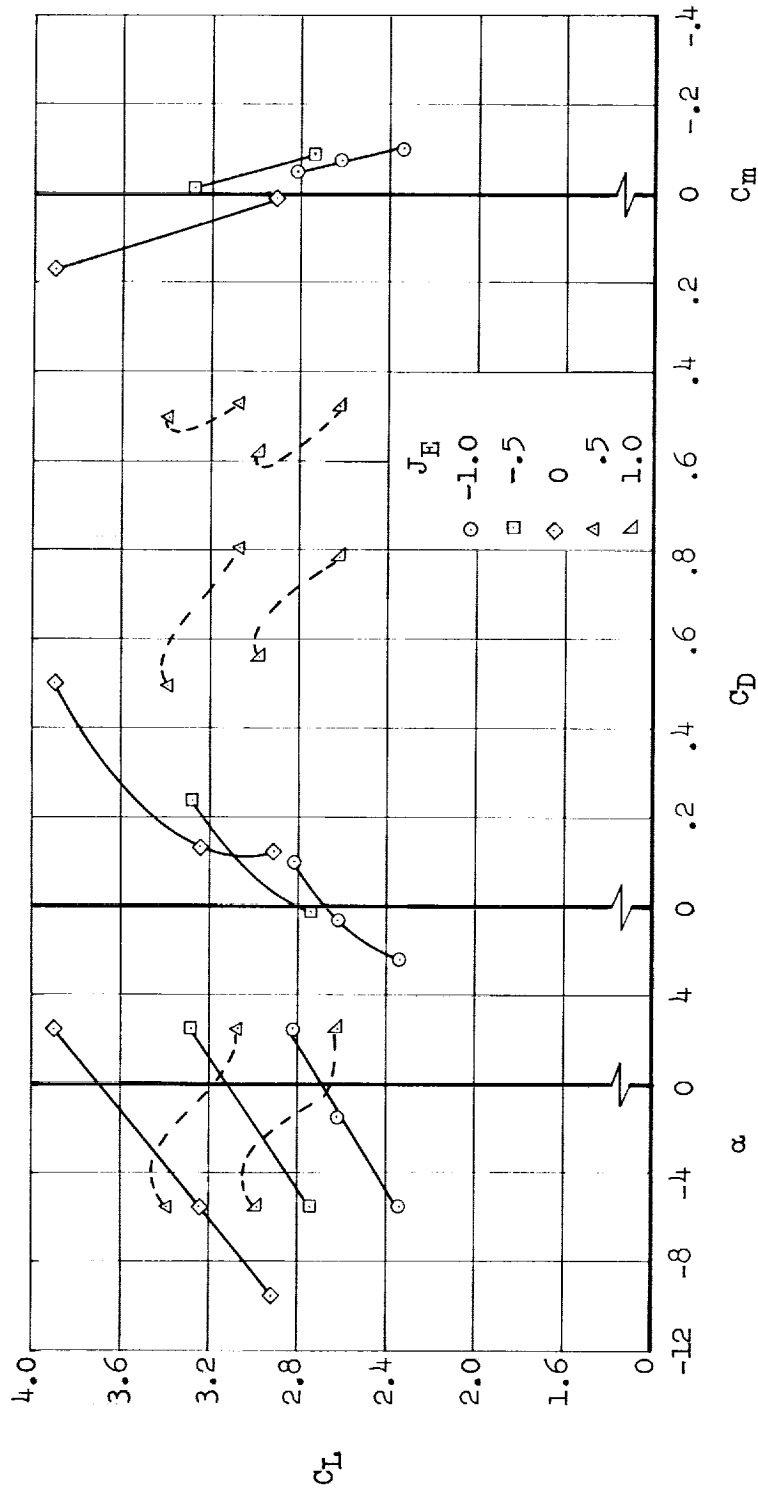
(a) h/D = 0.15; C_J = 3.4

Figure 7.- Longitudinal characteristics of the hover configuration (J_T = 0/0) at various ground heights. Flagged symbols are for tail on, with i_T = 26º.
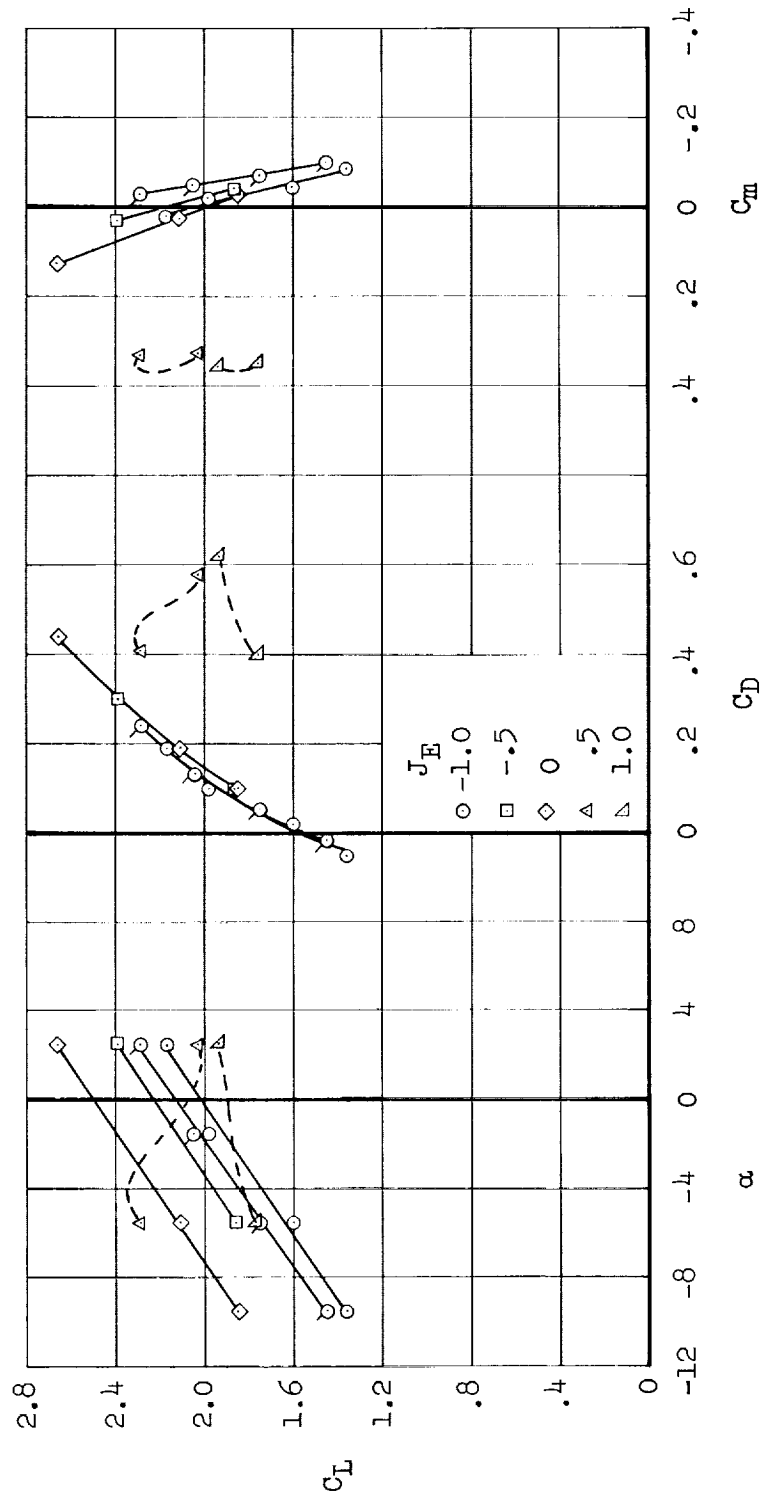
(a) h/D = 0.15; C_J = 2.1 - Continued.

Figure 7.- Continued.
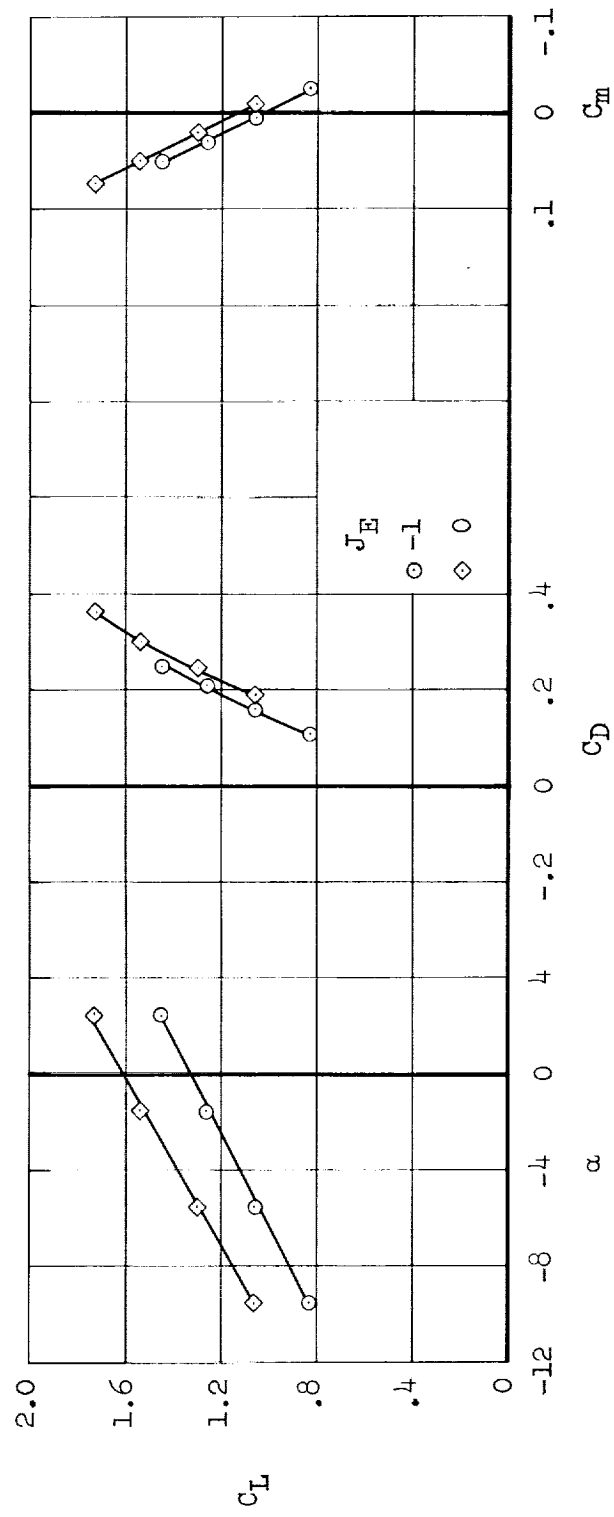
(a) h/D = 0.15; C_J = 1.1 - Concluded.

Figure 7.- Continued.
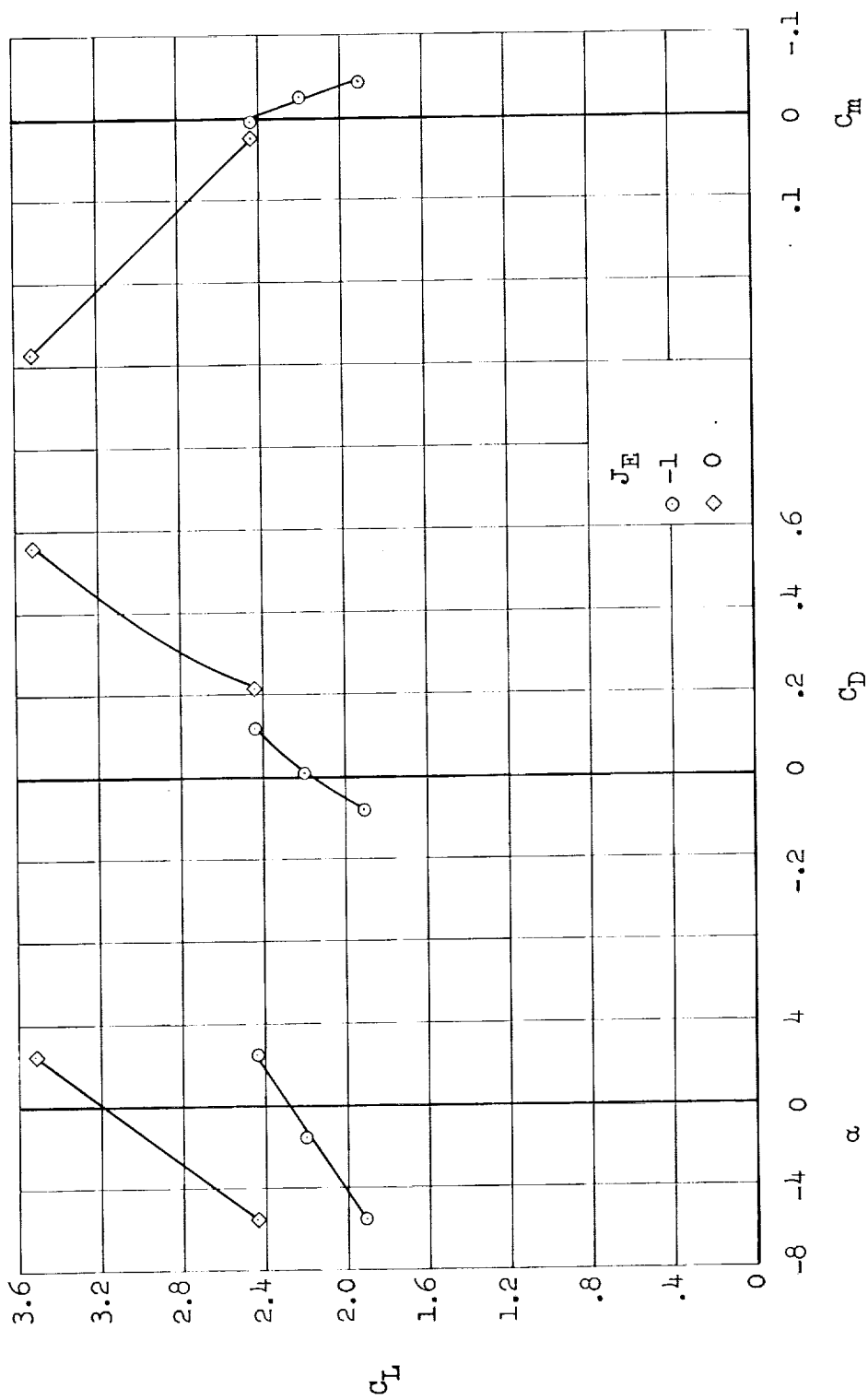
(b) h/D = 0.21; C_J = 3.4

Figure 7.- Continued.
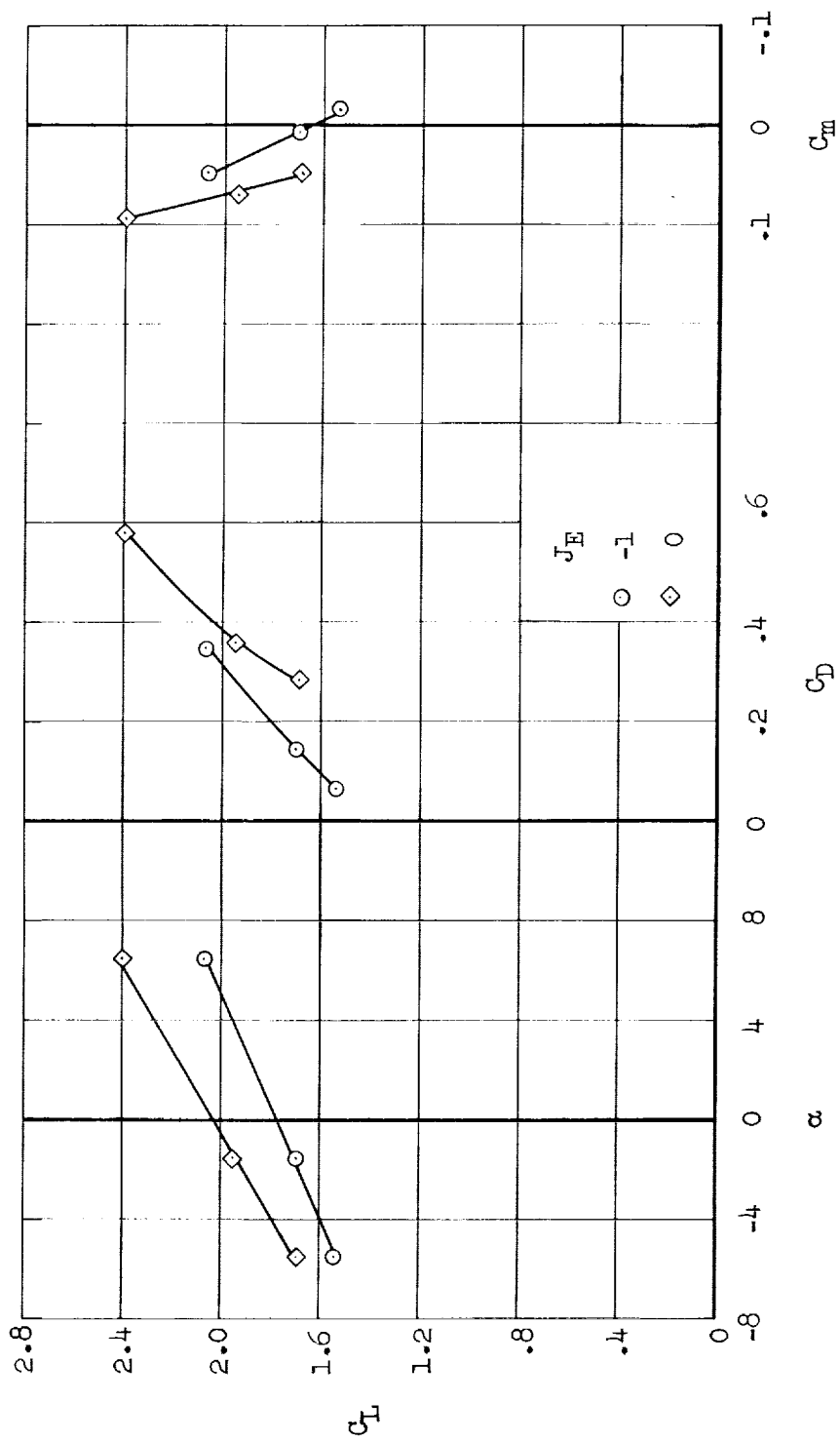
(b) $h/D = 0.21$; $C_J = 2.2$ - Continued.

Figure 7.- Continued.
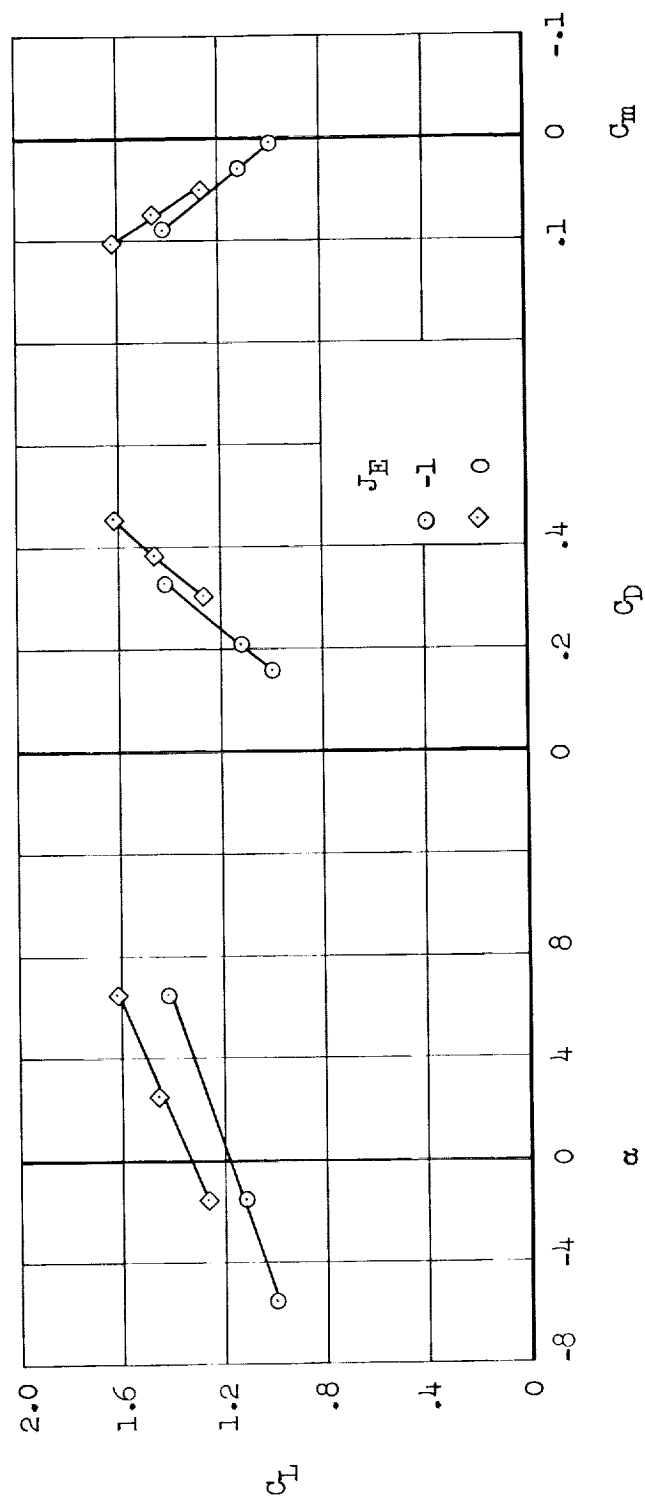
(b) h/D = 0.21; C_J = 1.1 - Concluded.

Figure 7.- Continued.
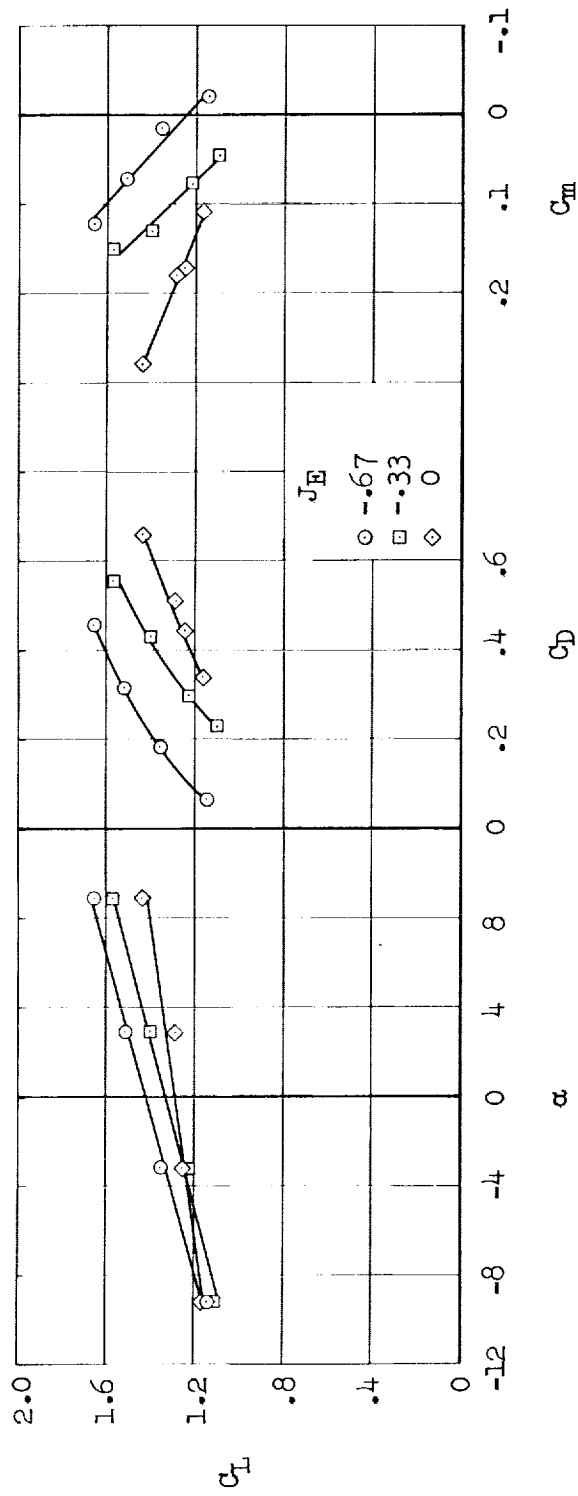
(c) h/D = 0.70; C_J = 2.6

Figure 7.- Continued.
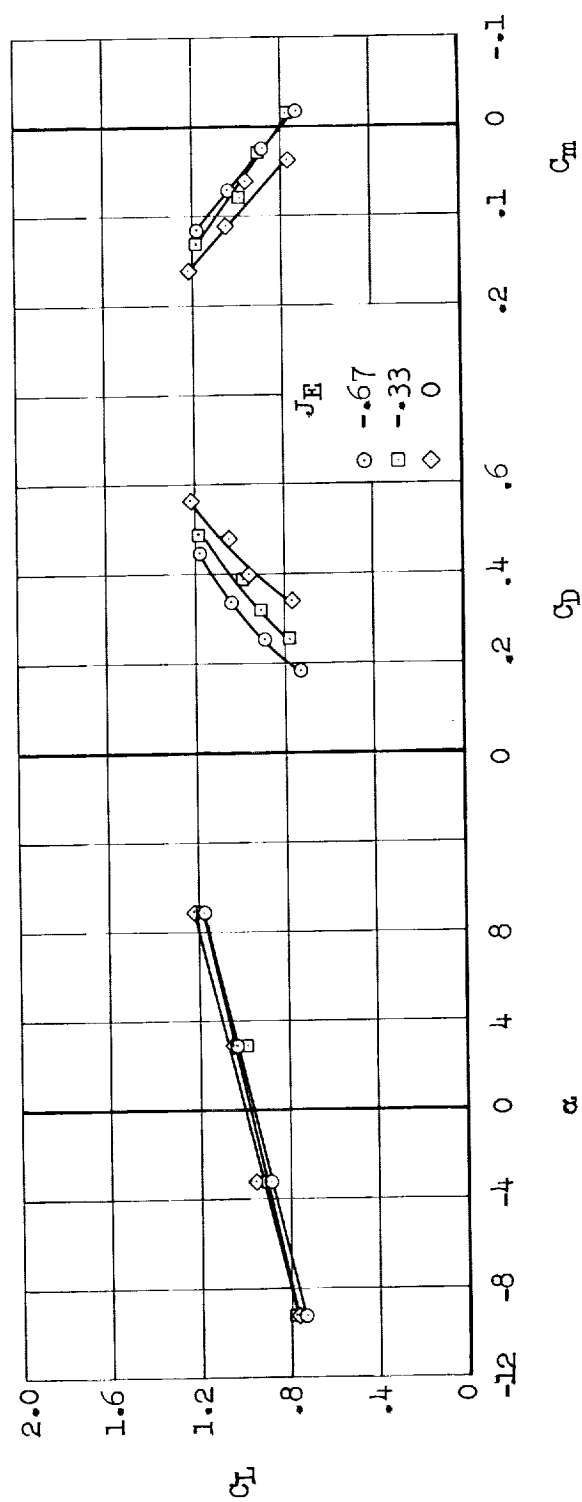
(c) $h/D = 0.70$; $C_J = 1.3$ - Continued.

Figure 7.- Continued.
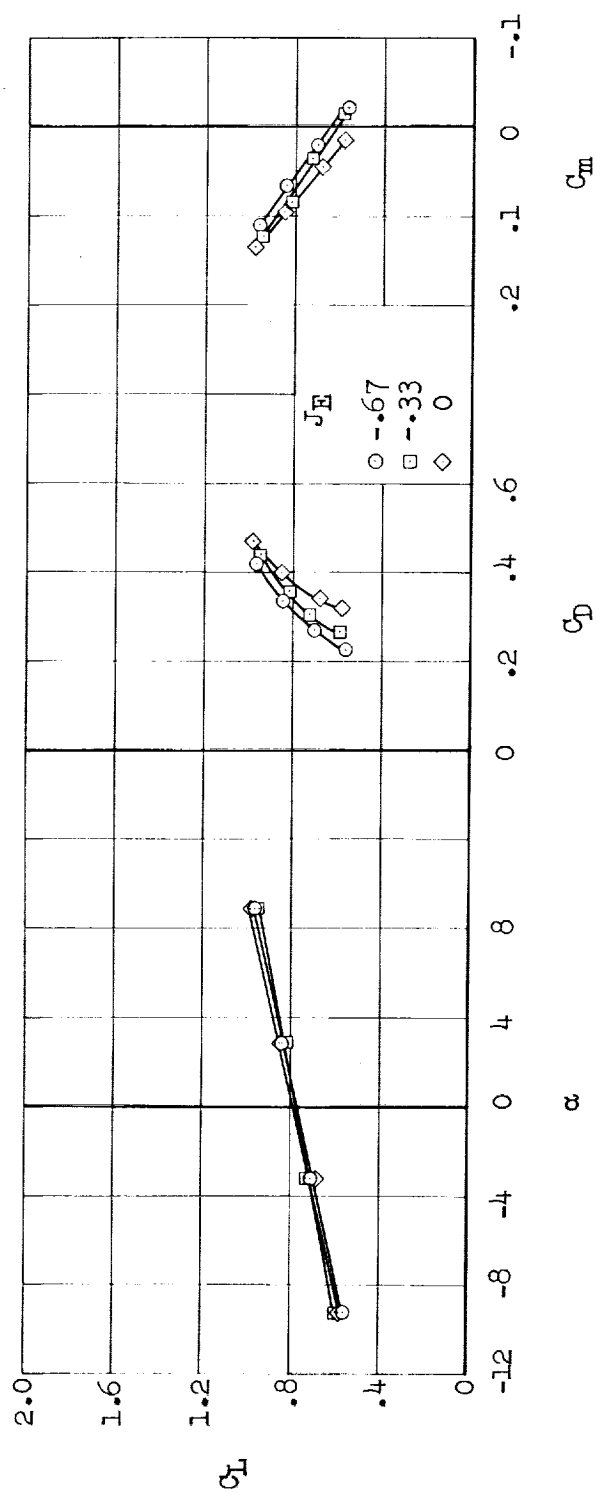
(c) $h/D = 0.70$; $C_J = 0.87$ - Concluded.

Figure 7.- Concluded.
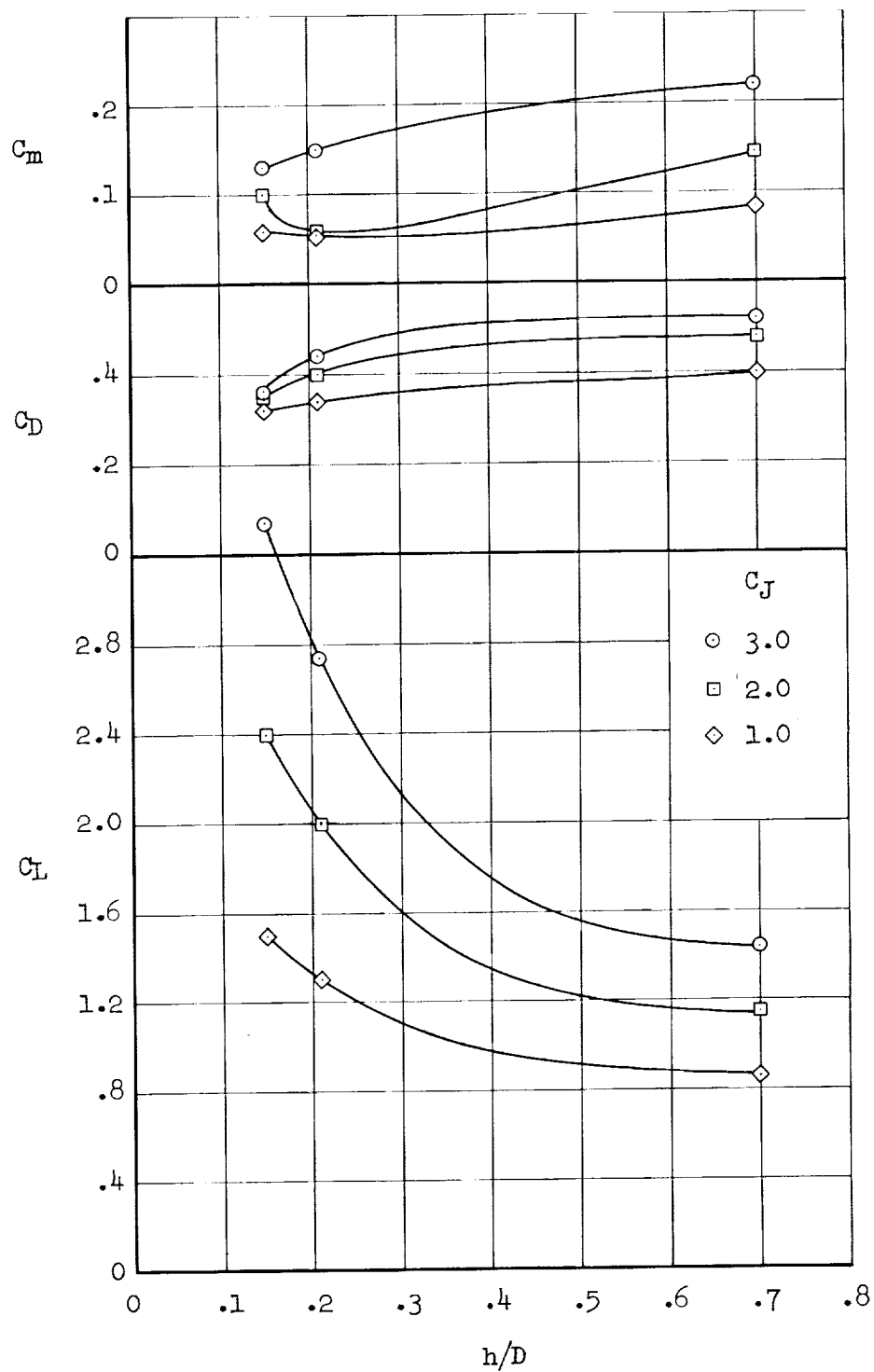
Figure 8.- Effect of ground height on the longitudinal characteristics of the hover configuration at $\alpha = 0$ and $J_E = 0$.

36
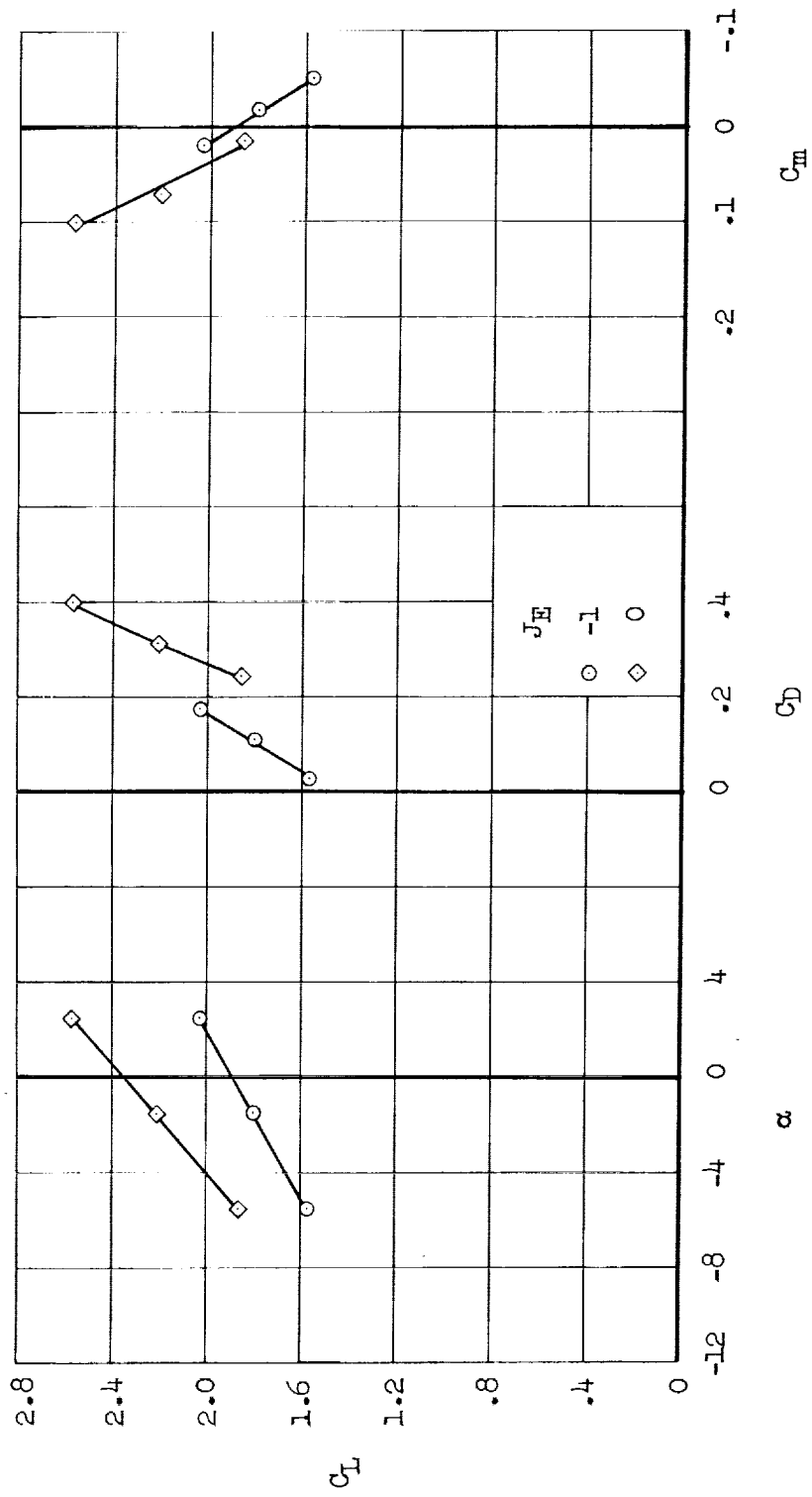
(a) $J_T = 0/0.25$; $C_J = 2.2$

Figure 9.- Longitudinal characteristics of the transition configuration at $h/D = 0.15$. Flagged symbols are for tail on, with $i_T = 26°$.
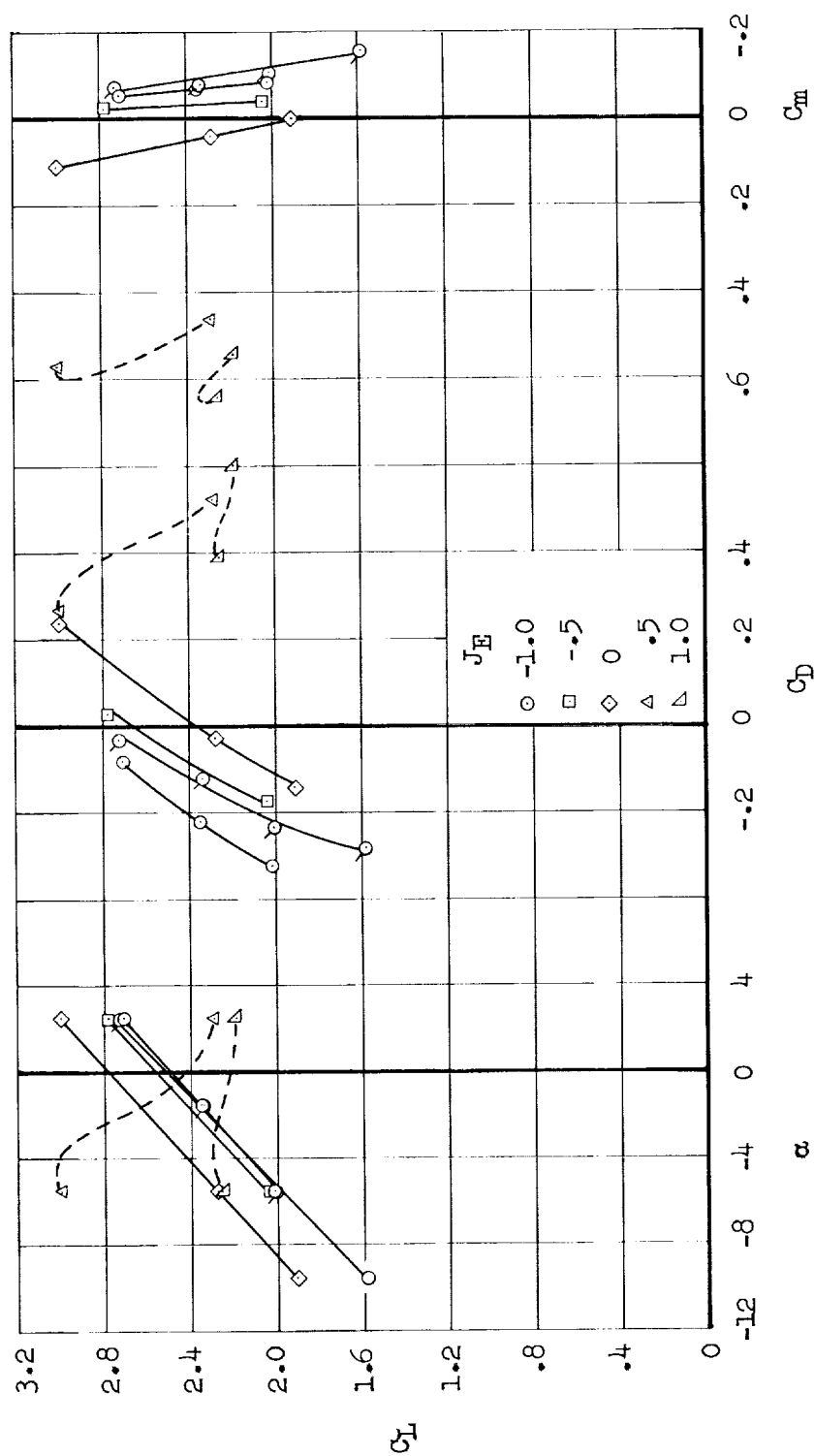
(b) $J_T = 0/0.5$; $C_J = 3.4$
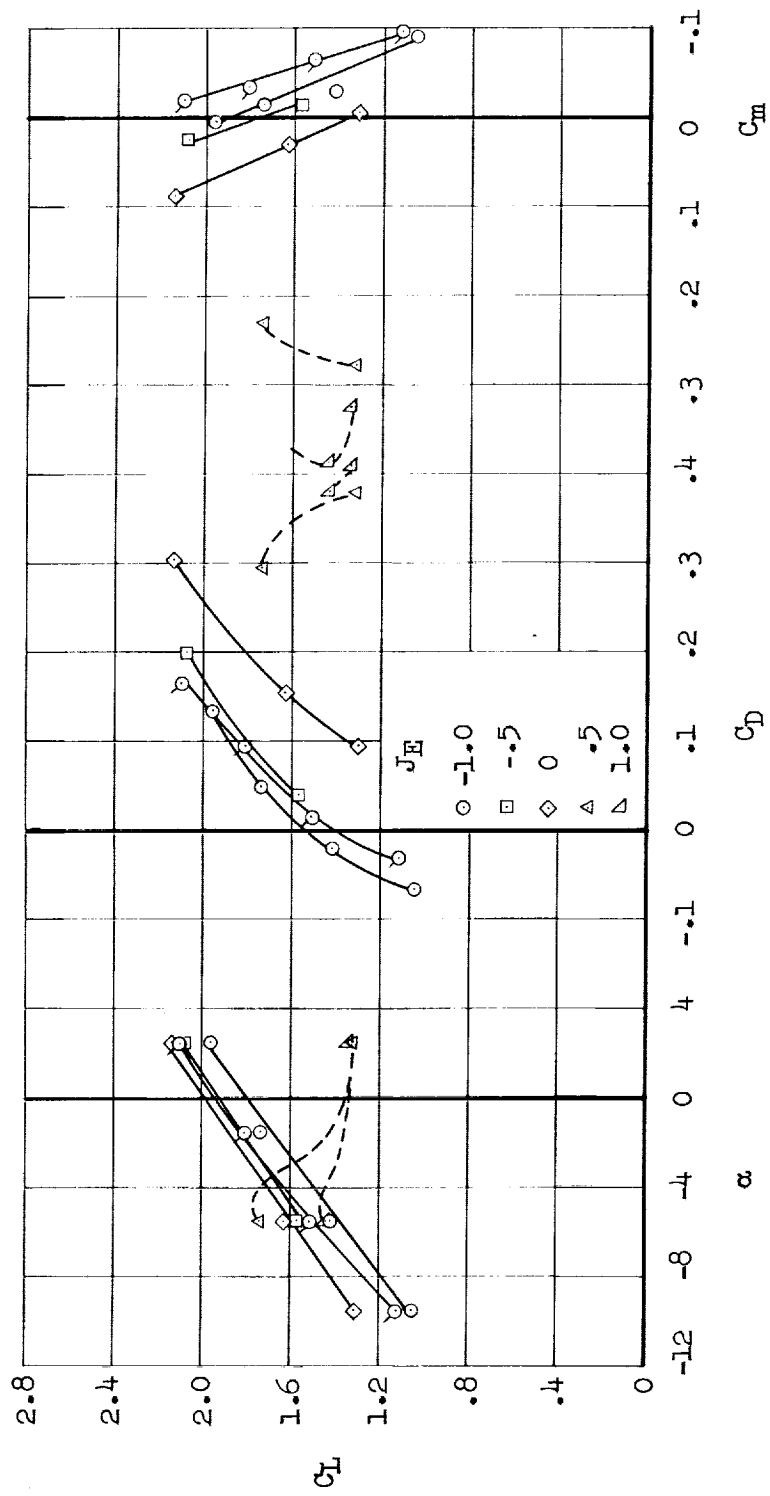
Figure 9.- Continued.

(b) $J_T = 0/0.5$; $C_J = 2.2$ - Continued.

Figure 9.- Continued.
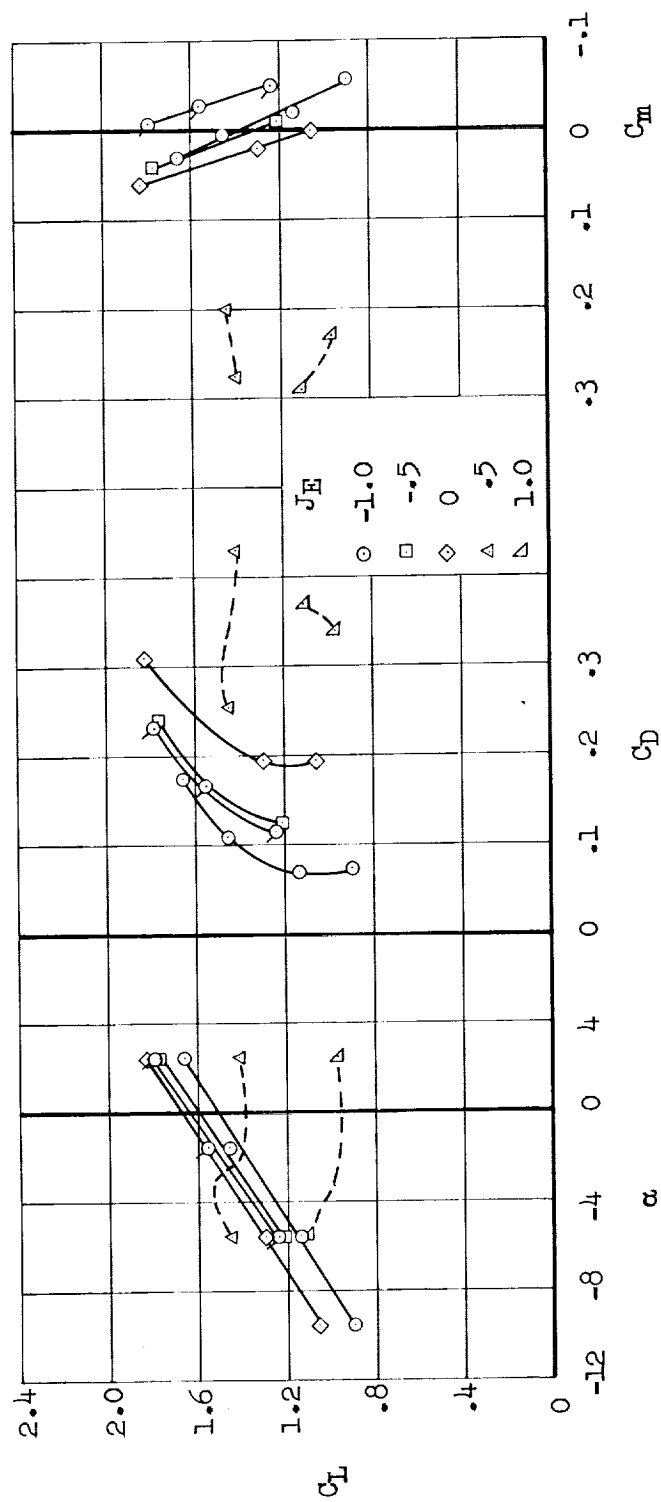
(b) $J_T = 0/0.5$; $C_J = 1.6$ - Concluded.

Figure 9.- Continued.
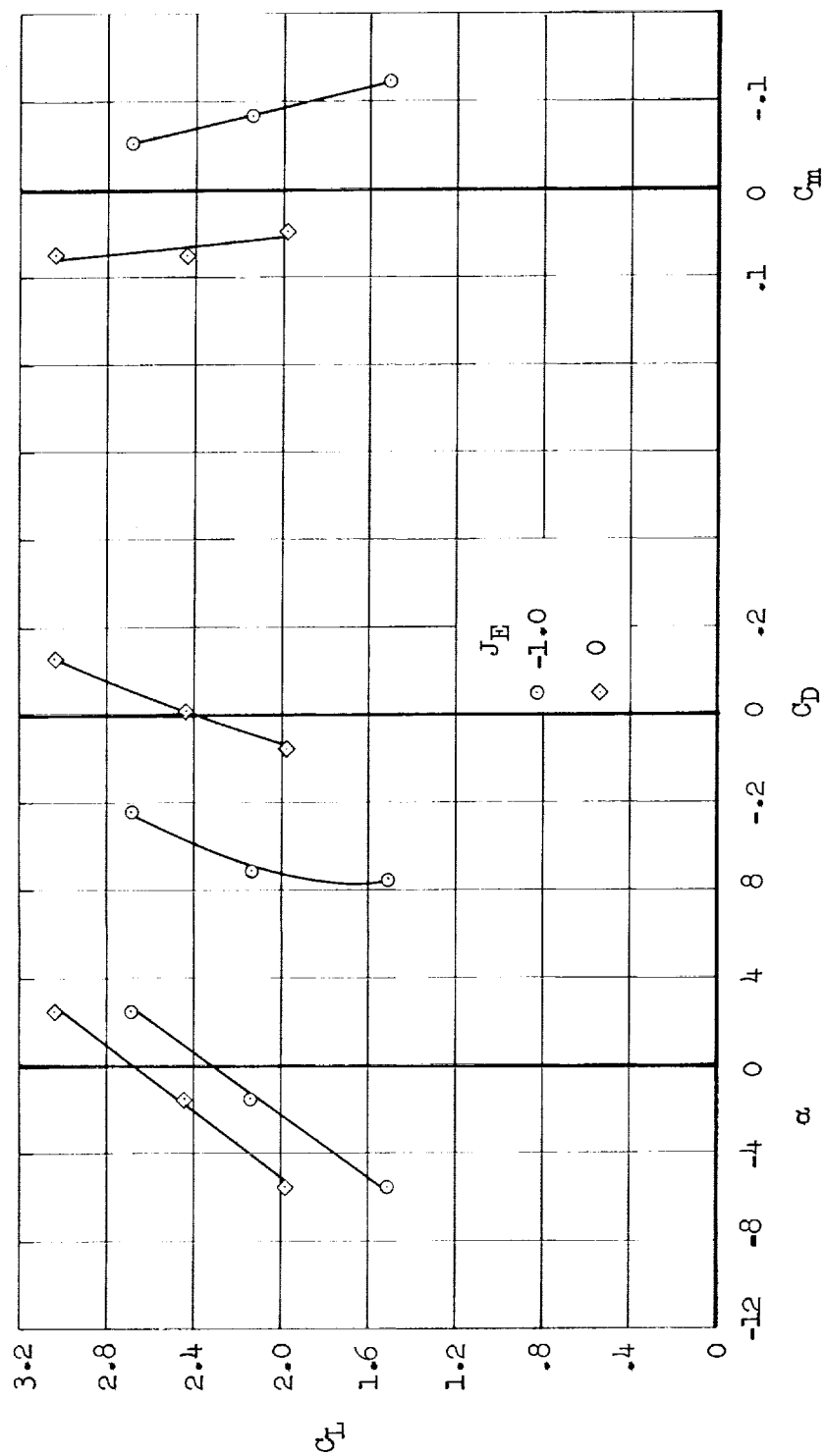
(c) $J_T = 0/0.75$; $C_J = 3.4$

Figure 9.- Continued.
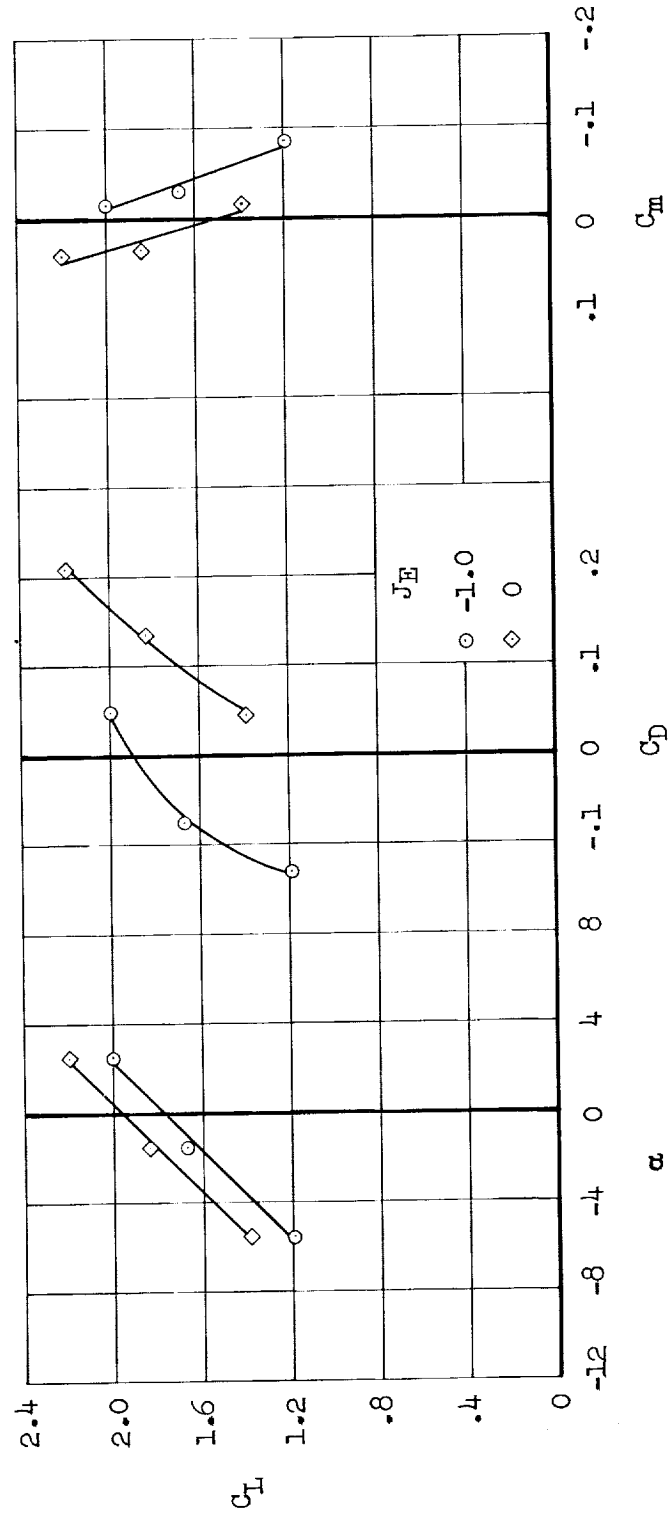
(c) $J_T = 0/0.75$; $C_J = 2.1$ - Concluded.

Figure 9.- Continued.
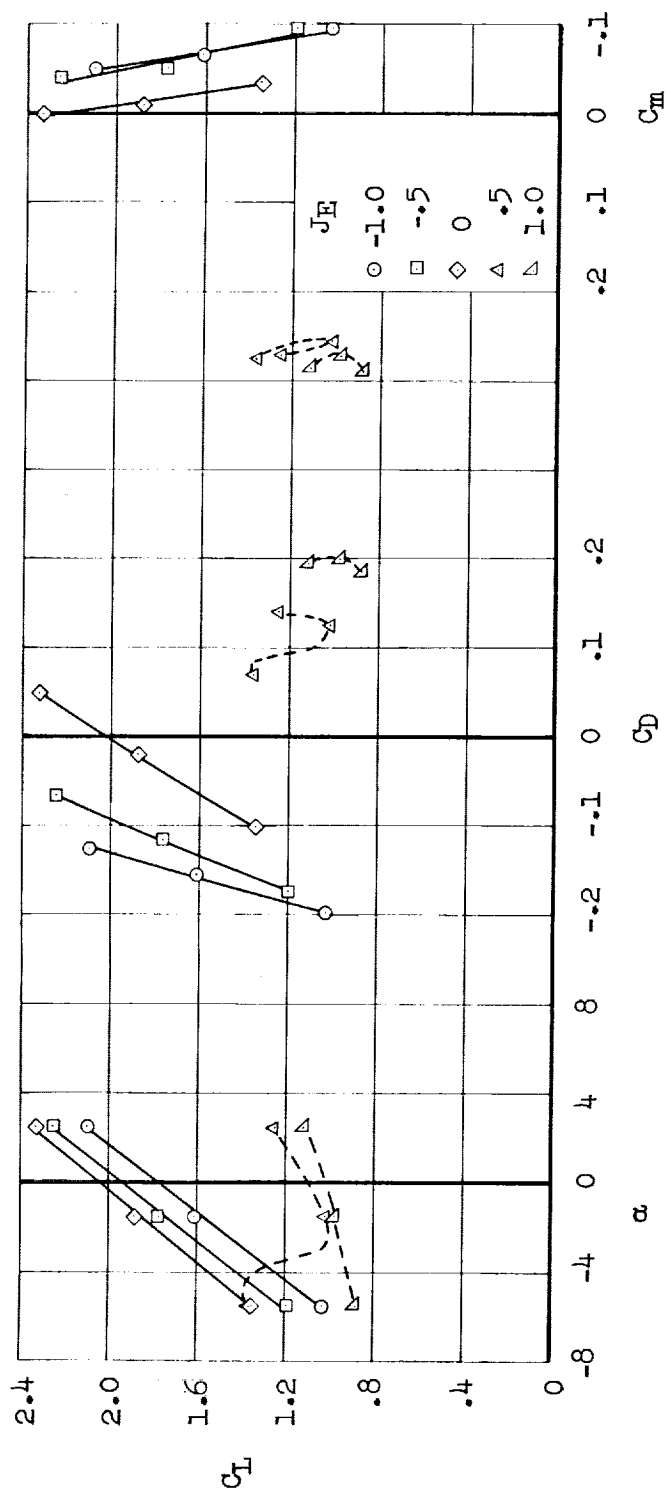
(d) $J_T = 0/1$; $C_J = 2.1$

Figure 9.- Continued.
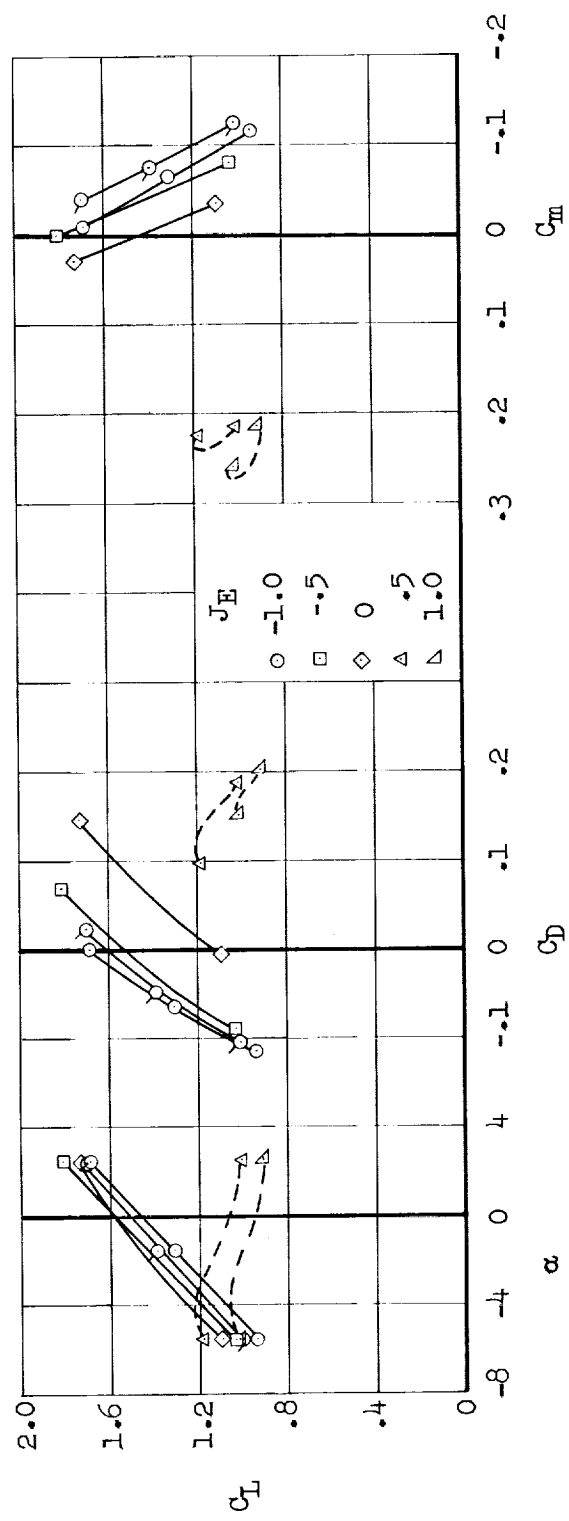
(d) $J_T = 0/1$; $C_J = 1.6$ - Continued.

Figure 9.- Continued.
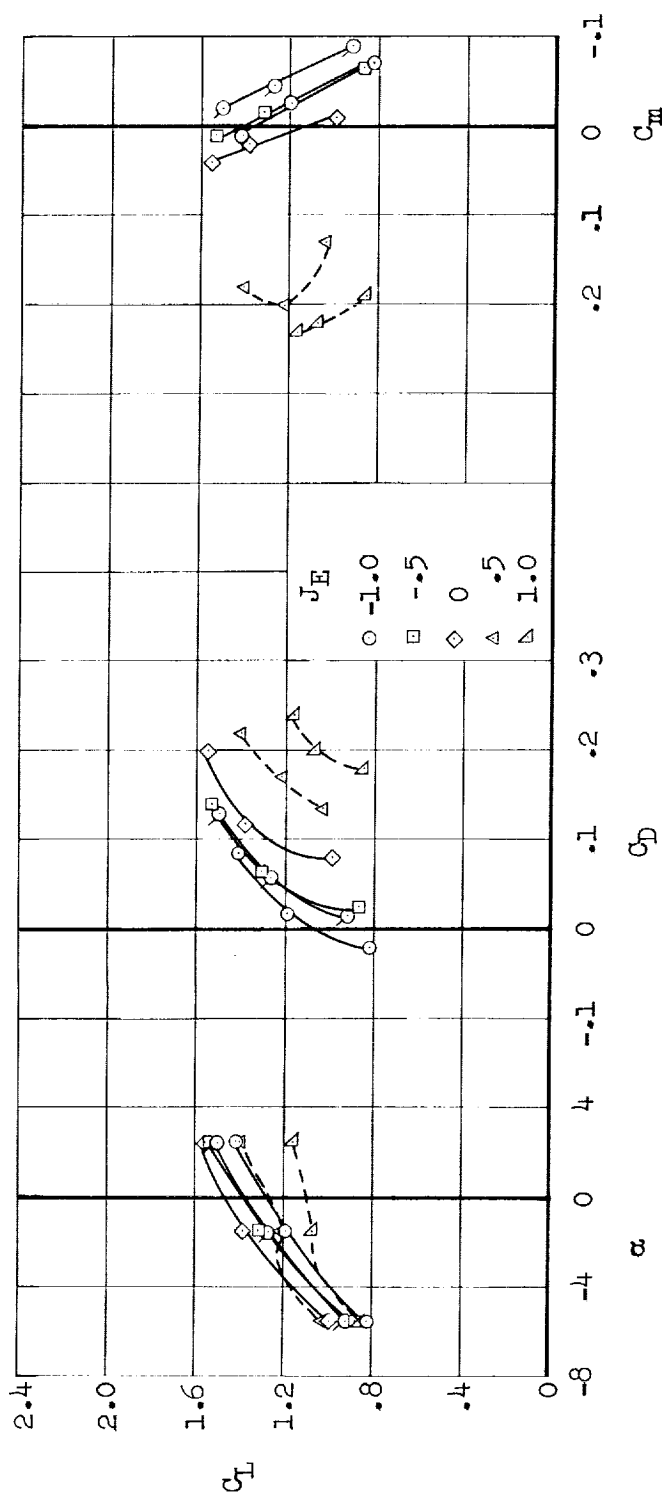
(a) $J_T = 0/1$; $c_J = 1.1$ - Concluded.

Figure 9.- Continued.
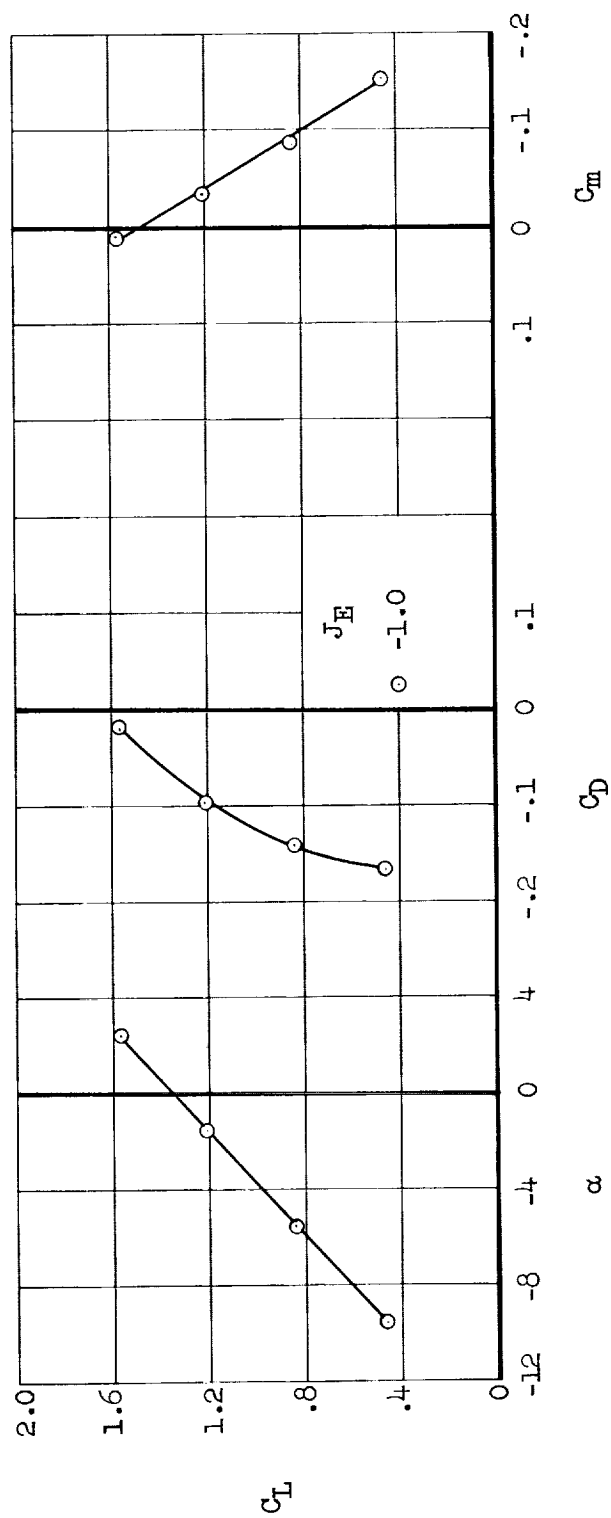
(e) $J_T = 0.25/1$; $C_J = 1.5$

Figure 9.- Continued.
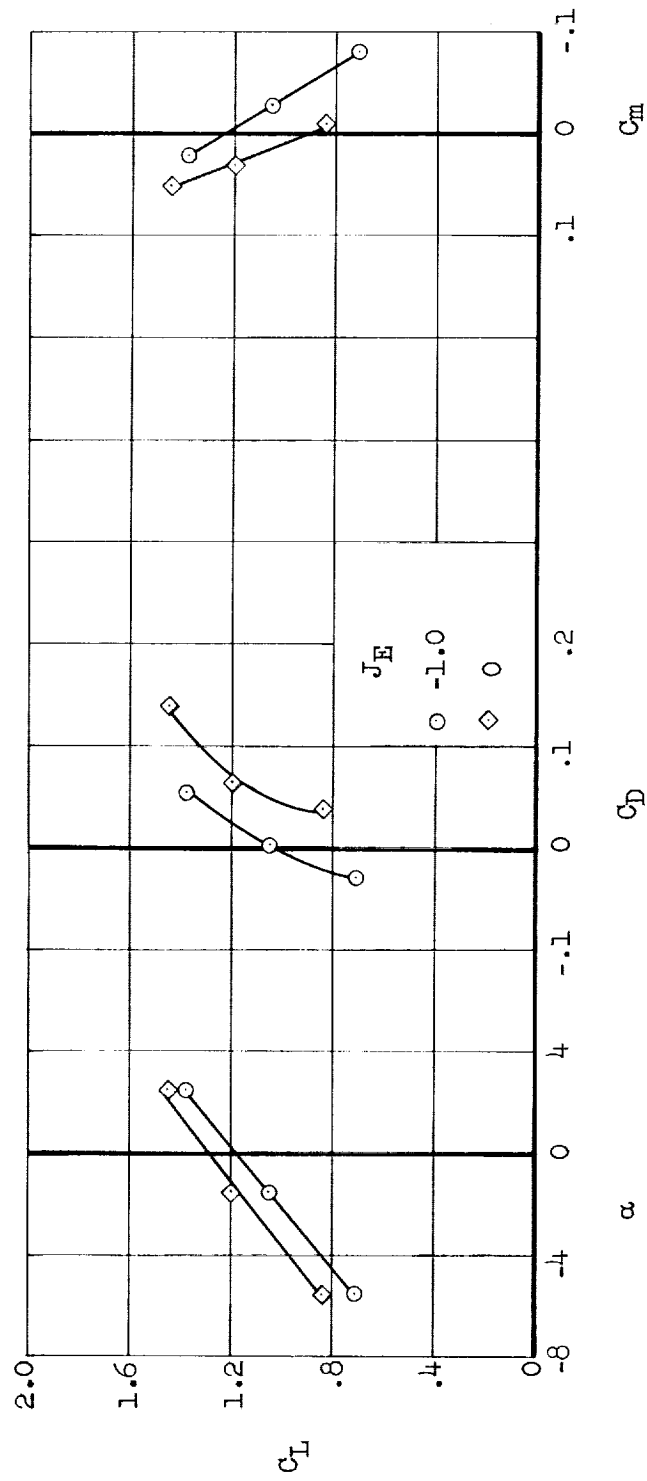
(e) $J_T = 0.25/1$; $C_J = 1.1$ - Continued.
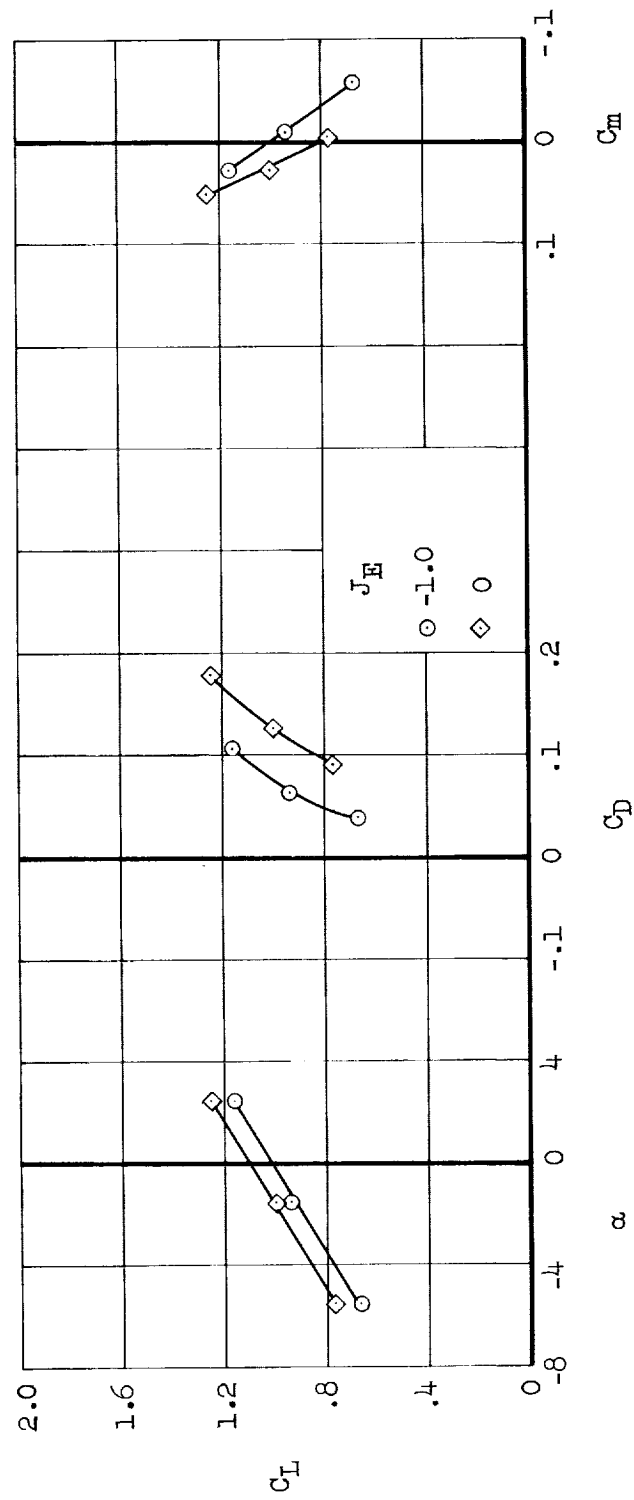
Figure 9.- Continued.

(e) $J_T = 0.25/1$; $C_J = 0.73$ - Concluded.
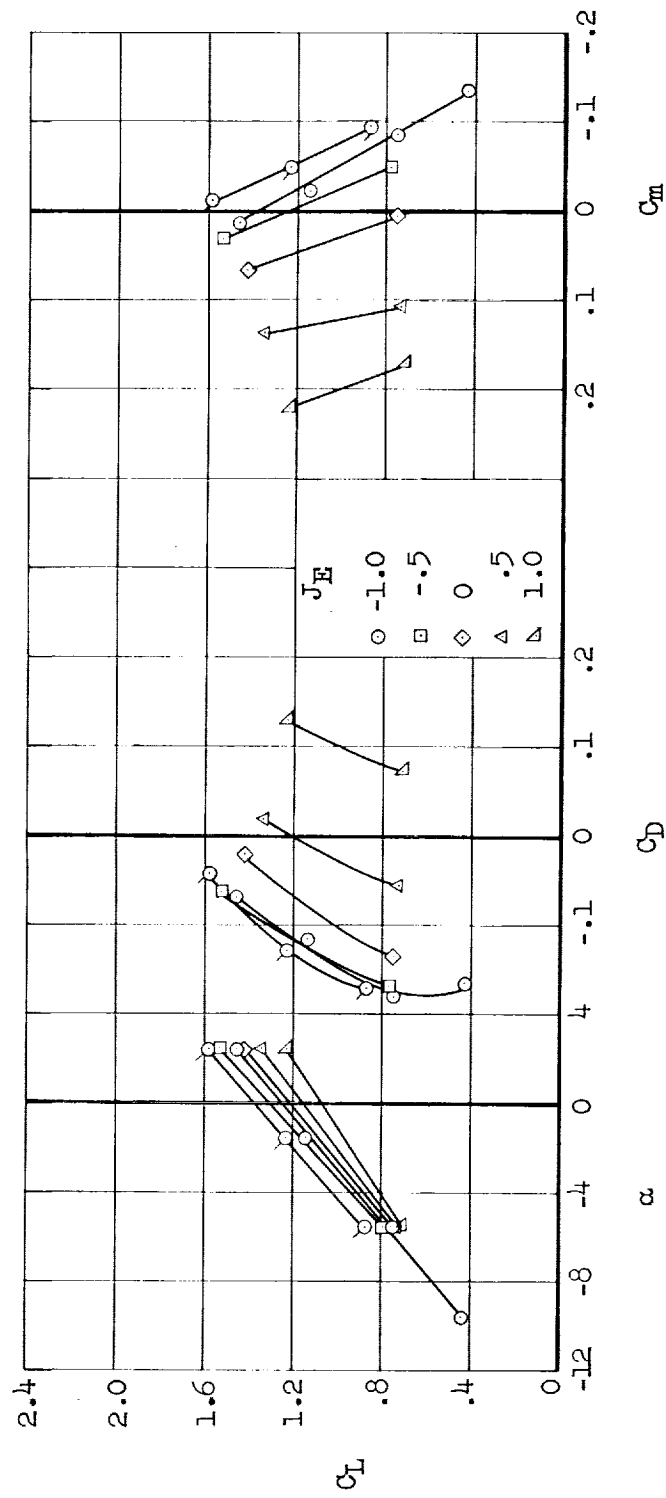
Figure 9.- Continued.

(f) $J_T = 0.5/1$; $C_J = 1.5$

Figure 9.- Continued.
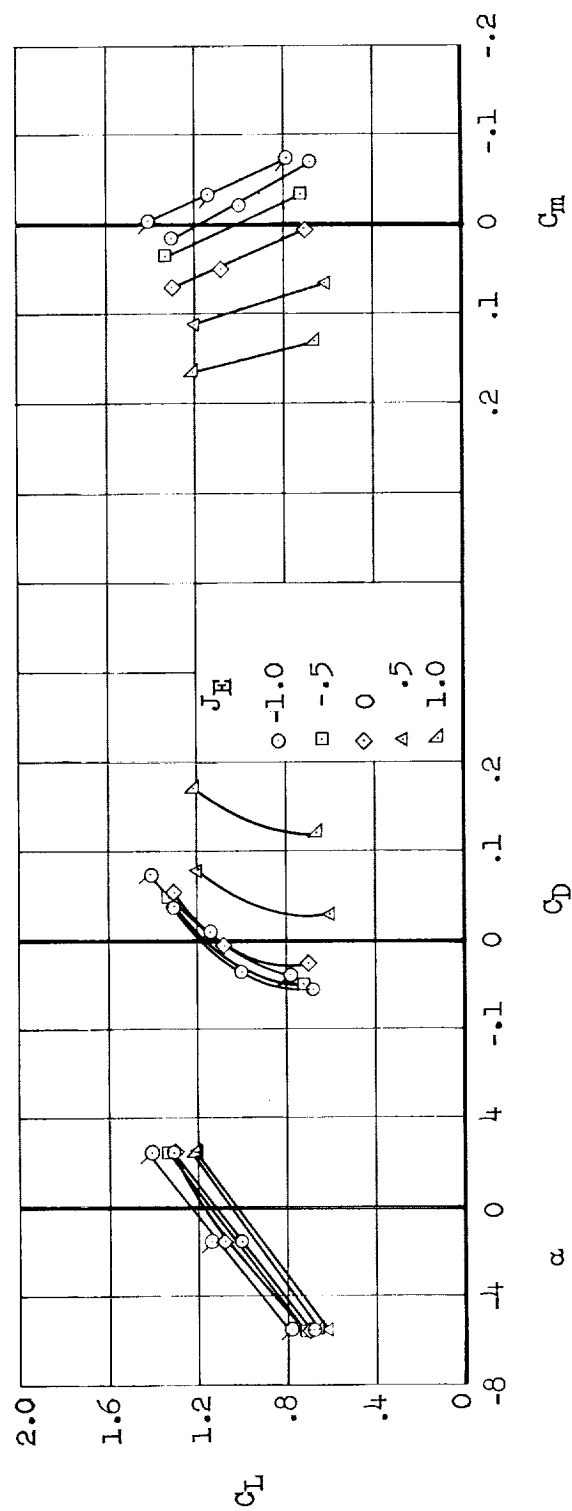
(f) $J_T = 0.5/1$; $C_J = 1.1$ - Continued.
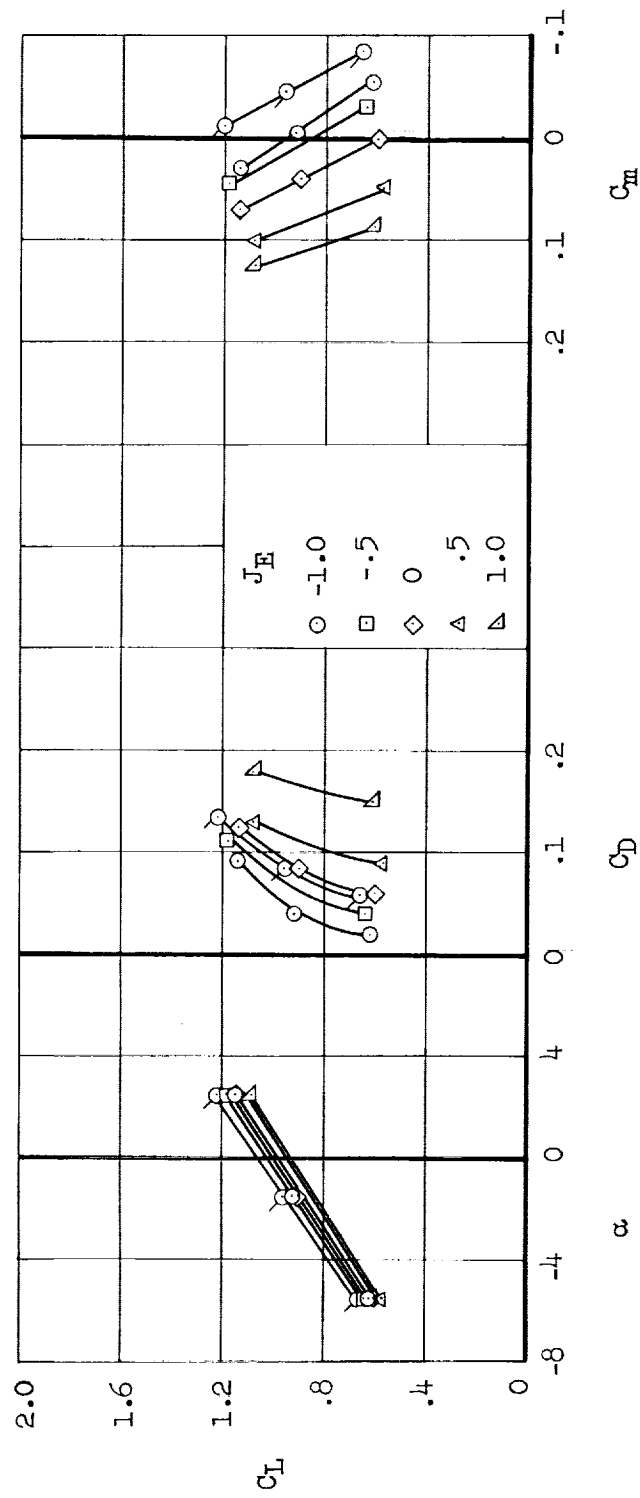
Figure 9.- Continued.

(f) $J_T = 0.5/1$; $C_J = 0.73$ - Concluded.
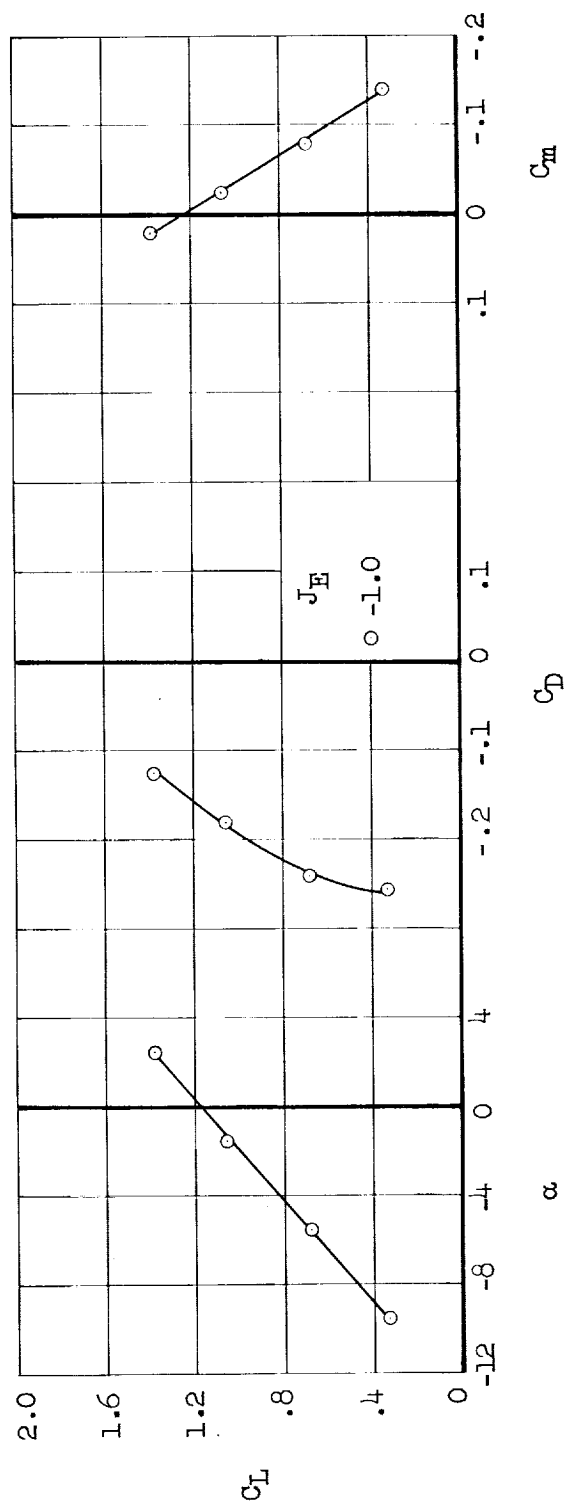
Figure 9.- Continued.

(g) $J_T = 0.75/1$; $C_J = 1.5$

Figure 9.- Continued.
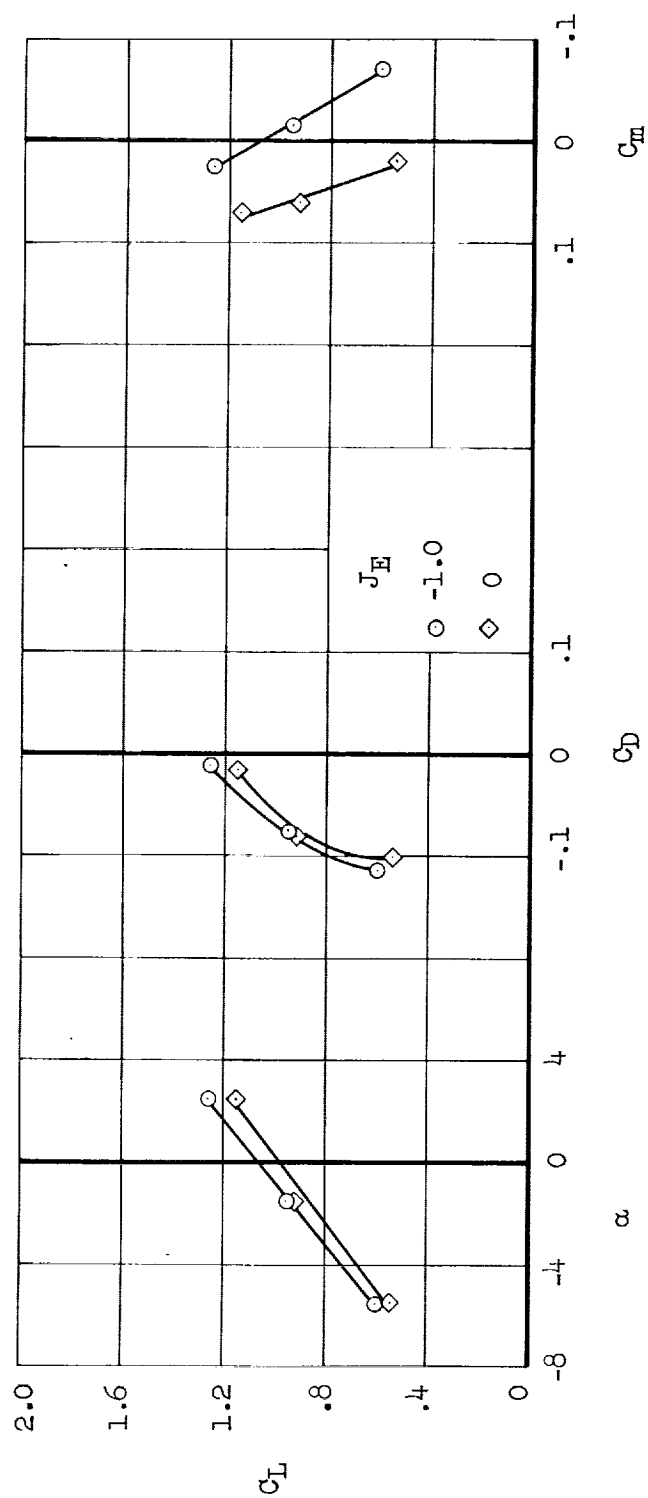
(g) $J_T = 0.75/1$; $C_J = 1.1$ - Continued.
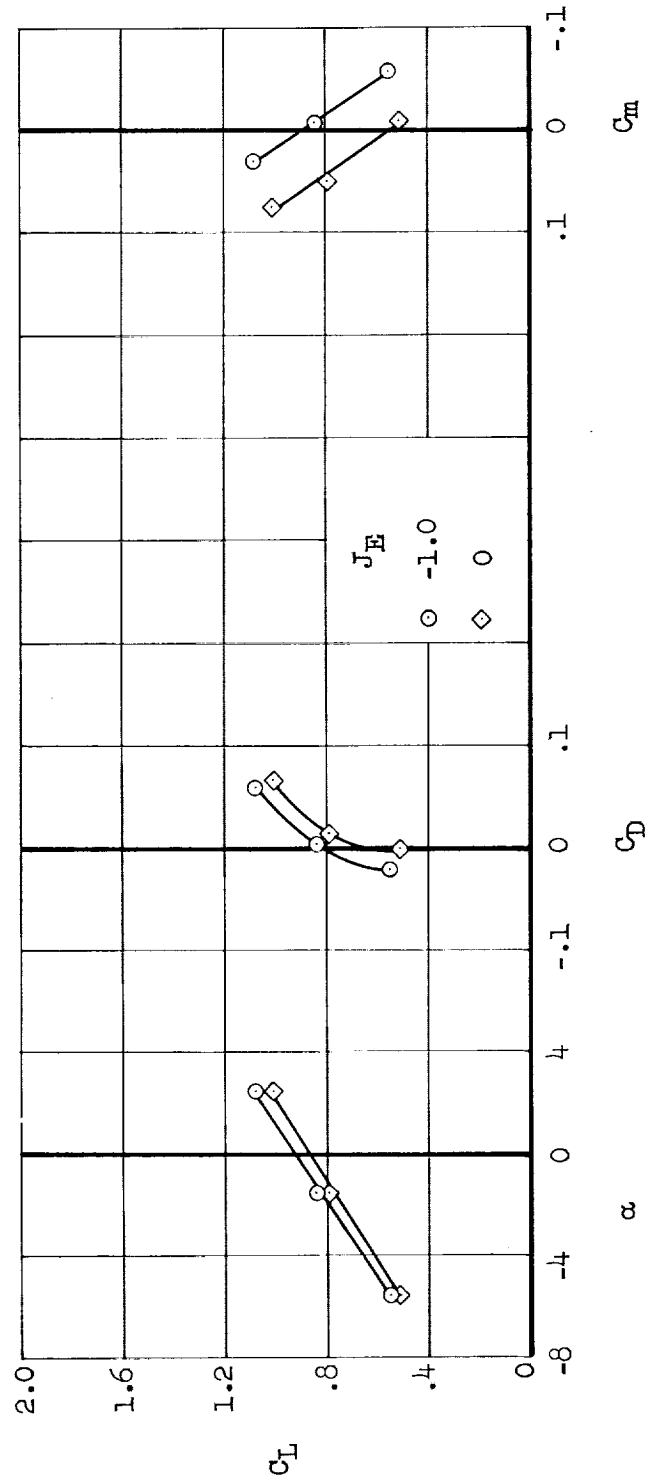
Figure 9.- Continued.

(g) $J_T = 0.75/1$; $C_J = 0.73$ - Concluded.

Figure 9.- Concluded.
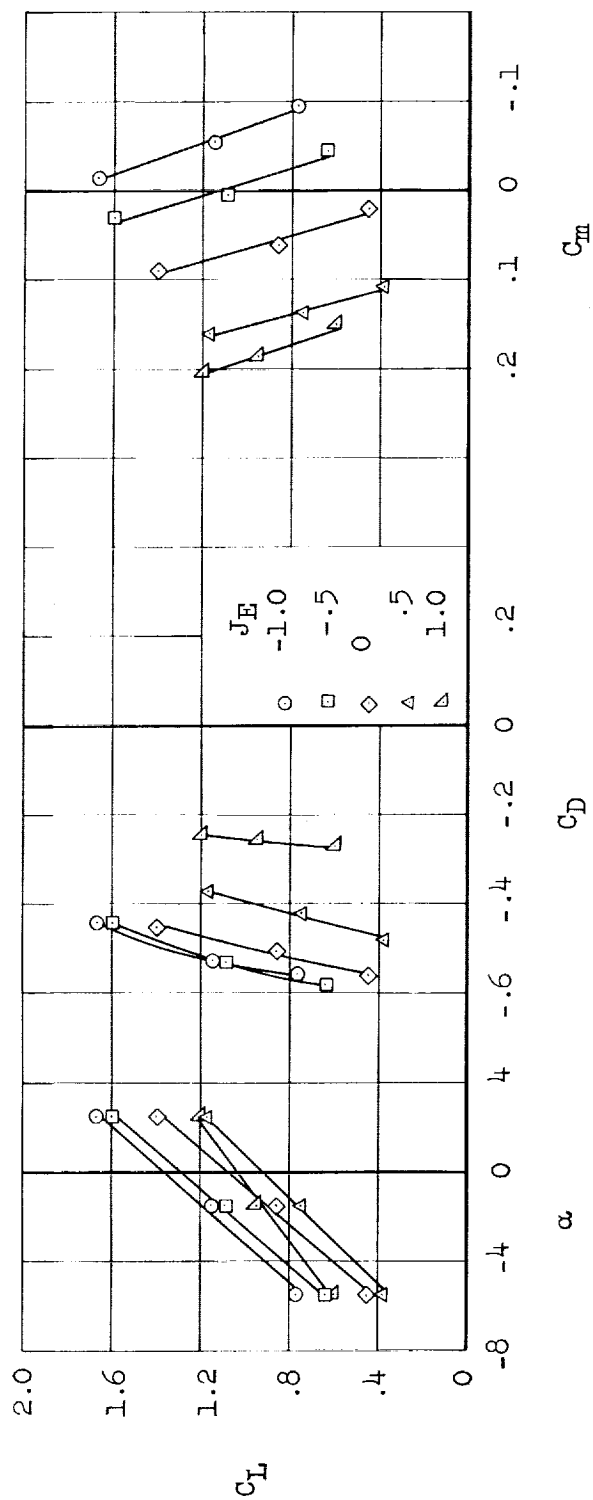
(a) $h/D = 0.15$; $C_J = 2.1$

Figure 10.- Longitudinal characteristics of the cruise flight configuration ($J_T = 1/1$) at various ground heights. Flagged symbols are for tail on, with $i_T = 26°$.
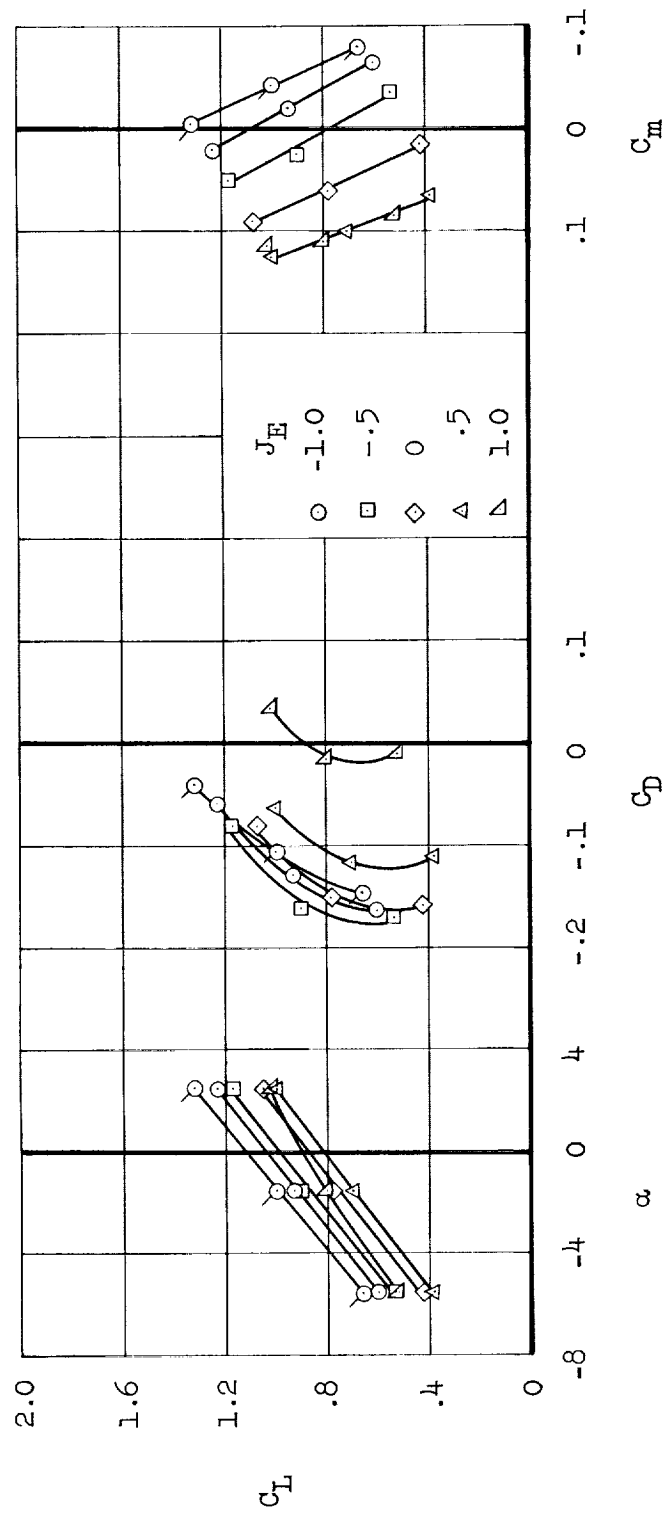
(a) h/D = 0.15; C_J = 1.1 - Continued.

Figure 10.- Continued.
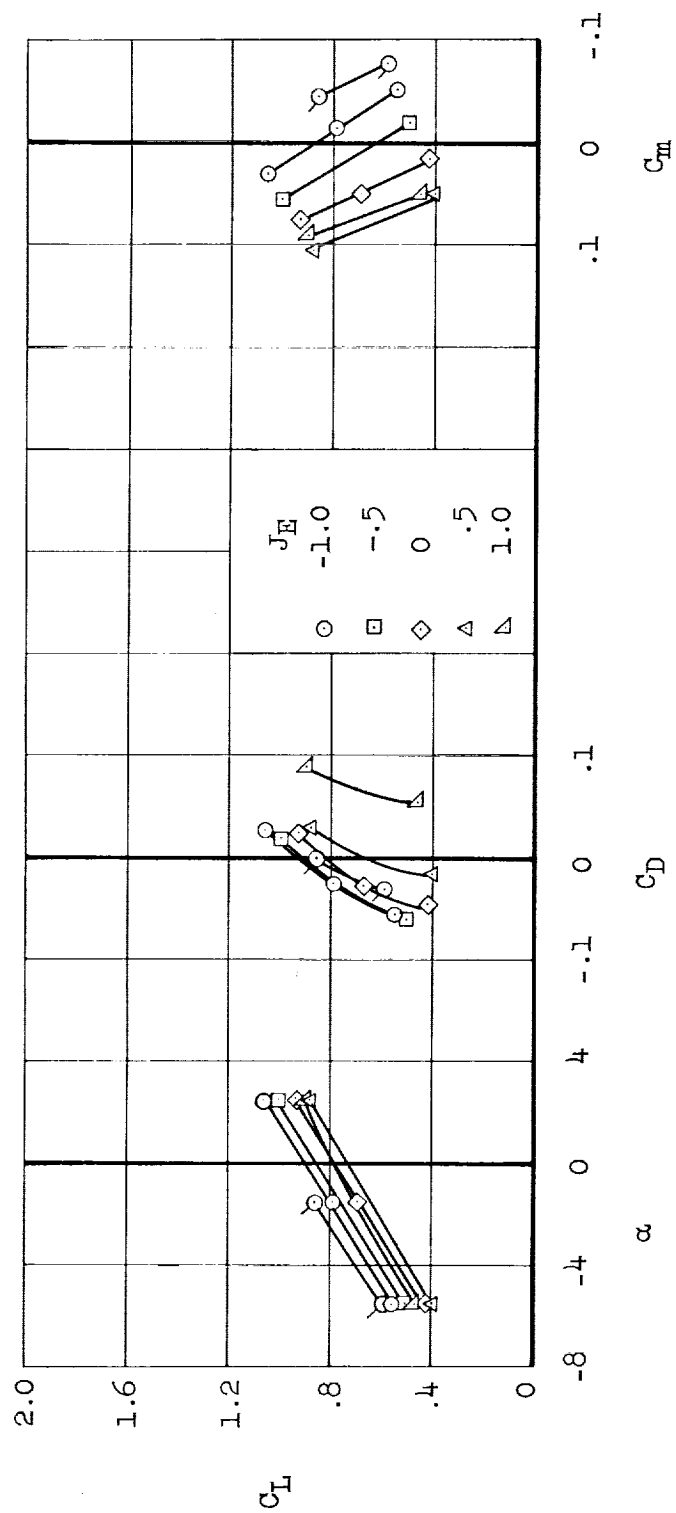
(a) h/D = 0.15; C_J = 0.73 - Concluded.

Figure 10.- Continued.
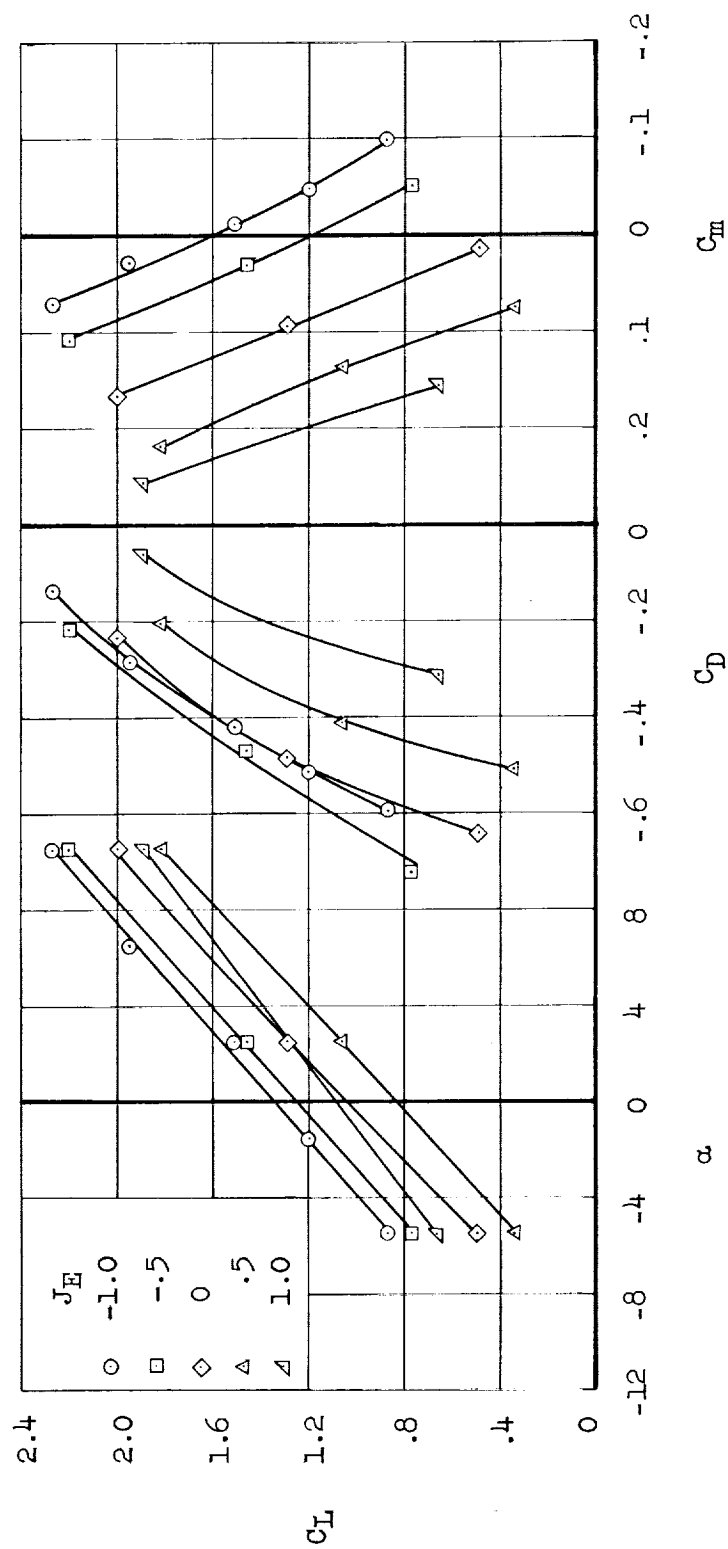
(b) $h/D = 0.21$; $C_J = 2.2$

Figure 10.- Continued.

58
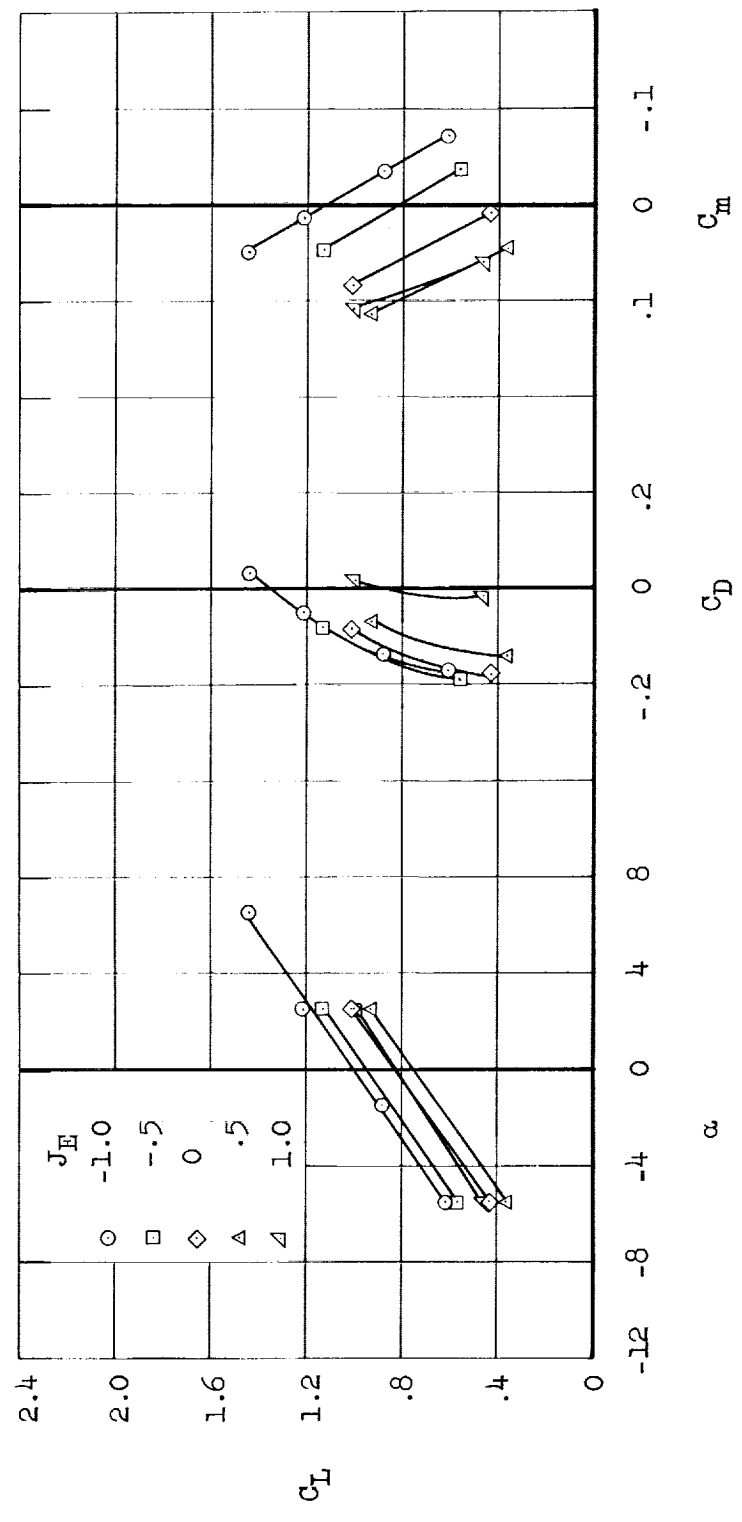
(b) h/D = 0.21; C_J = 1.1 - Continued.

Figure 10.- Continued.
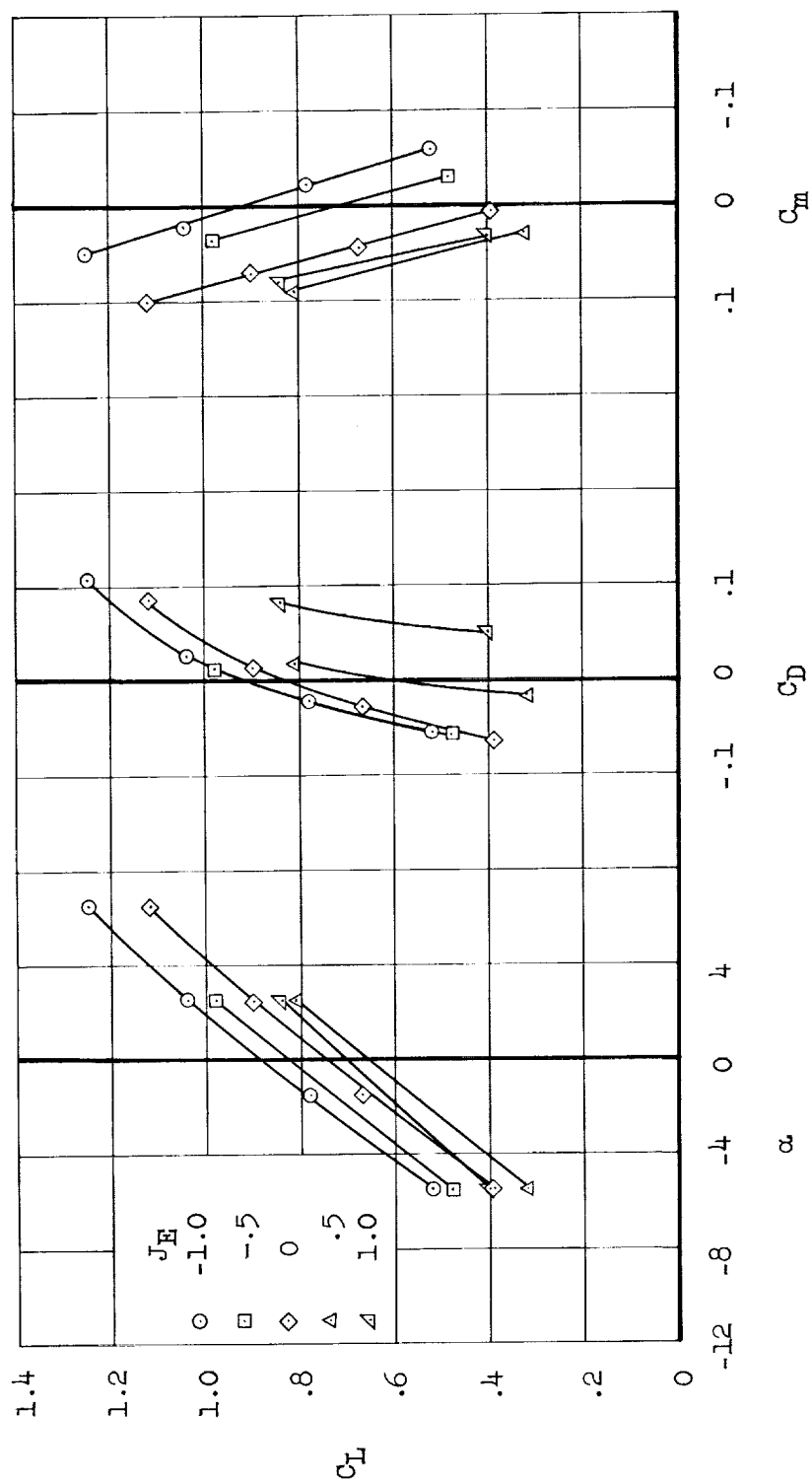
(b) h/D = 0.21; C_J = 0.76 - Concluded.

Figure 10.- Continued.
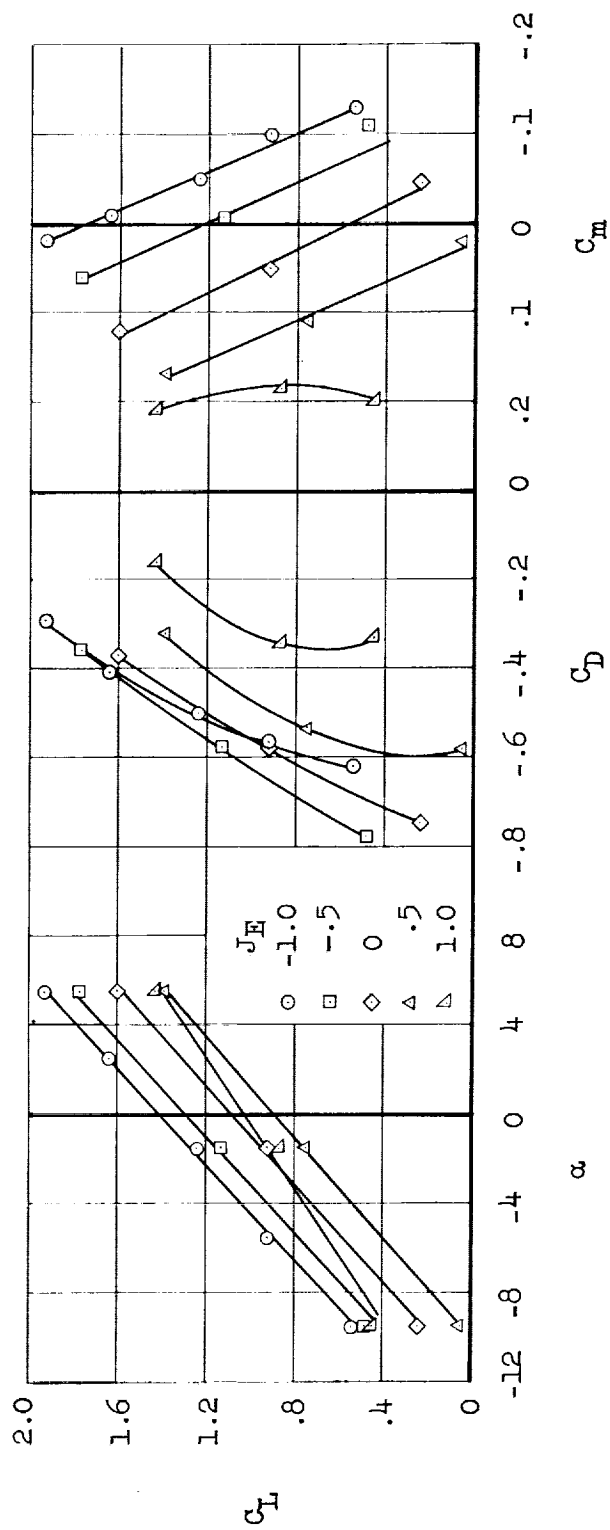
(c) h/D = 0.28; C_J = 2.2

Figure 10.- Continued.
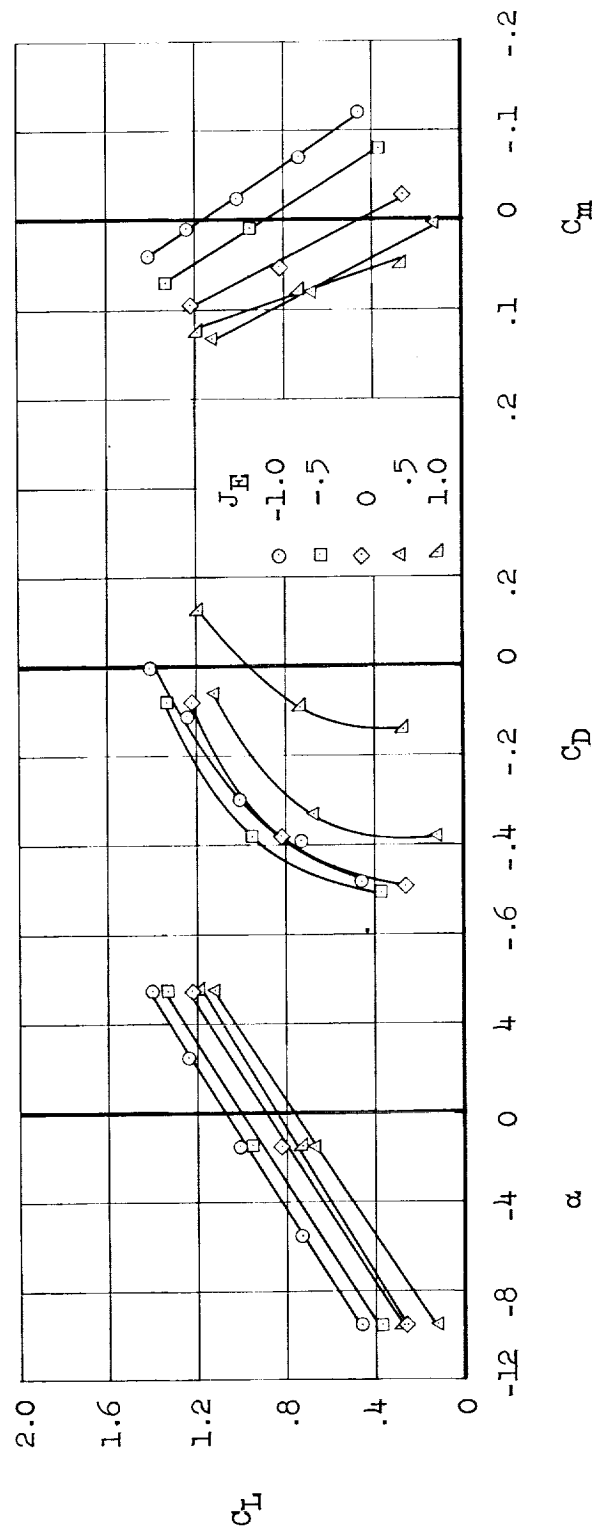
(c) h/D = 0.28; C_J = 1.1 - Concluded.

Figure 10.- Concluded.
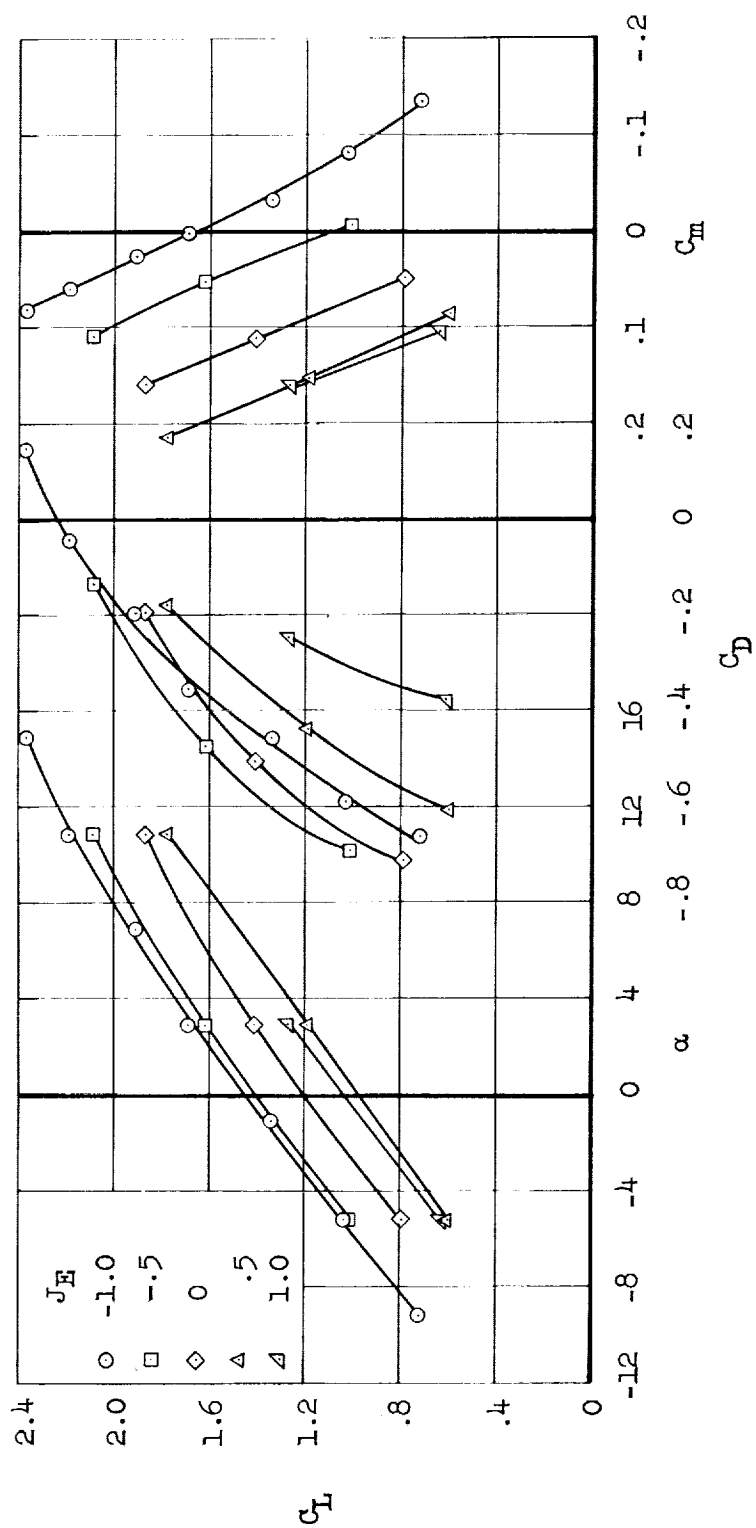
(a) Tail off; $C_J = 2.2$.

Figure 11.- Longitudinal characteristics of the cruise flight configuration ($J_T = 1/1$) at $h/D = 0.70$.
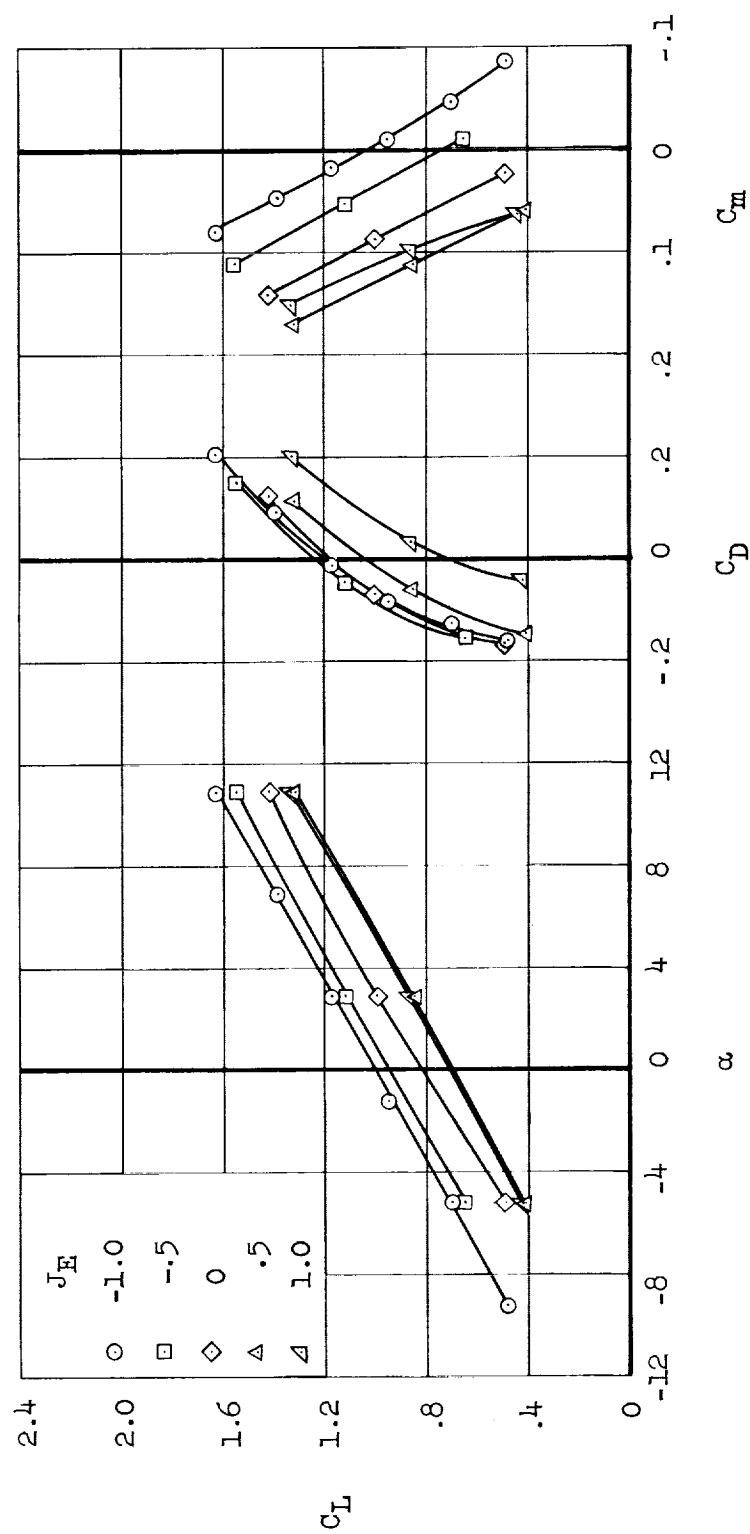
(a) Tail off; $C_J = 1.1$ - Continued.

Figure 11.- Continued.
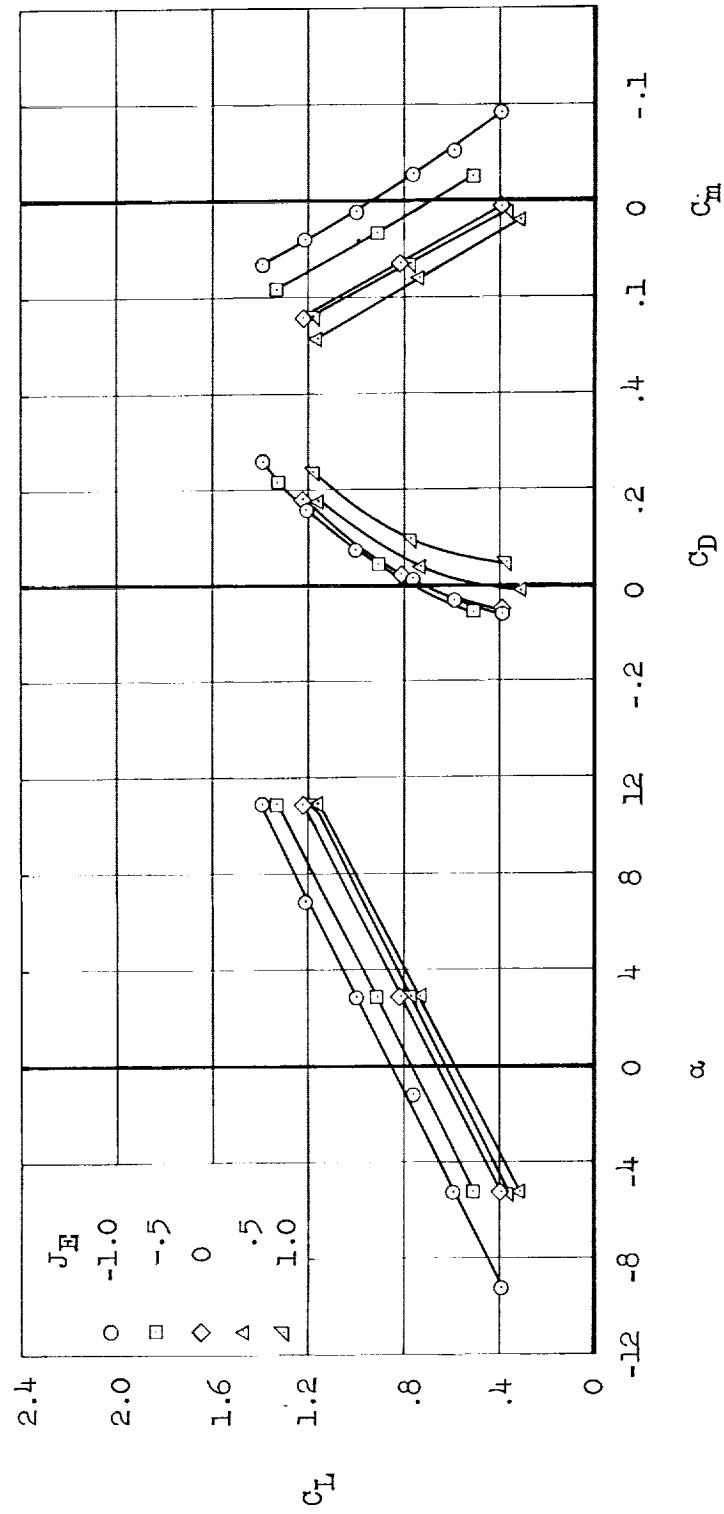
(a) Tail off; $C_J = 0.76$ - Continued.

Figure 11.- Continued.
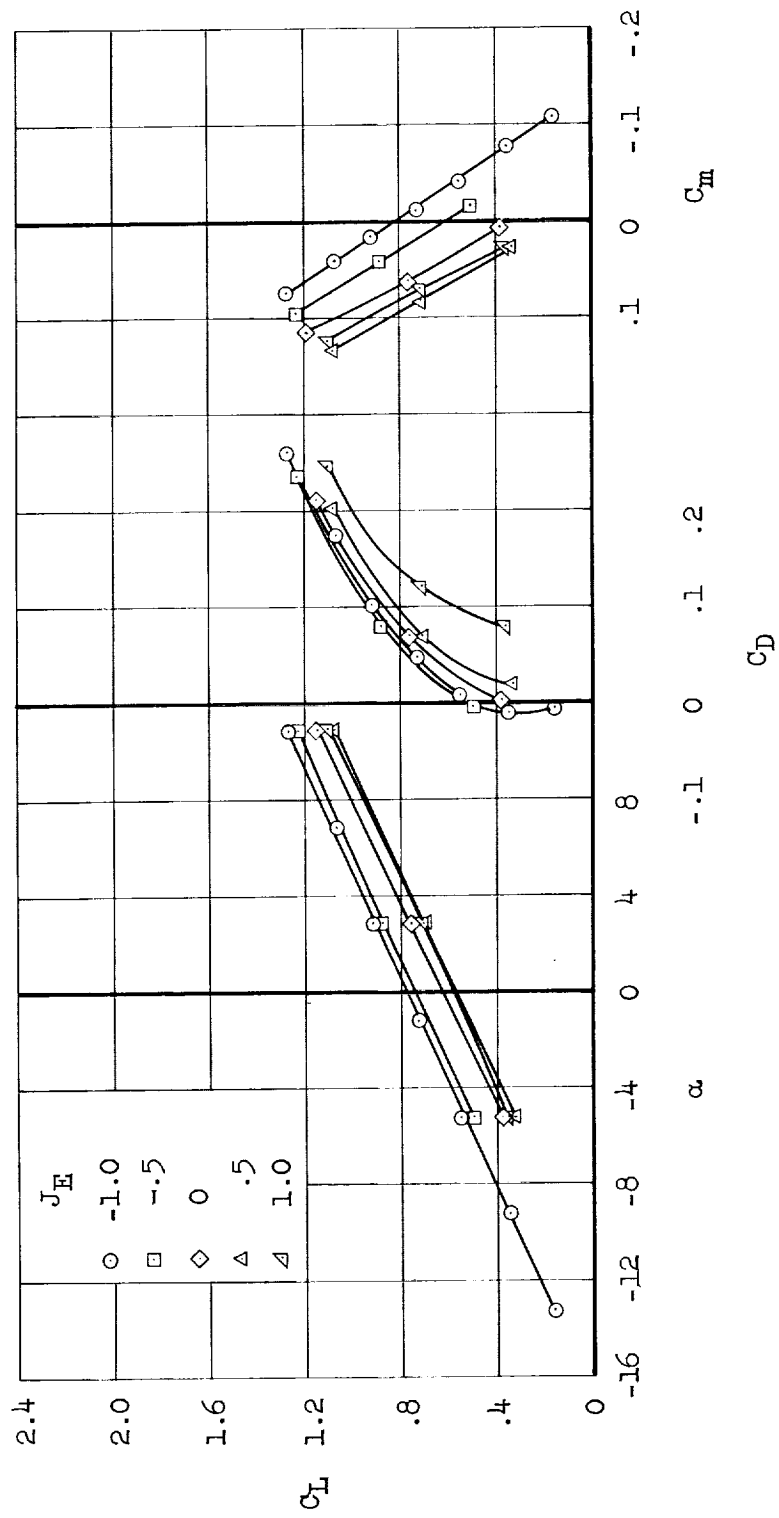
(a) Tail off; $C_J = 0.63$ - Continued.
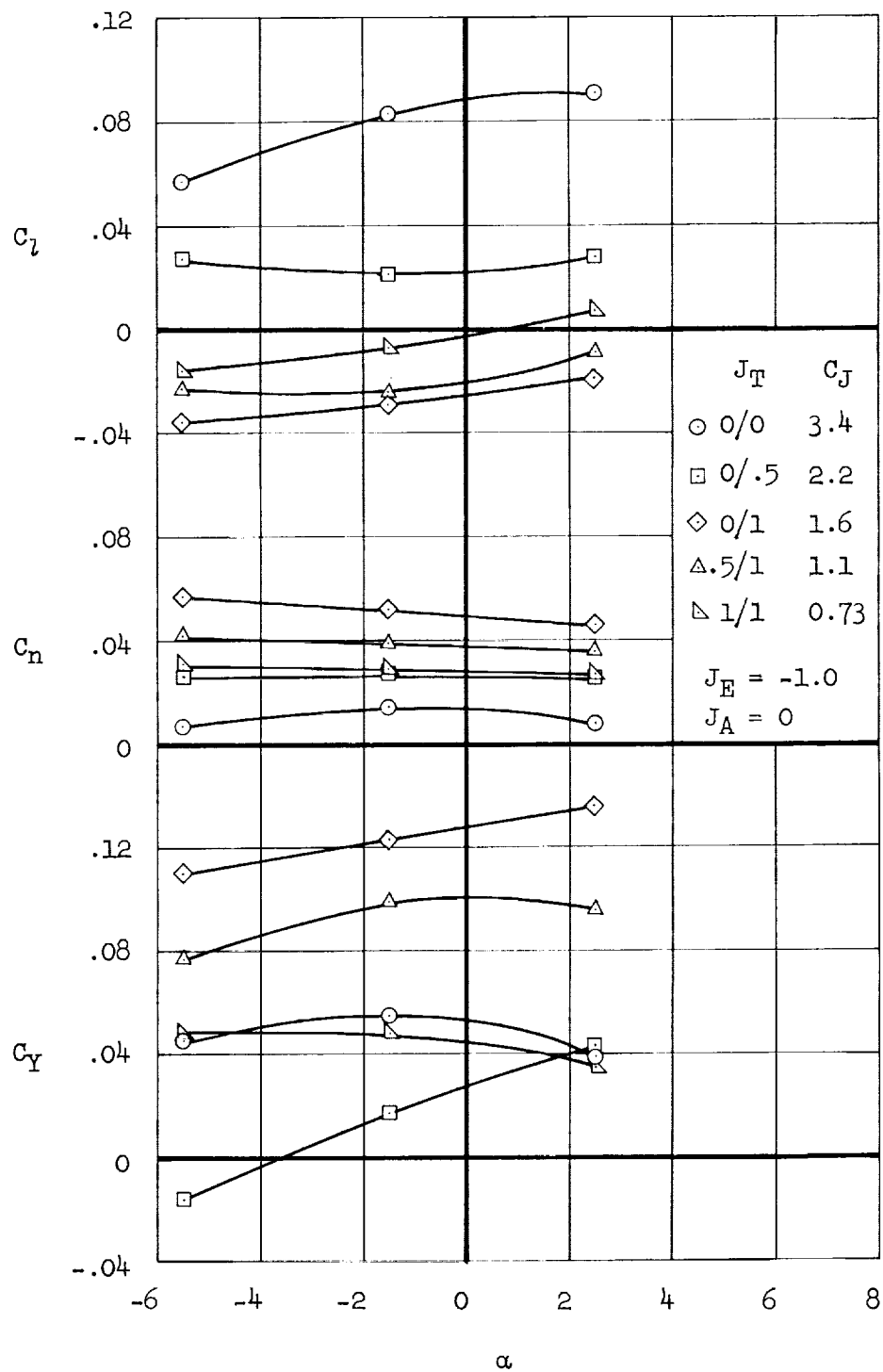
Figure 11.- Continued.

66
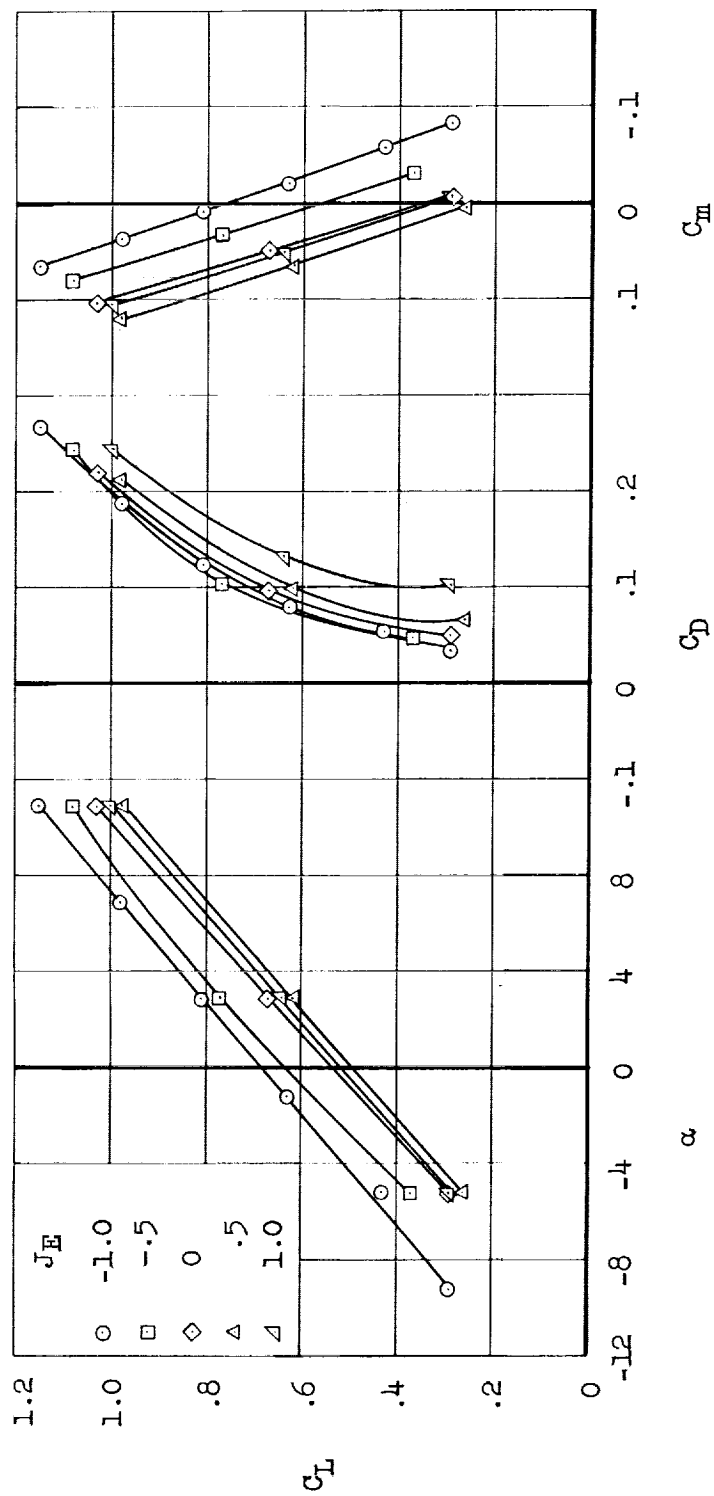
(a) Tail off; $C_J = 0.45$ - Concluded.

Figure 11.- Continued.
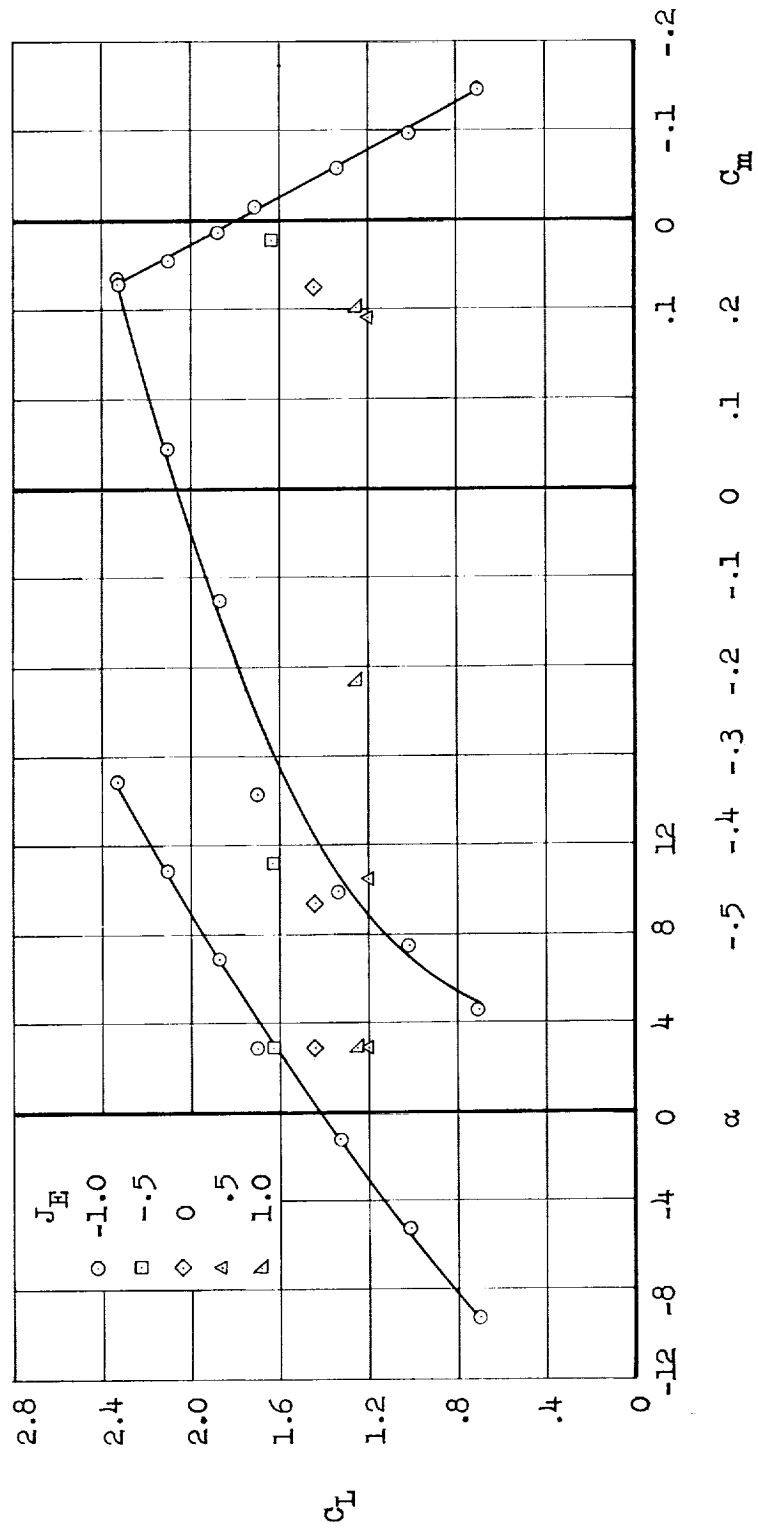
(b) Tail on, with $i_T = 26^{\circ}$; $C_J = 2.2$.

Figure 11.- Continued.
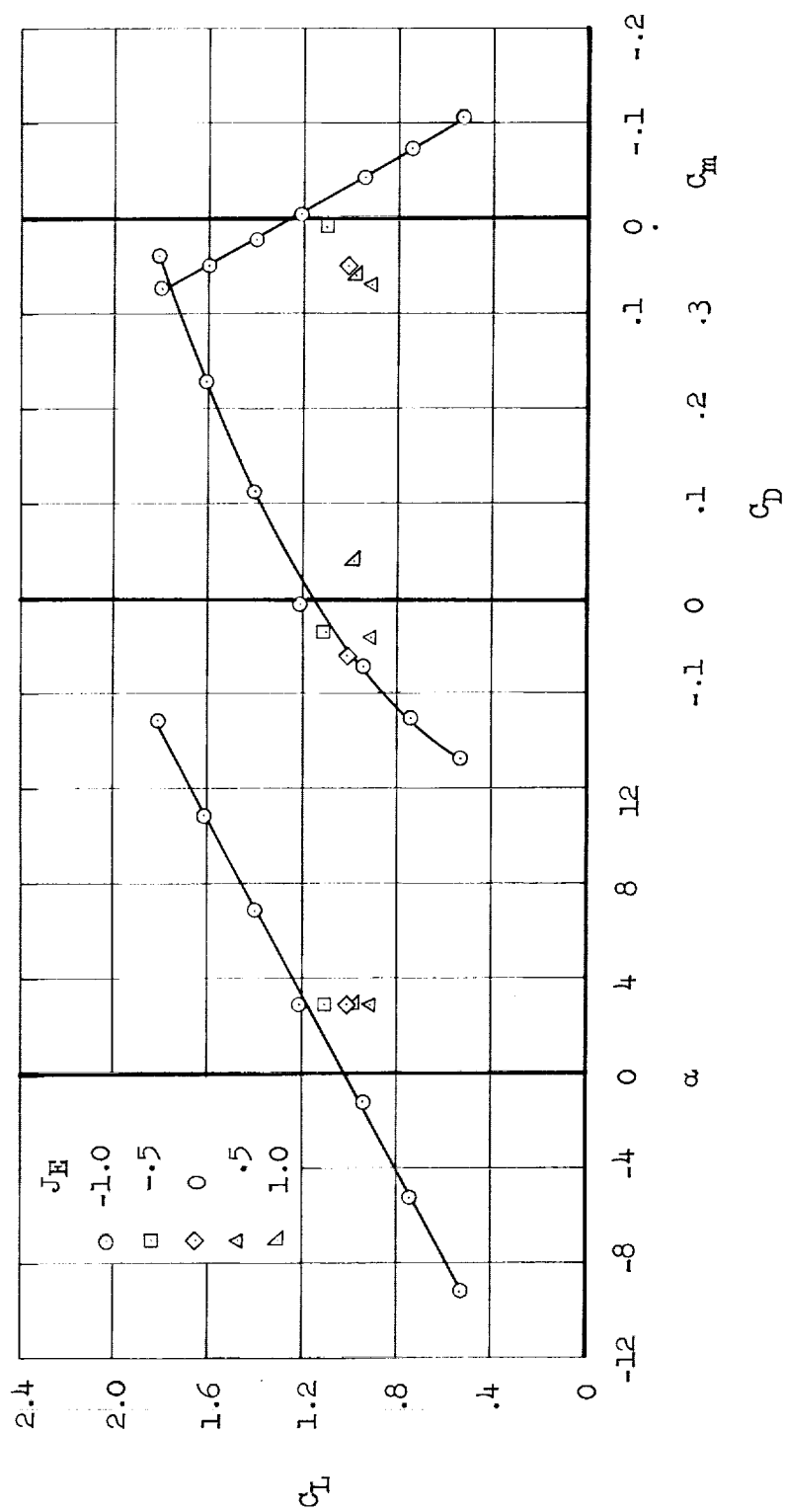
(b) Tail on, with $i_T = 26°$; $C_J = 1.1'$ - Continued.

Figure 11.- Continued.
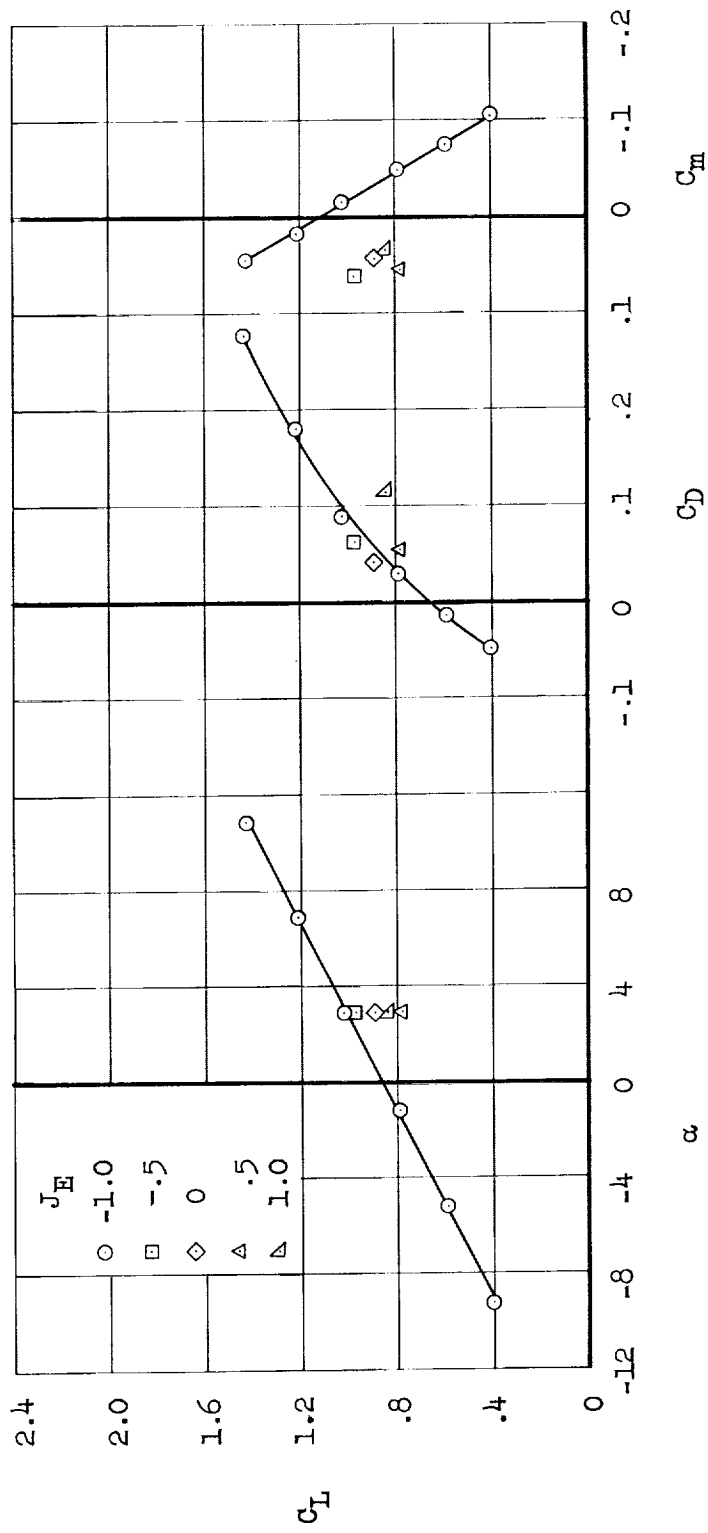
(b) Tail on, with $i_T = 26°$; $C_J = 0.75$ - Continued.

Figure 11.- Continued.
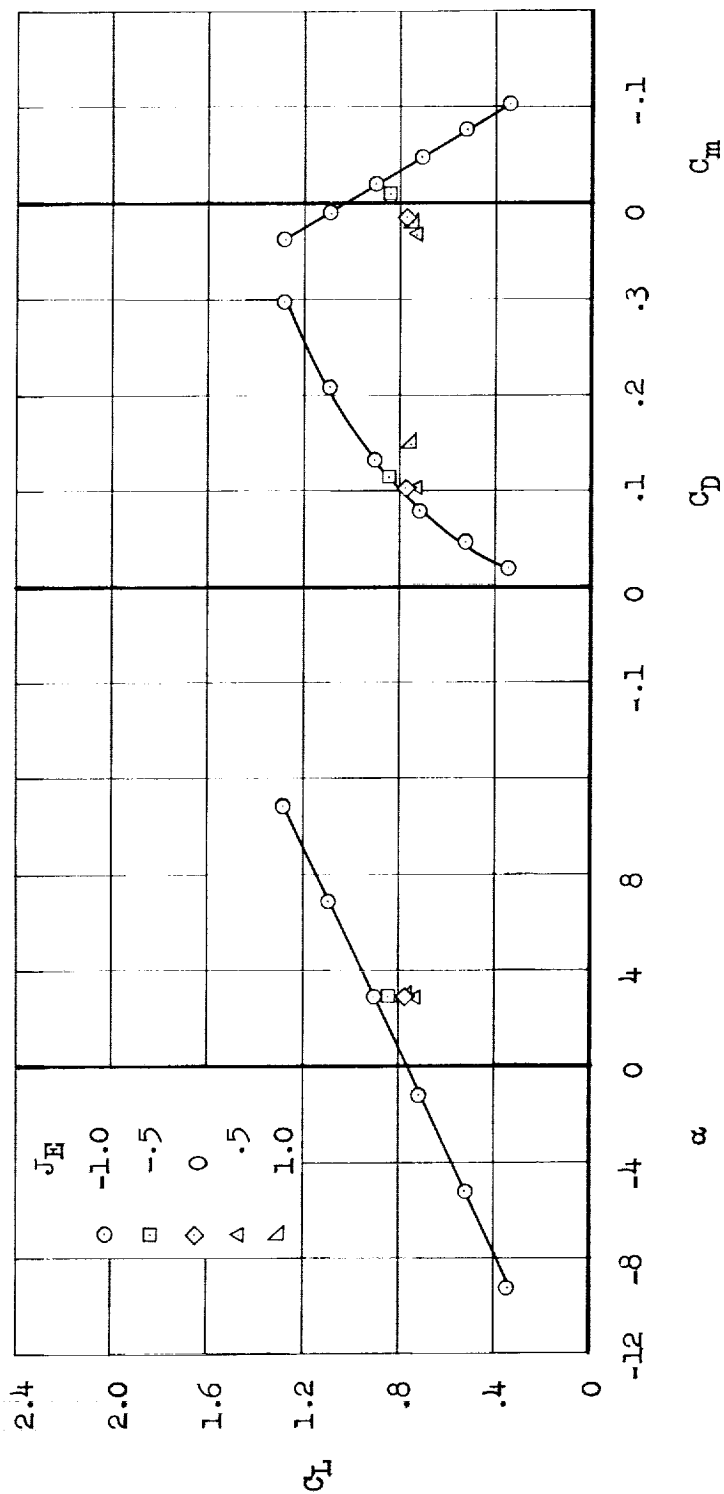
(b) Tail on, with $i_T = 26°$; $C_J = 0.56$ - Continued.

Figure 11.- Continued.
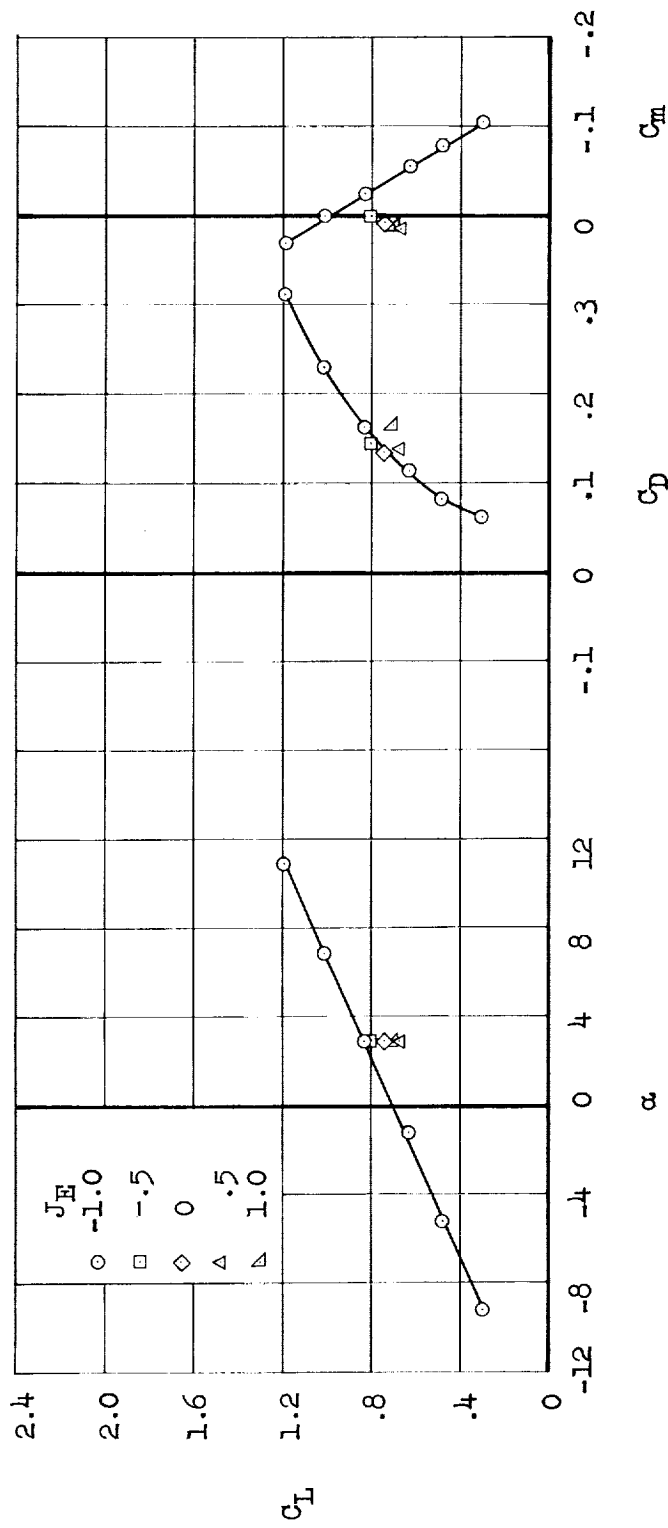
(b) Tail on, with $i_T = 26^\circ$; $C_J = 0.45$ - Concluded.

Figure 11.- Concluded.
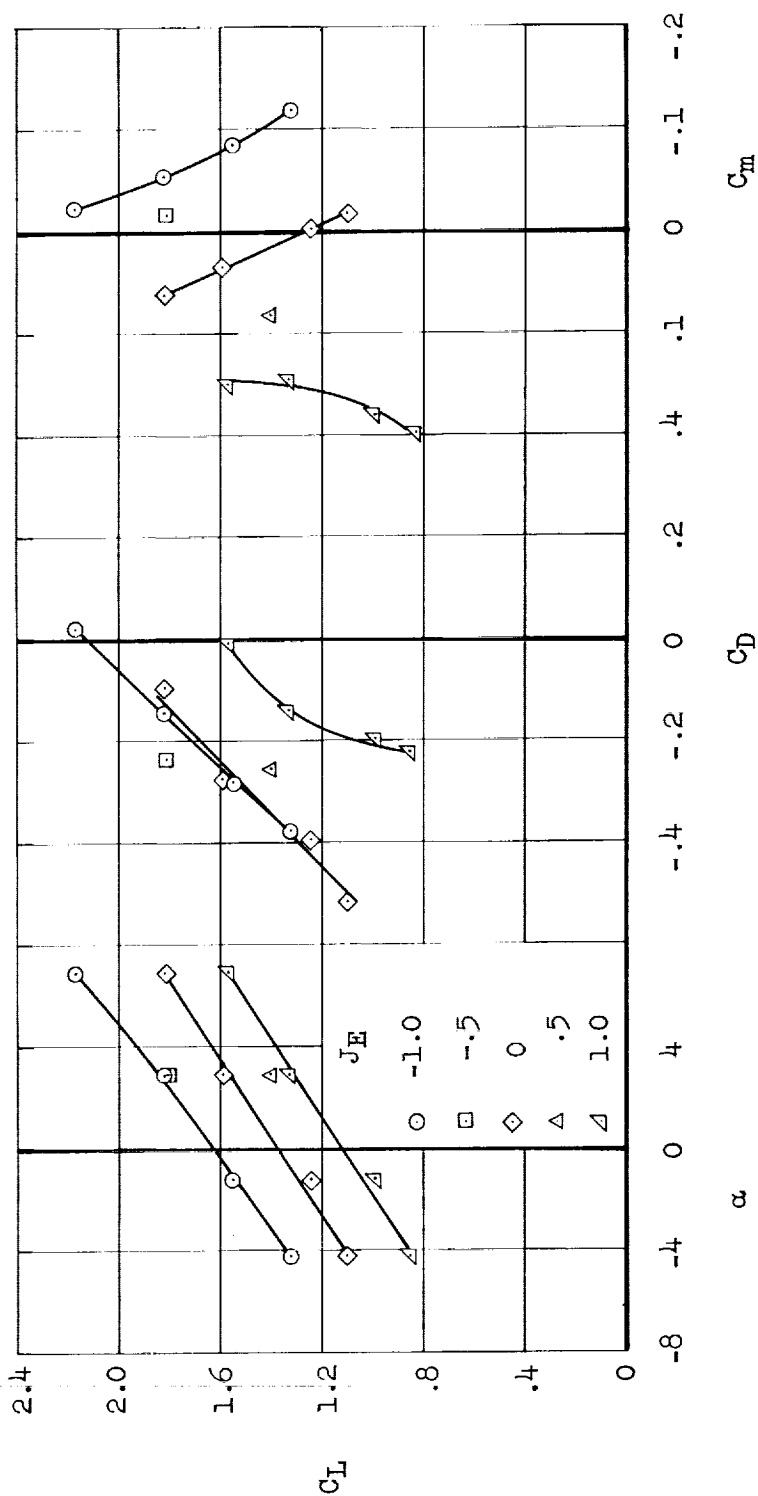
(a) $C_J = 2.2$

Figure 12.- Longitudinal characteristics of the cruise flight configuration ($J_T = 1/1$) at
$h/D = 0.70$, with flaps on the control vanes; tail off.
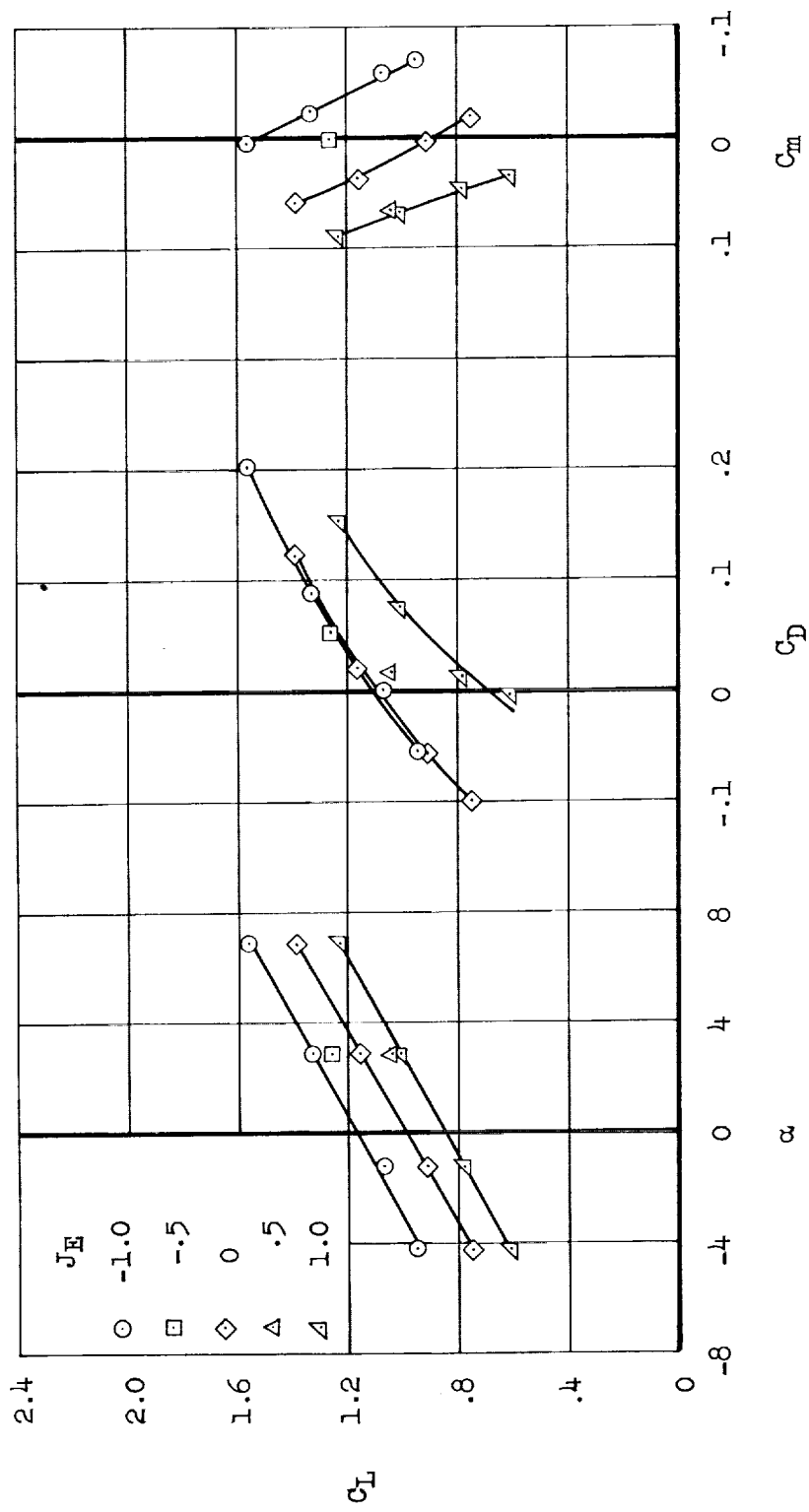
(b) $C_J = 1.1$

Figure 12.- Continued.
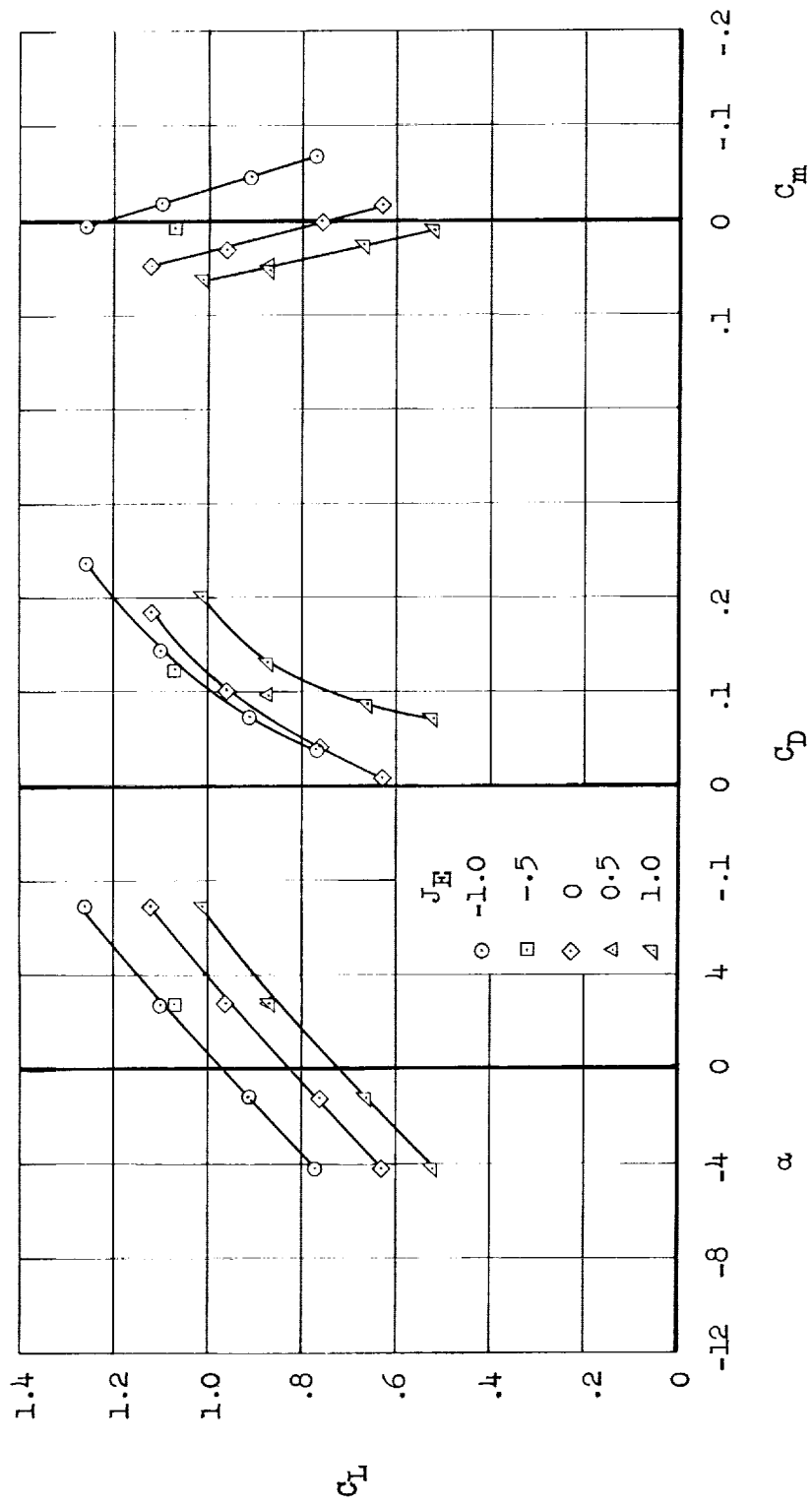
(c) $C_J = 0.76$

Figure 12.- Concluded.
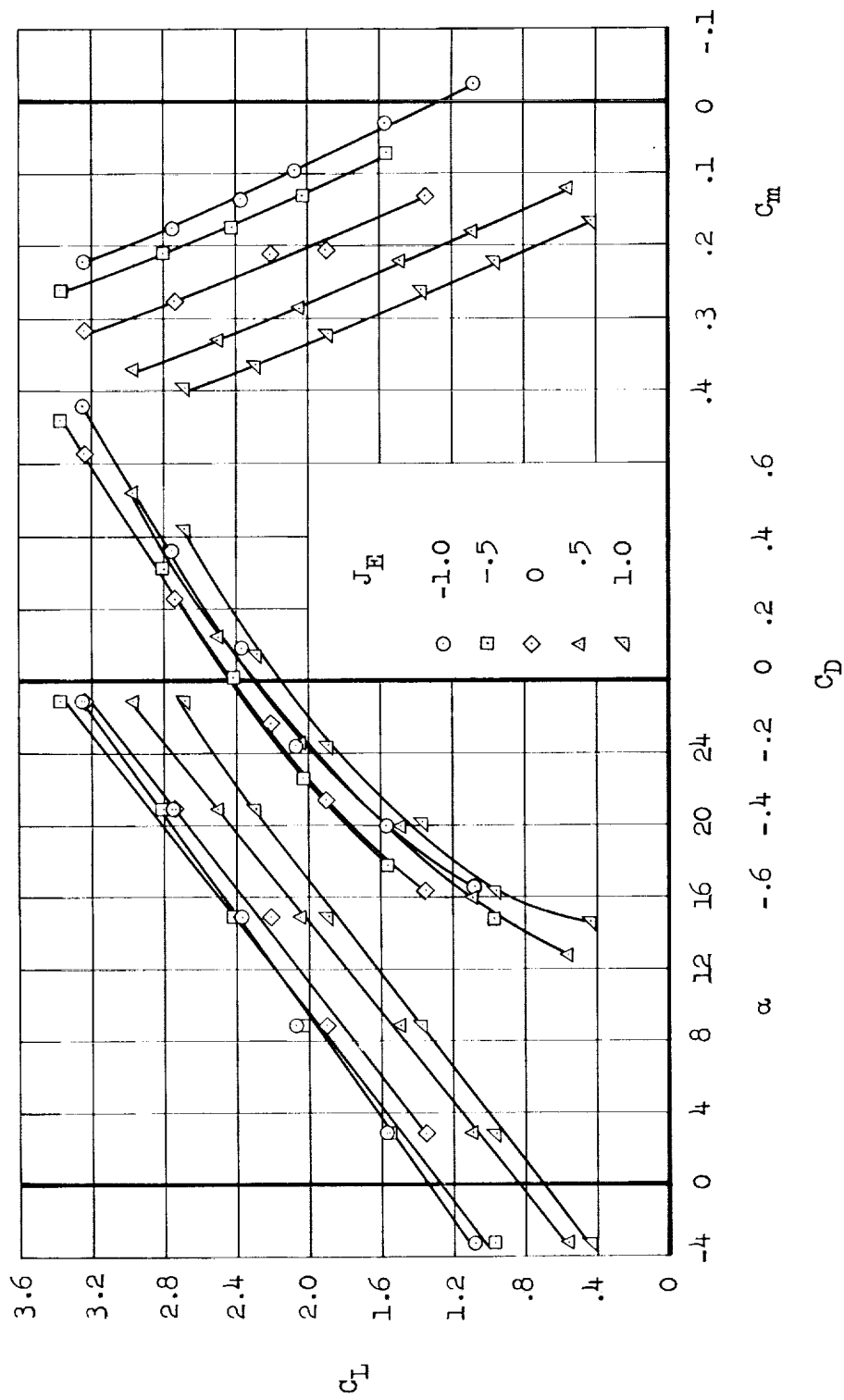
(a) Tail off; $C_J = 2.3$.

Figure 13.- Longitudinal characteristics of the original cruise flight configuration ($J_T = 1/1$) at $h/D = 0.70$.
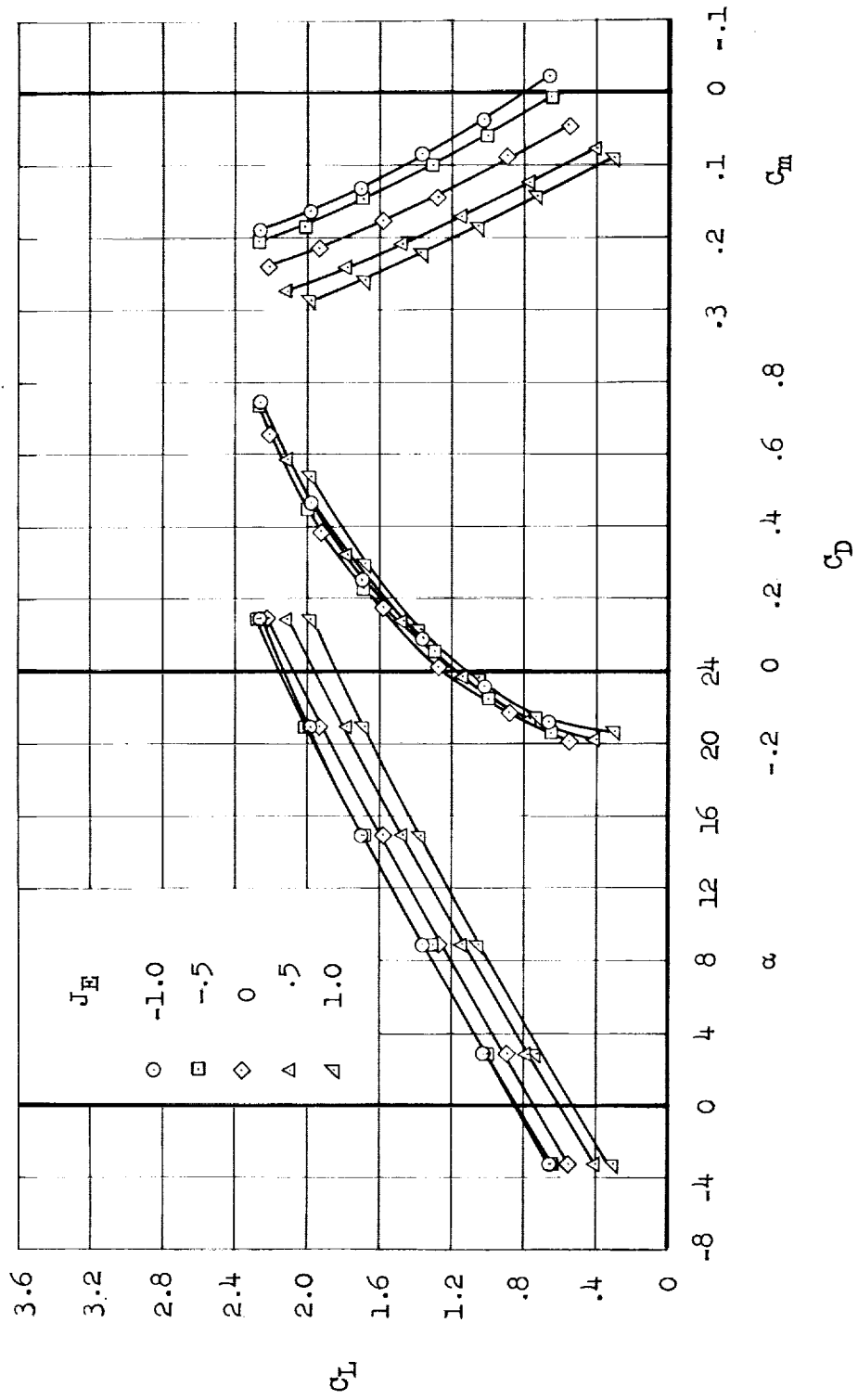
(a) Tail off; $C_J = 1.1$ - Continued.

Figure 13.- Continued.
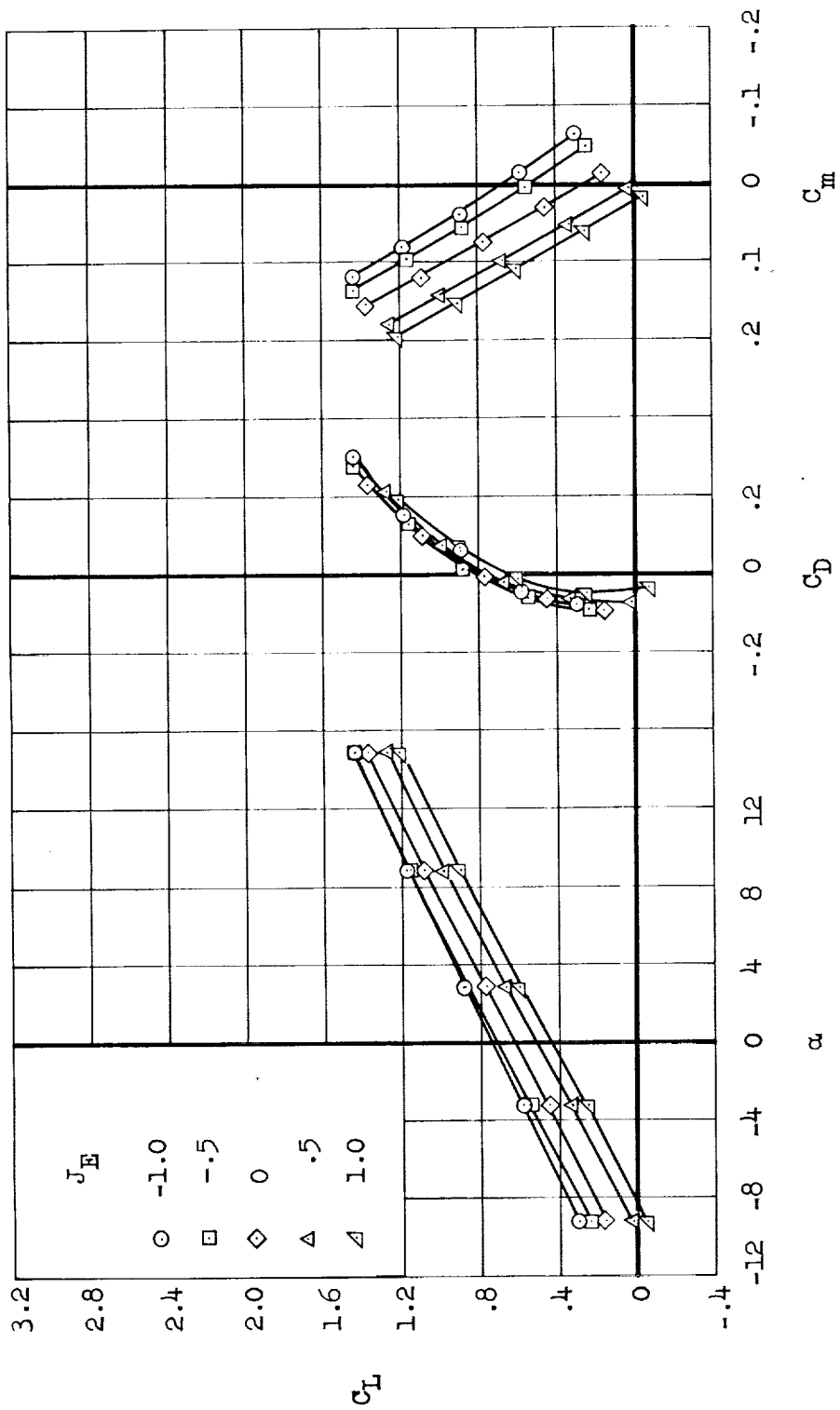
(a) Tail off; $C_J = 0.76$ - Continued.

Figure 13.- Continued.
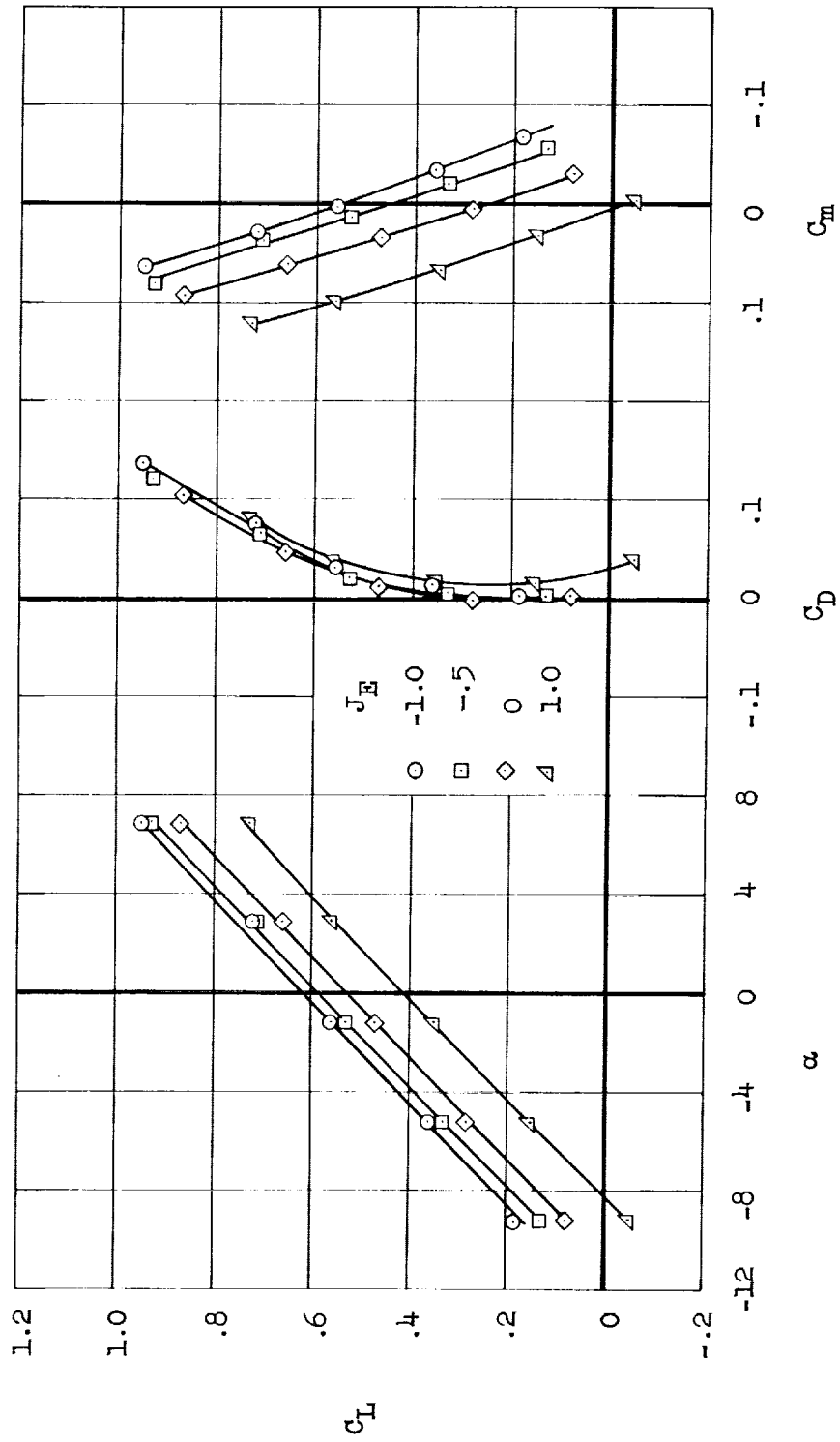
(a) Tail off; $C_J = 0.58$ - Continued.

Figure 13.- Continued.
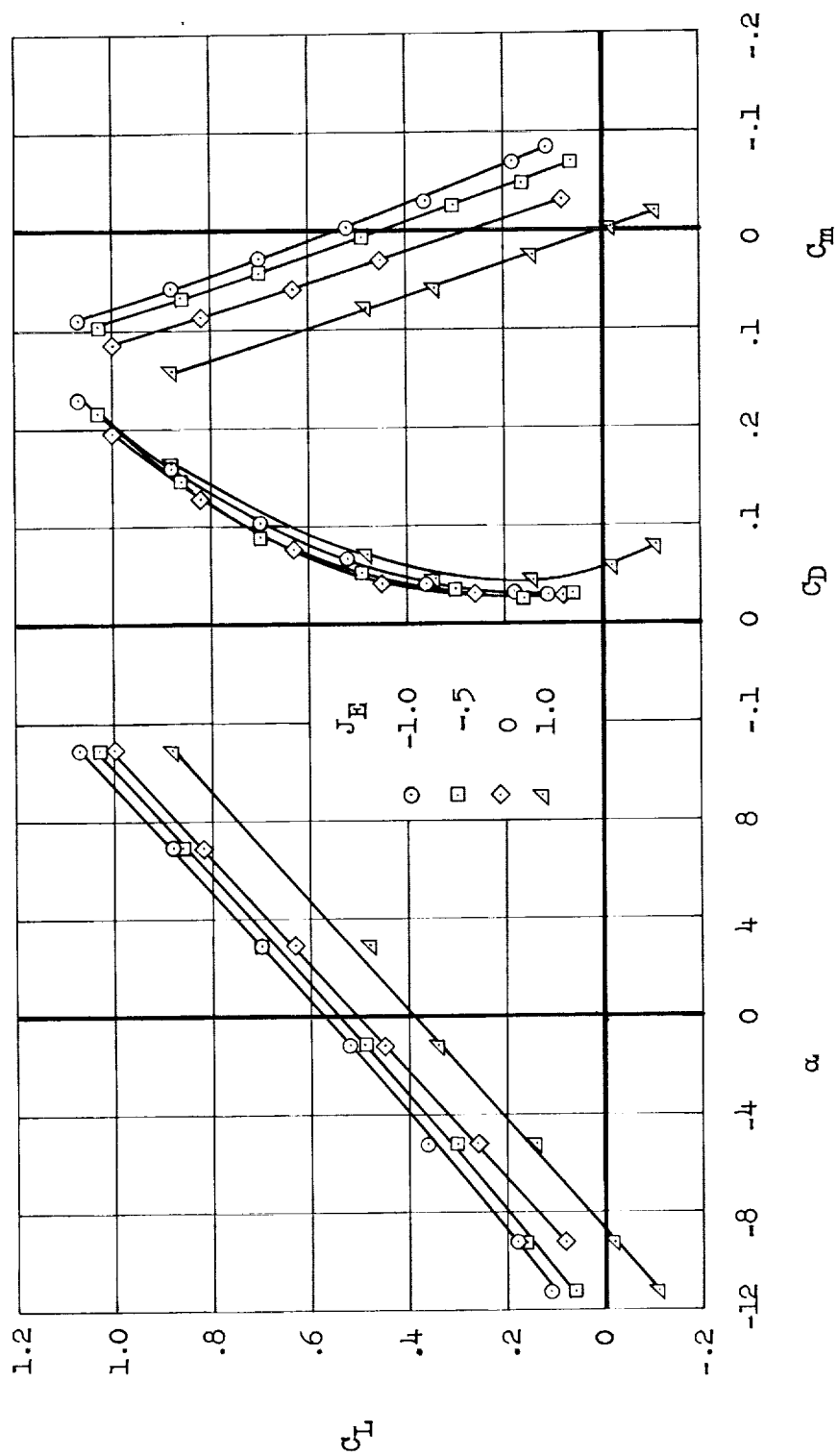
(a) Tail off; $C_J = 0.45$ - Concluded.

Figure 13.- Continued.

$J_E = -1.0$
$C_J = 0.45$
o Tail off
□ $i_T = 20^o$
◇ $i_T = 26^o$
△ $i_T = 32^o$
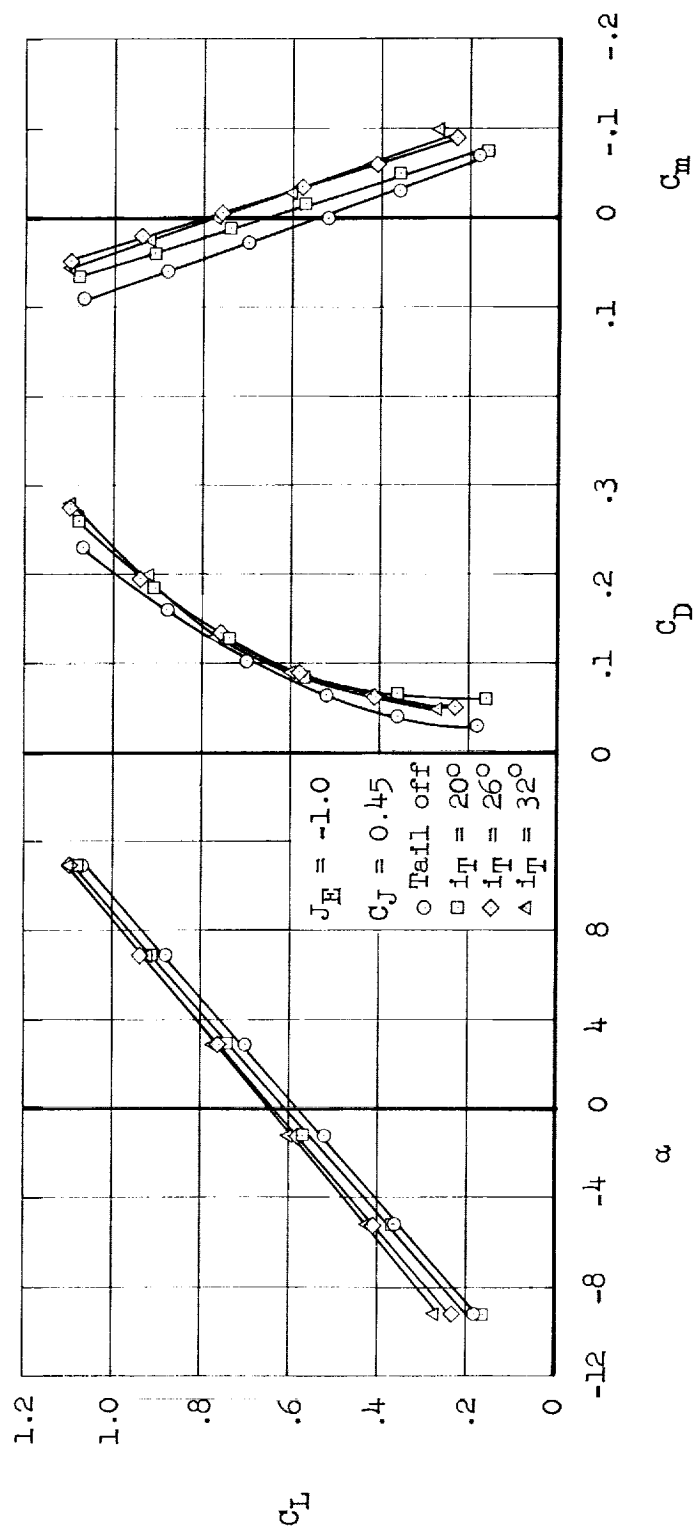
(b) Tail on; various i_T.

Figure 13.- Concluded.

(a) Effect of α without rotor intake guide vanes.

Figure 14.- Lateral characteristics of various transition configurations at $h/D = 0.15$.
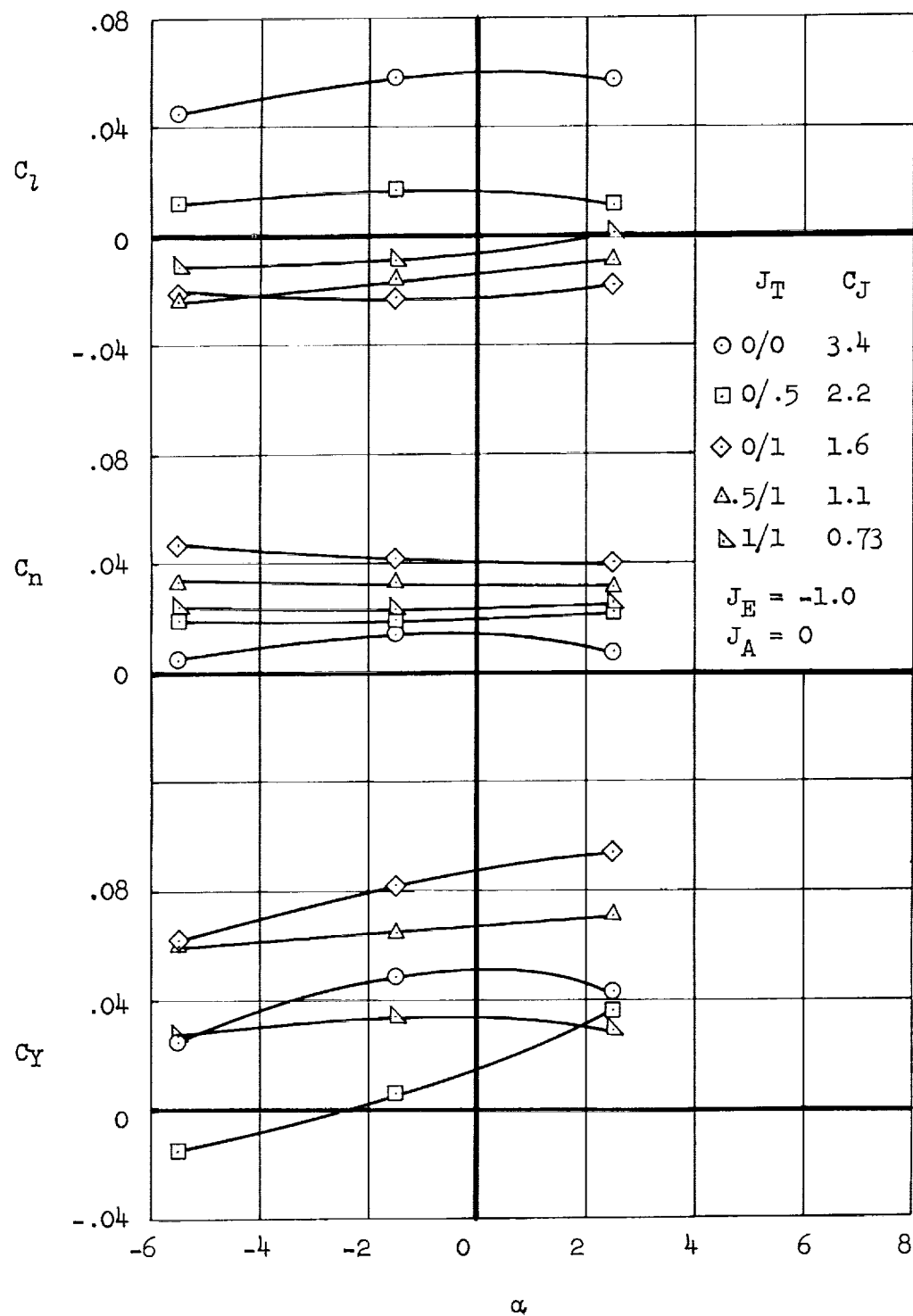
(b) Effects of α with rotor intake guide vanes.

Figure 14.- Continued.
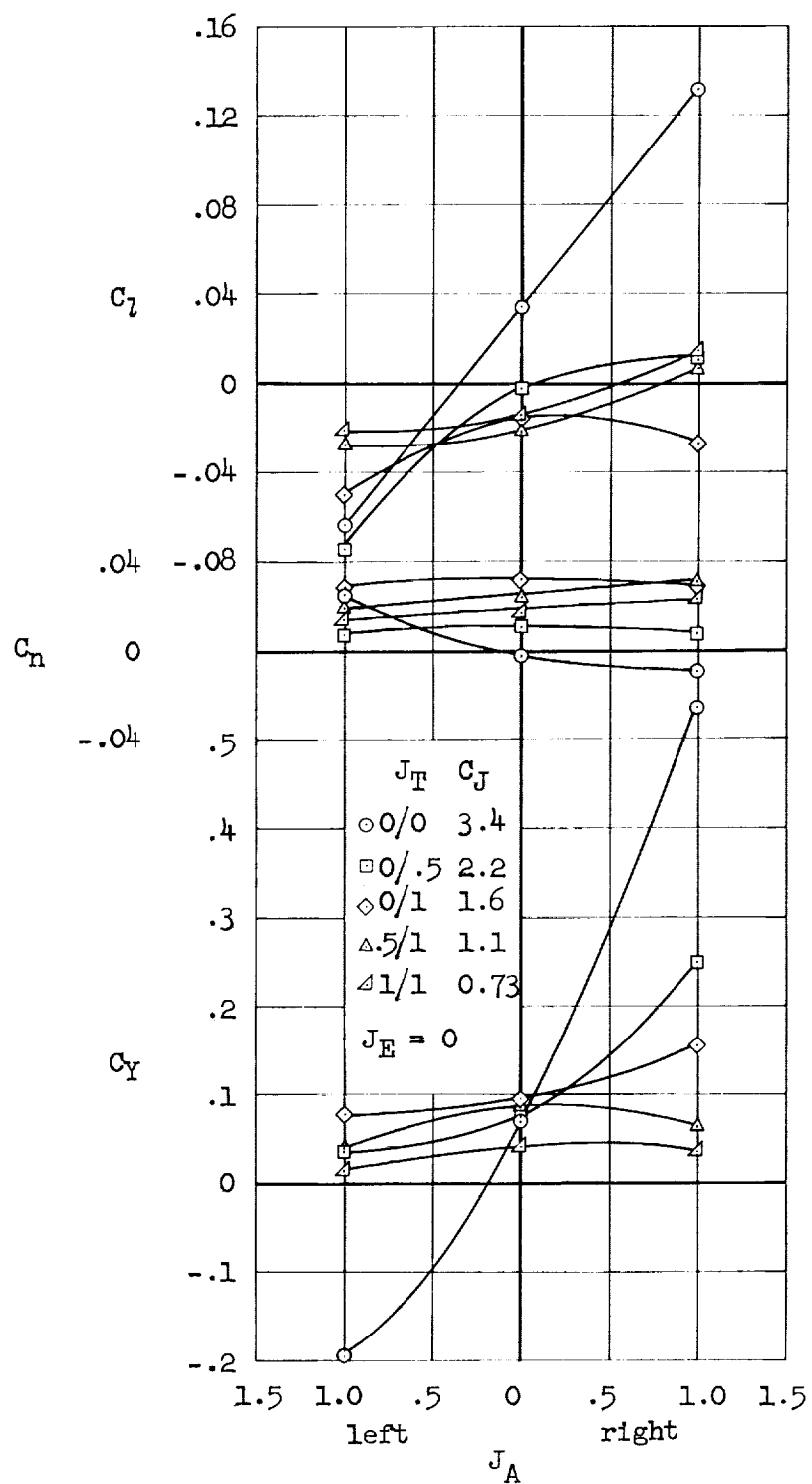
(c) Effect of J_A with rotor intake guide vanes.

Figure 14.- Concluded.
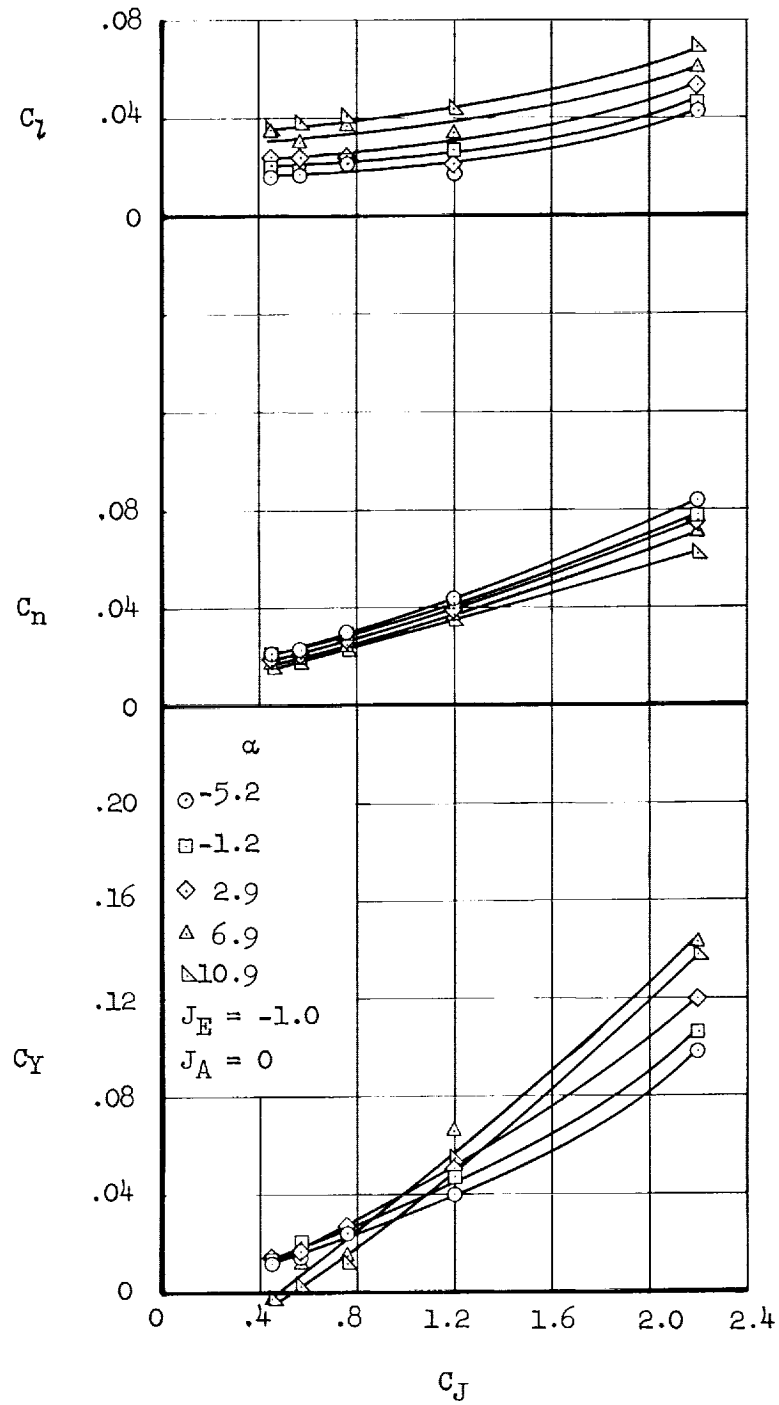
(a) For various α; without rotor intake guide vanes.

Figure 15.- Variation of lateral characteristics with C_J for the cruise flight configuration (J_T = 1/1) at h/D = 0.70.
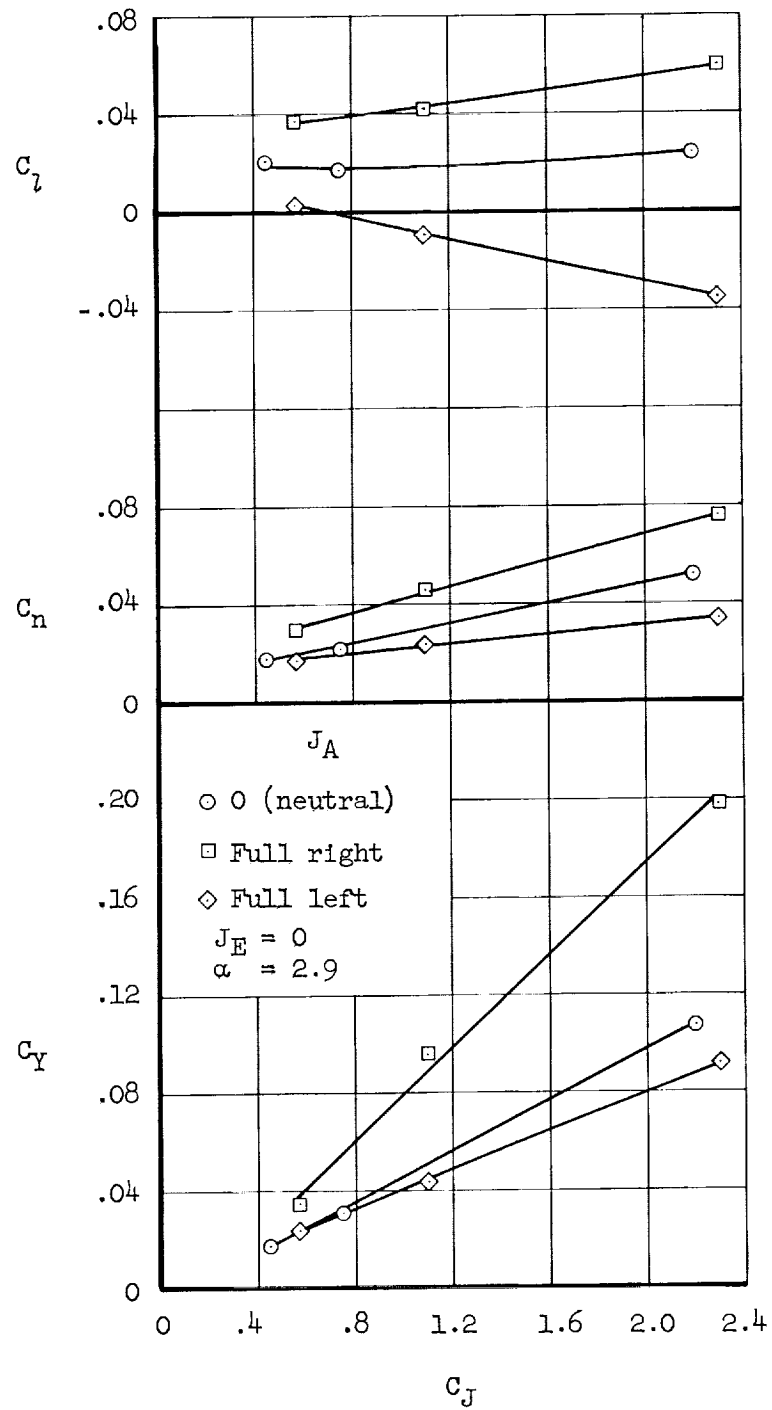
(b) For various lateral control positions; without rotor intake guide vanes.

Figure 15.- Continued.
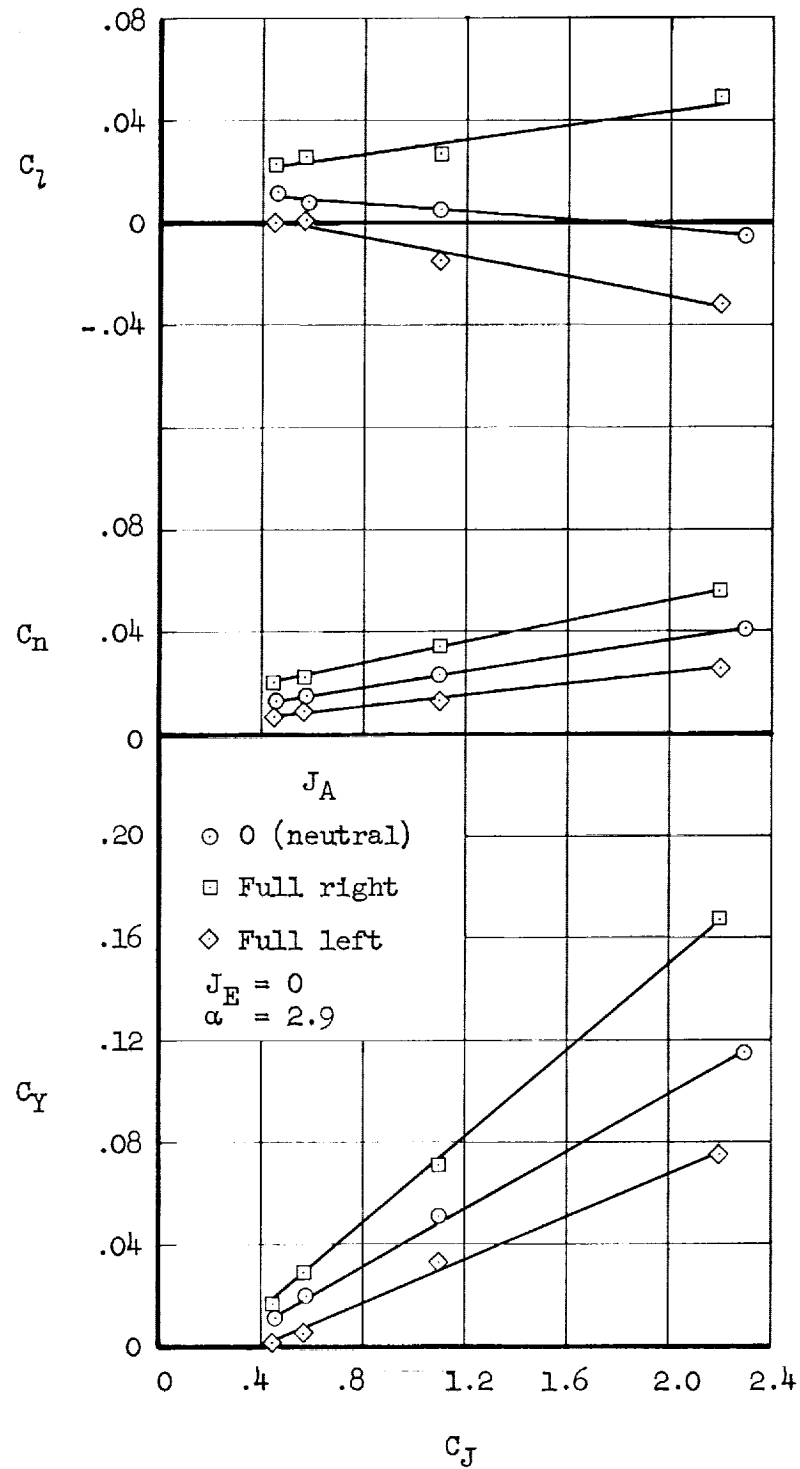
(c) For various lateral control positions; with rotor intake guide vanes.

Figure 15.- Concluded.
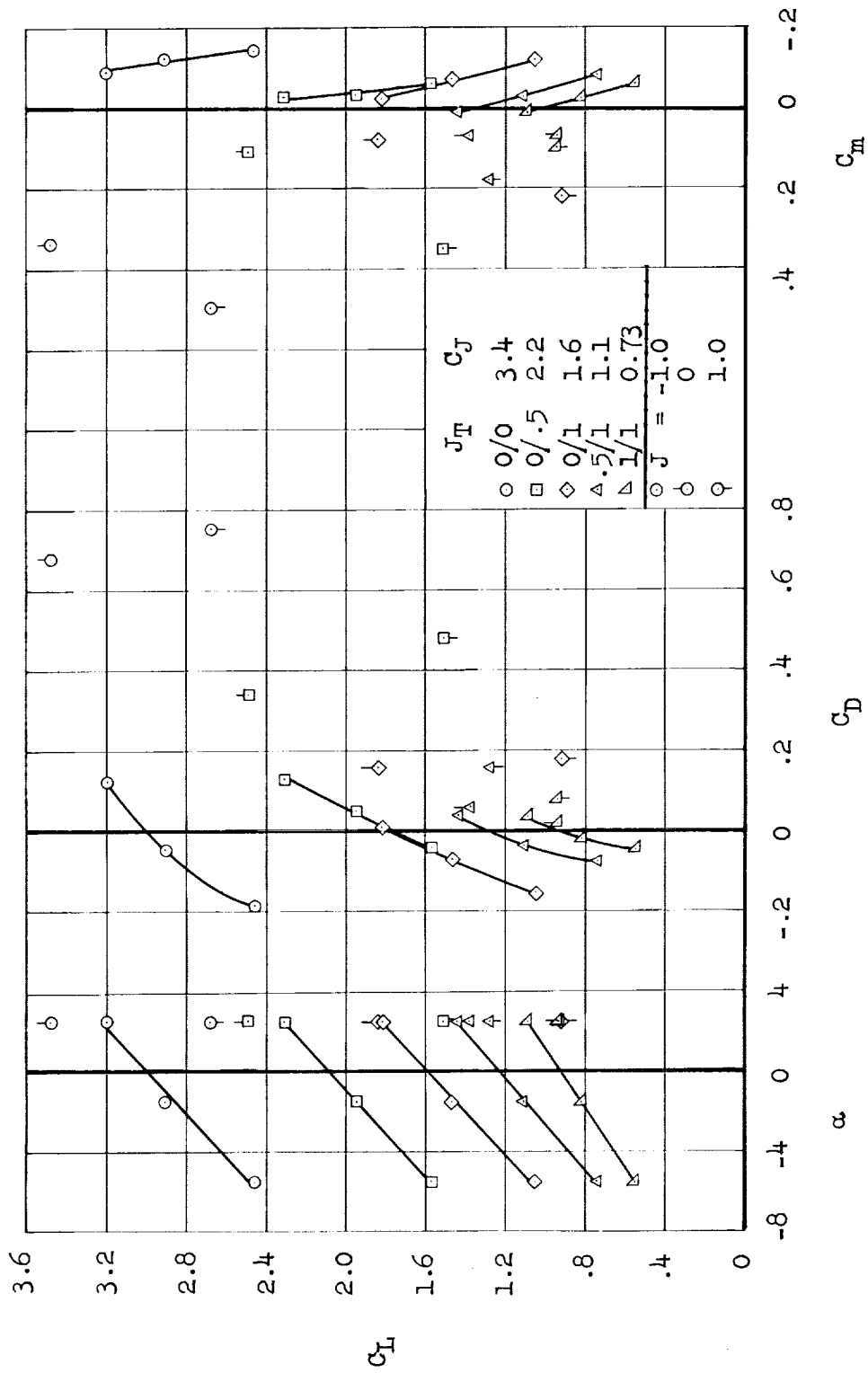
(a) At $h/\bar{D} = 0.15$, for various transition configurations.

Figure 16.- Longitudinal characteristics with rotor intake guide vanes.

(b) At h/D = 0.70, for the cruise flight configuration (J_T = 1/1).

Figure 16.- Concluded.
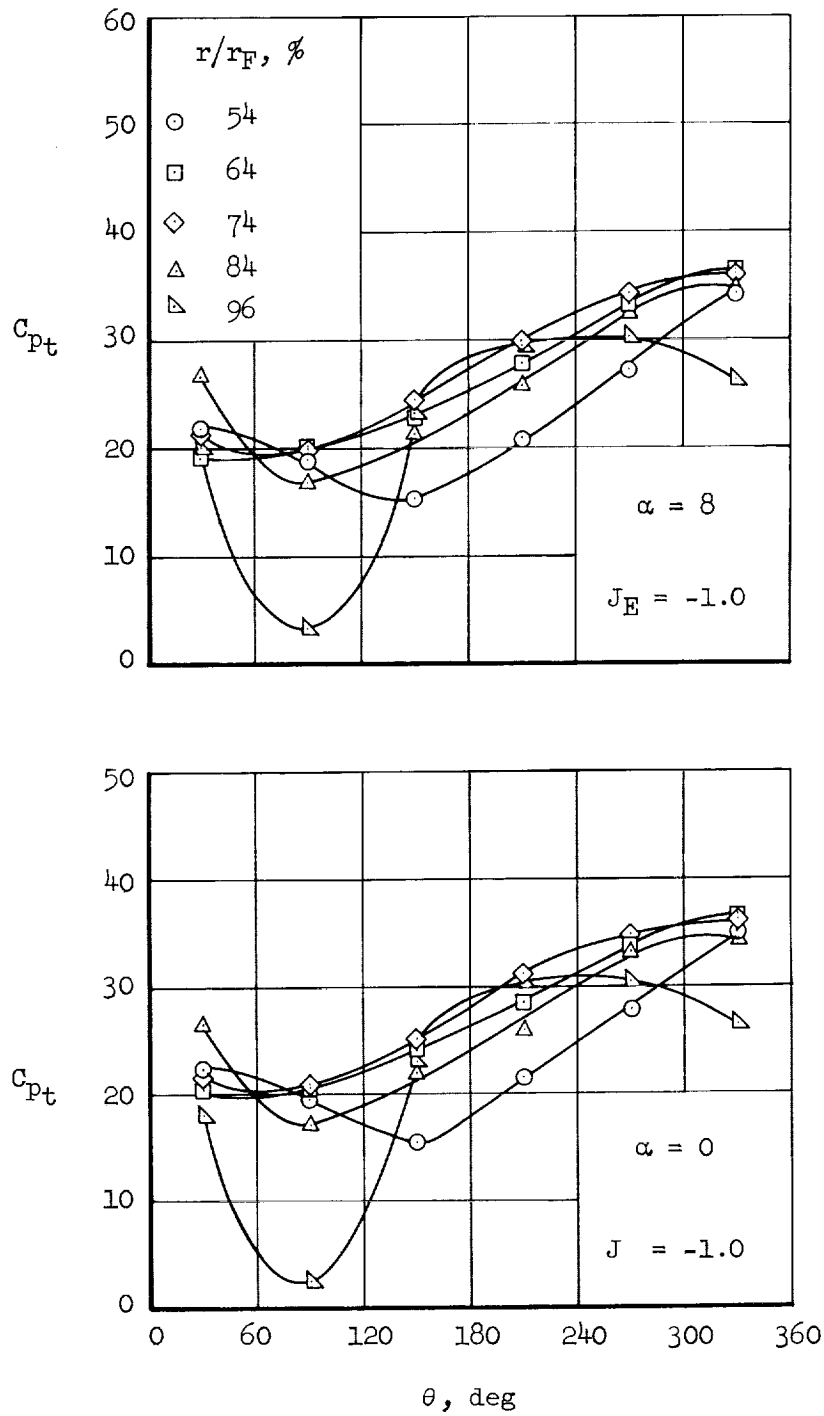
(a) $C_J = 2.2$

Figure 17.- Circumferential pressure profiles beneath the turborotor at various radii from the rotor axis; h/D = 0.70; no intake guide vanes.
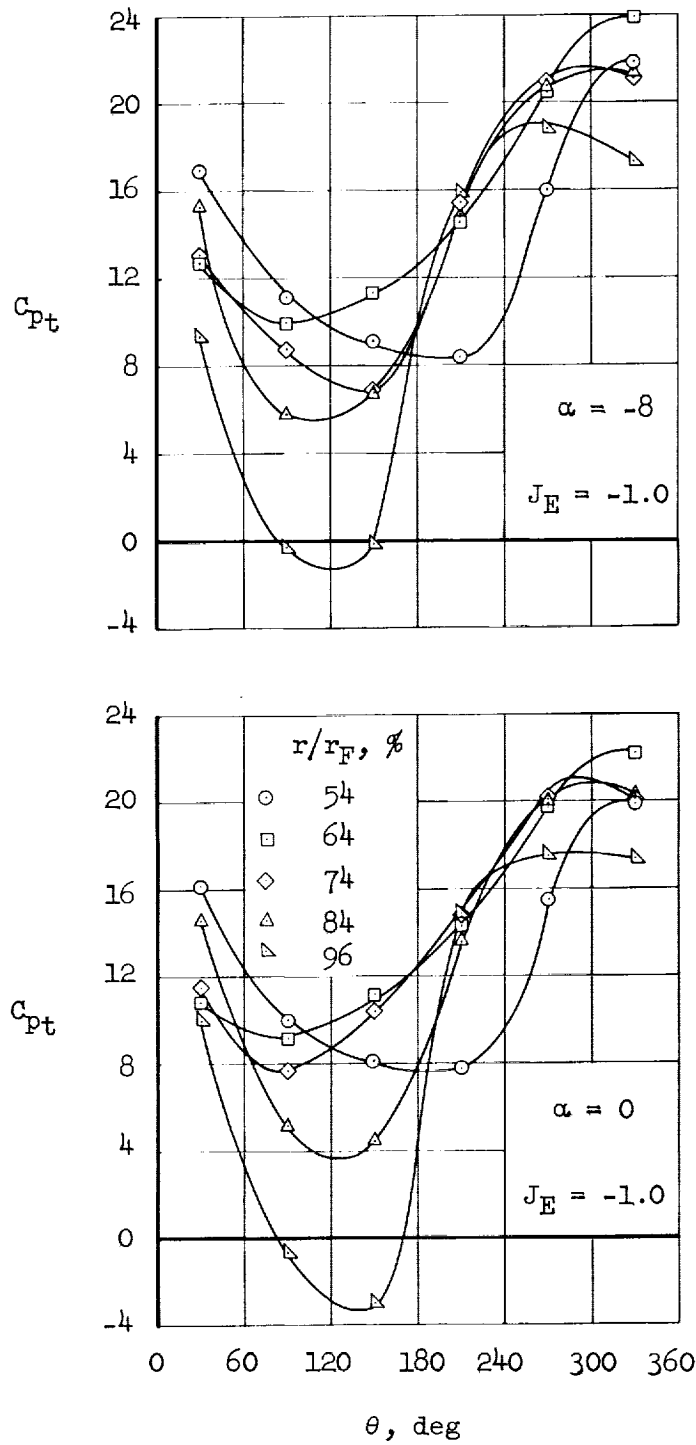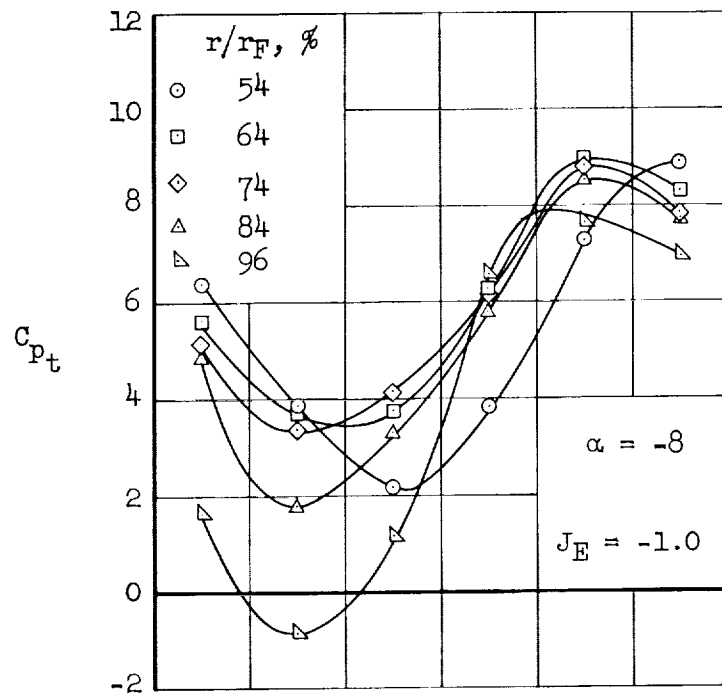
(b) $C_J = 1.1$

Figure 17.- Continued.
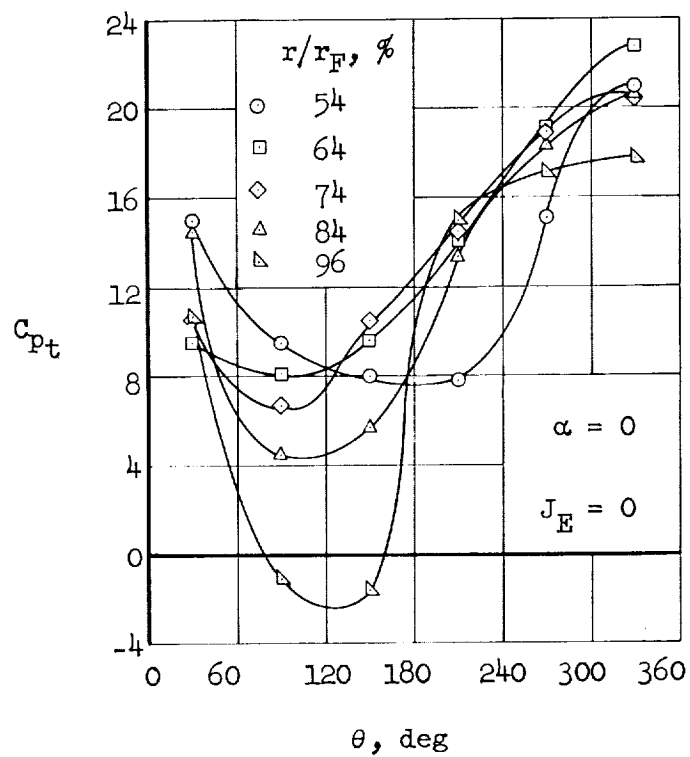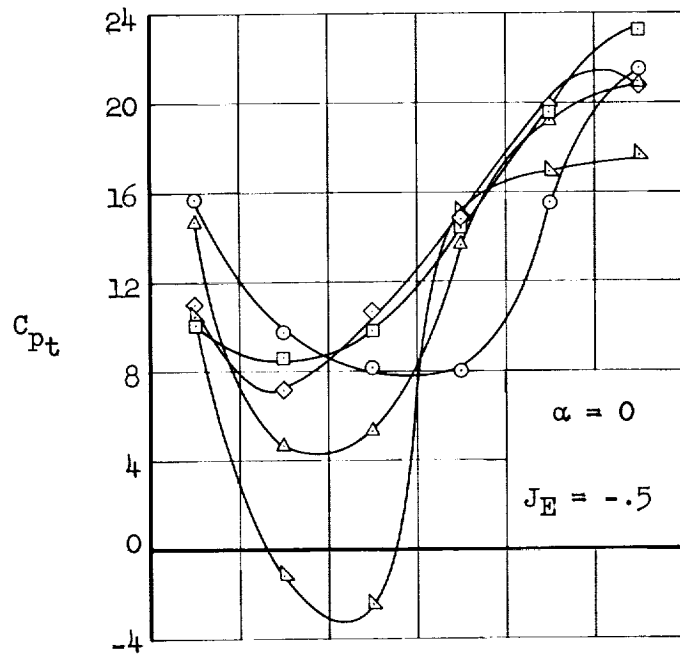
(b) $C_J = 1.1$ - Continued.
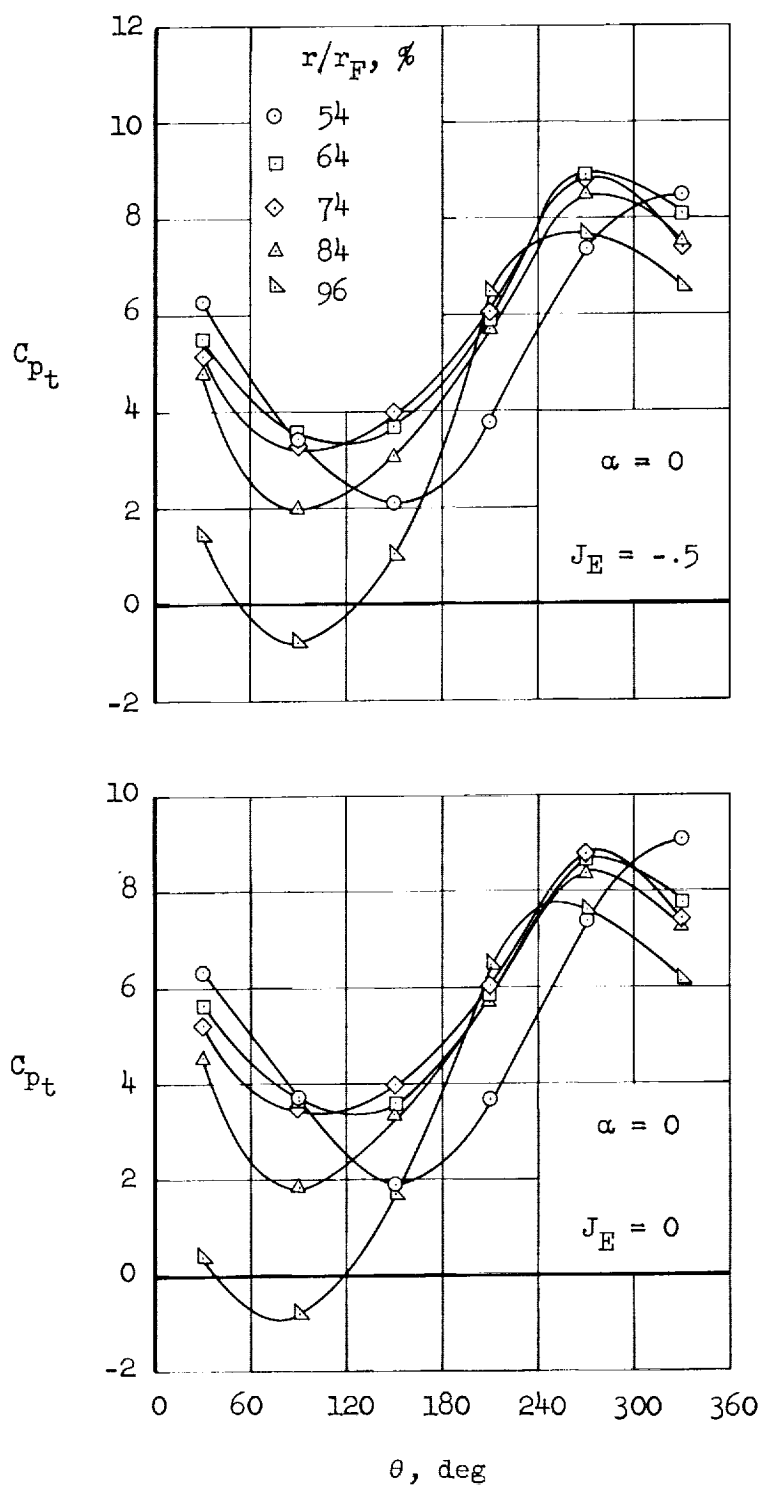
Figure 17.- Continued.
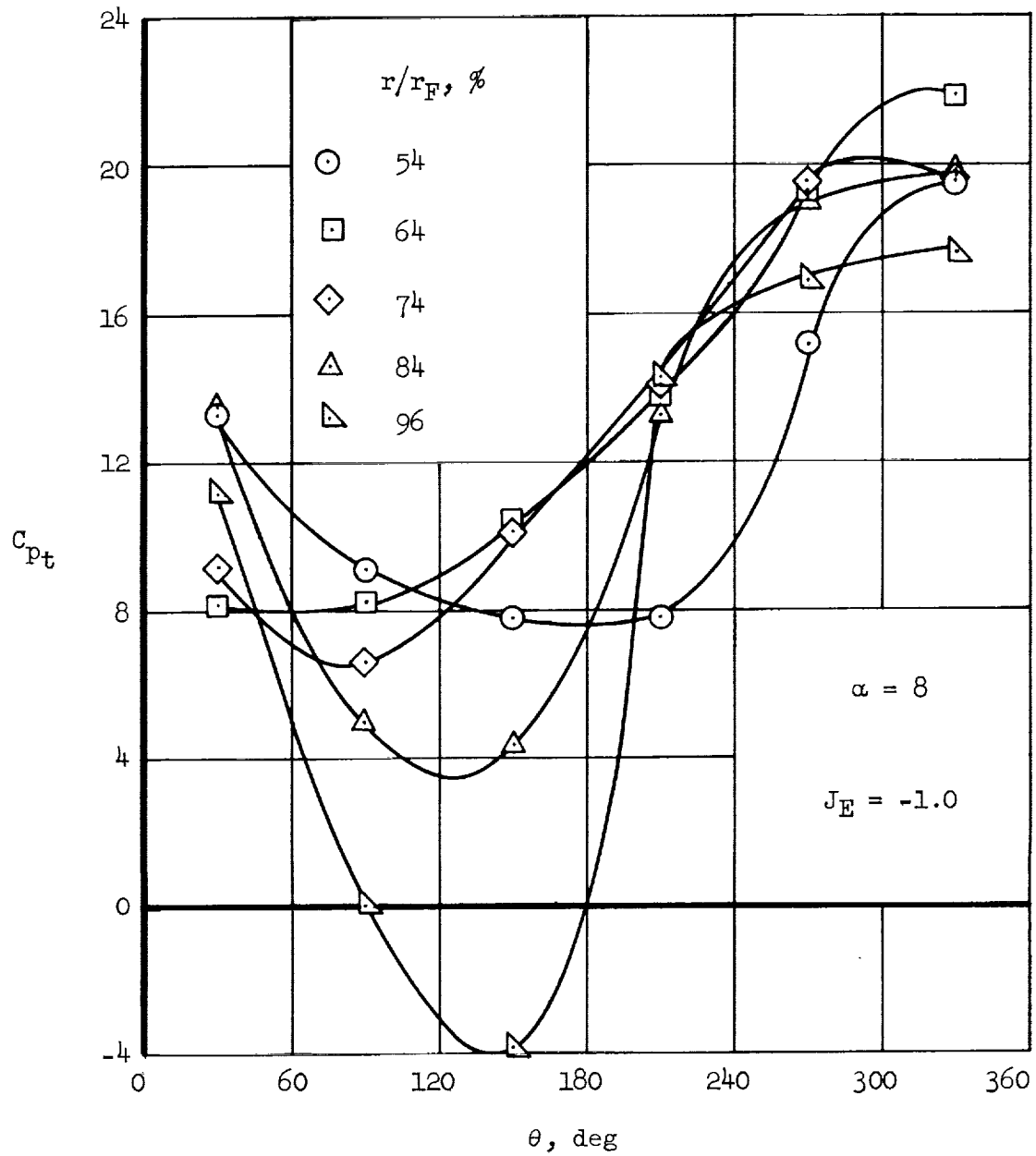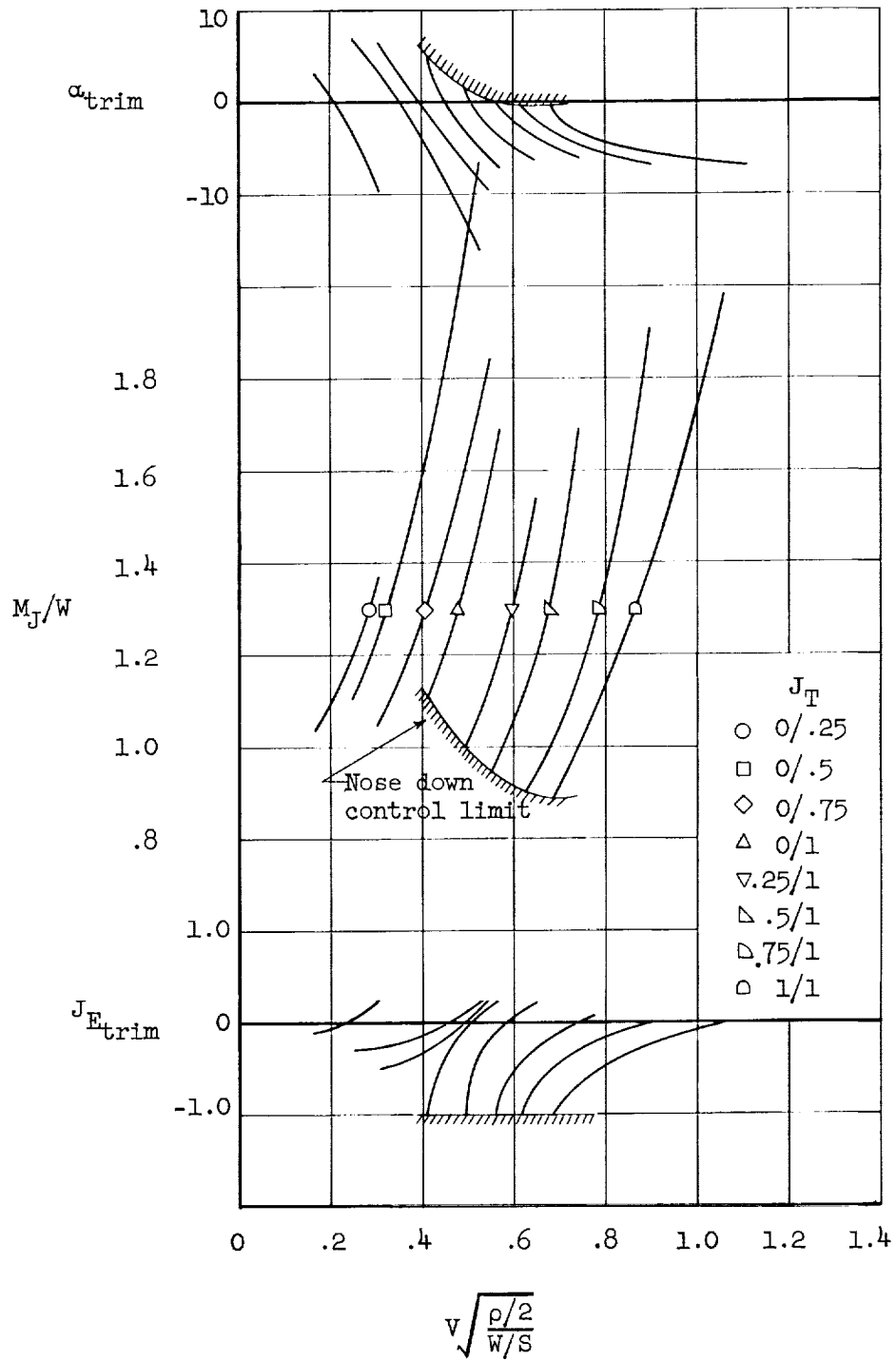
(b) $C_J = 1.1$ - Concluded.

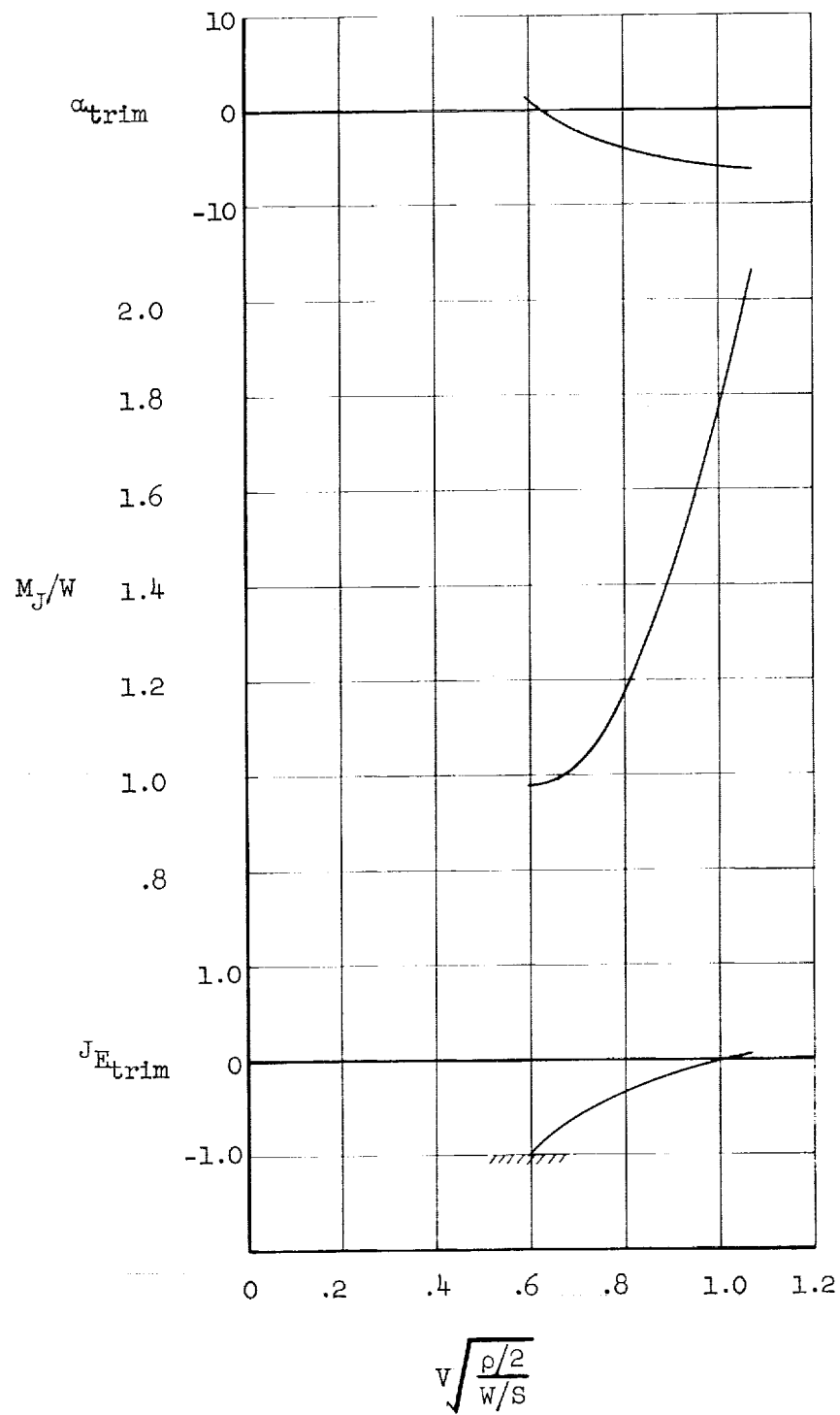Figure 17.- Continued.
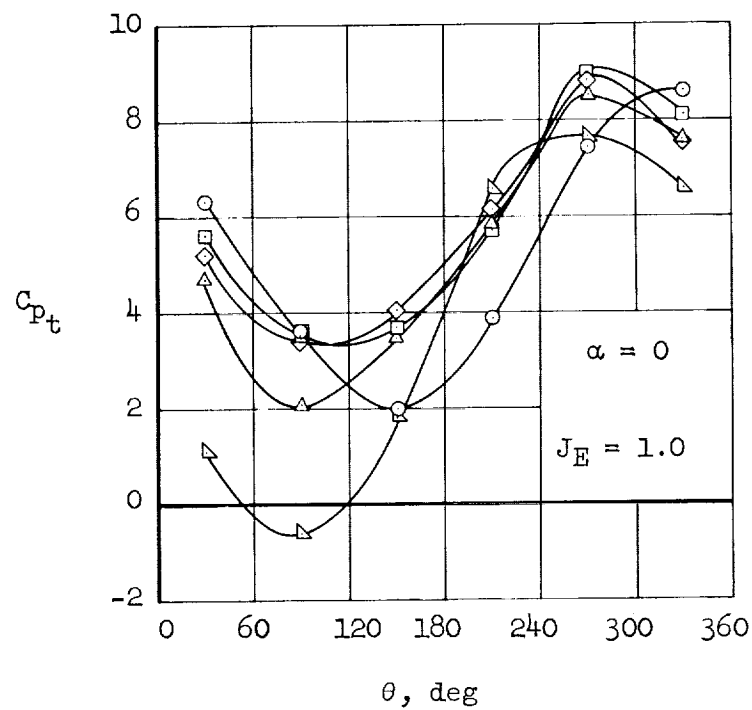
(c) $C_J = 0.45$

Figure 17.- Continued.
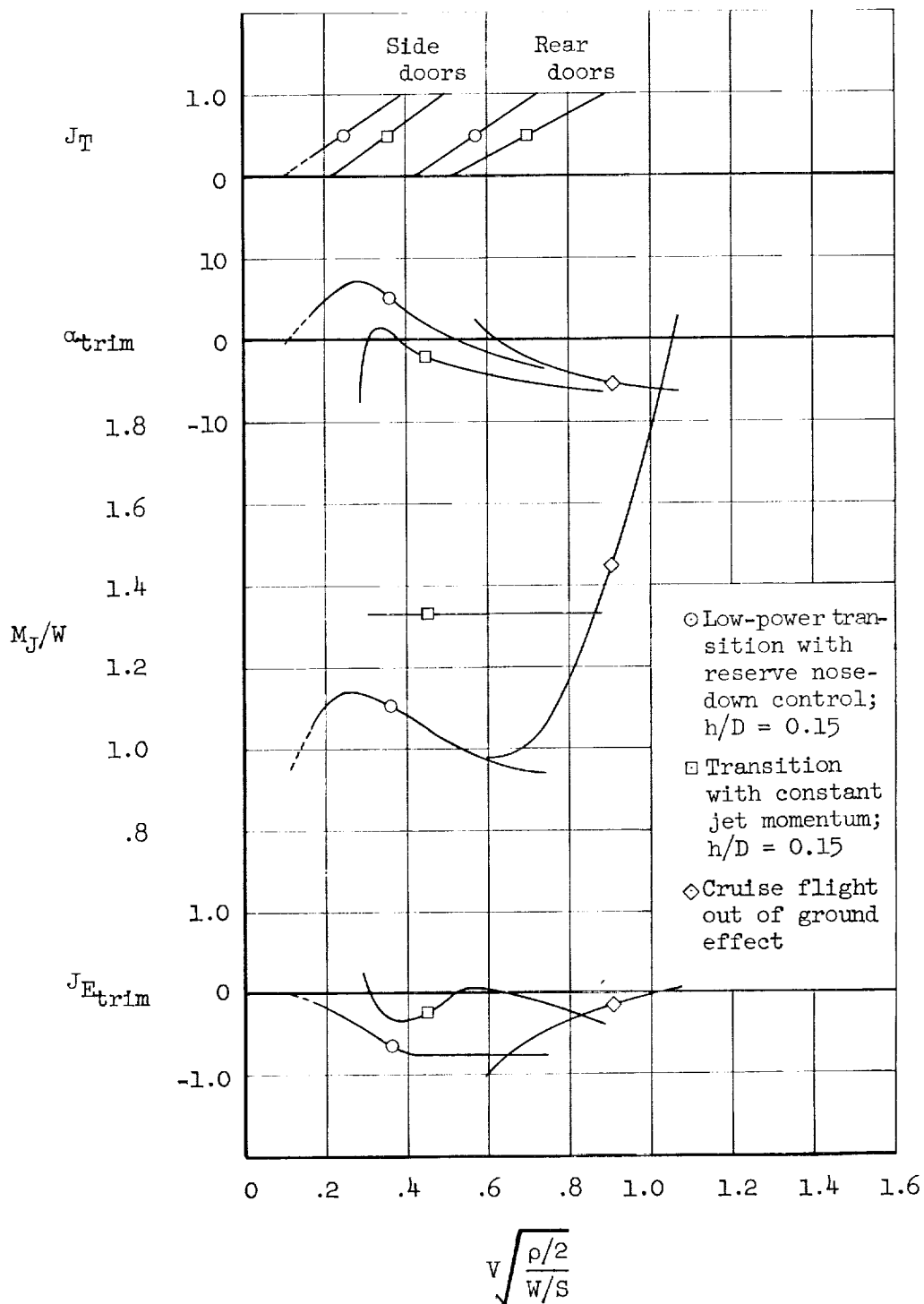
(c) $C_J = 0.45$ - Concluded.

Figure 17.- Concluded.

(a) For transition configurations at h/D = 0.15.

Figure 18.- Performance summary showing the variation of basic aircraft
variables required for trimmed, level, unaccelerated flight. Tail
off configuration with modified trailing edge.

(b) For the cruise configuration out of ground effect ($h/D = 0.70$).

Figure 18.- Continued.

(c) Cross plots of figure 4(a) showing two variations of trim conditions for transition flight.

Figure 18.- Concluded.